CHALMERS
UNIVERSITY OF TECHNOLOGY

An Adaptive Control Approach Based on Dynamic Movement Primitives for Human-Robot Handover

Master's thesis in Systems, Control and Mechatronics

DOMINIK WIDMANN

Department of Signals and Systems
CHALMERS UNIVERSITY OF TECHNOLOGY
Gothenburg, Sweden 2016

MASTER'S THESIS 2016:49

An Adaptive Control Approach Based on Dynamic Movement Primitives for Human-Robot Handover

DOMINIK WIDMANN

Department of Signals and Systems
Division of Automatic Control, Automation and Mechatronics
CHALMERS UNIVERSITY OF TECHNOLOGY
Gothenburg, Sweden 2016

An Adaptive Control Approach Based on Dynamic Movement Primitives for Human-Robot Handover
DOMINIK WIDMANN

© DOMINIK WIDMANN, 2016.

Supervisor and Examiner: Yiannis Karayiannidis, Assistant Professor, Department of Signals and Systems, Chalmers University of Technology

Master's Thesis 2016:49
Department of Signals and Systems
Division of Automatic Control, Automation and Mechatronics
Chalmers University of Technology
SE-412 96 Gothenburg
Telephone +46 31 772 1000

Typeset in LaTeX
Gothenburg, Sweden 2016

An Adaptive Control Approach Based on Dynamic Movement Primitives for Human-Robot Handover
DOMINIK WIDMANN
Department of Signals and Systems
Chalmers University of Technology

Abstract

Recent advancements on robotic technology expect a strong collaboration between humans and robots in the near future. Such collaboration relies on natural interaction between human and robot, demanding human-like behavior of the robot. A common scenario of human-robot collaboration is a human-robot handover. For this to be done seamlessly and in a human fashion, the robot has to anticipate the human agent's motion by predicting place and time of the handover on-line as soon as the human initiates the handover process. We consider the prediction problem as a model-based estimation problem where the point attractor and the timescale constant of the system are estimated on-line. Using Dynamic Movement Primitives as a parameterization of human motion, point attractor and timescale are successfully estimated on-line using different estimation laws based on adaptive control methods. Their stability is shown and their performance is evaluated using experimental data of human-human handovers. Thanks to the good prediction of the handover place, the presented algorithms are found to be applicable to improve human-robot collaboration.

Keywords: Dynamic movement primitive, parameter estimation, handover, human-robot collaboration.

Acknowledgements

I would like to thank my supervisor Yiannis Karayiannidis from Chalmers University of Technology for his support, feedback and many interesting discussions. Furthermore, I would like to acknowledge Christian Smith, Axel Demborg and Elon Såndberg from KTH in Stockholm, who provided us with useful experimental data on human-human handovers.

Dominik Widmann, Gothenburg, June 2016

Contents

List of Figures **xi**

List of Tables **xv**

1 Introduction **1**
- 1.1 Context . . . 1
- 1.2 Related Work . . . 1
- 1.3 Approach and Structure . . . 4

2 Background **5**
- 2.1 Notation Conventions . . . 5
- 2.2 Dynamic Movement Primitives . . . 5
  - 2.2.1 Attractor System . . . 6
  - 2.2.2 Multiple DOF . . . 7
  - 2.2.3 Stability and Invariance . . . 7
  - 2.2.4 Off-line Learning of Attractor Dynamics . . . 8
  - 2.2.5 Alternative Formulations . . . 10
- 2.3 On-line Parameter Estimation . . . 10
  - 2.3.1 Integral Adaptive Law . . . 11
  - 2.3.2 Least-Squares Adaptive Law . . . 12
  - 2.3.3 Persistence of Excitation and Parameter Identification . . . 13
  - 2.3.4 Hybrid Adaptive Law . . . 13
- 2.4 The Continuous Extended Kalman filter . . . 13
  - 2.4.1 Classical Extended Kalman Filter . . . 14
  - 2.4.2 Modified Extended Kalman Filter with prescribed Degree of Stability . . . 15
  - 2.4.3 Adaptive Laws as EKFs . . . 17

3 Problem Description **19**
- 3.1 Problem Formulation: Predictor Structure . . . 19
- 3.2 Limitations . . . 20
- 3.3 Parameterization of Human Motion Using a DMP . . . 20
- 3.4 Parameterization of Human Motion Using a Specialized DMP . . . 24

4 Parameter Estimation Based on DMPs **29**
- 4.1 Adaptive Law-Based Parameter Estimation of DMPs . . . 29
  - 4.1.1 Continuous Goal Estimation for Known Timescales . . . 30

4.1.2 Continuous Goal and Timescale Estimation 33
4.2 EKF-Based Parameter Estimation of DMPs 36
4.2.1 Classical EKF-Based State Estimation 37
4.2.2 Modified EKF-Based State Estimation 42
4.2.3 Modified EKF-Based Parameter Estimation 45

5 Parameter Estimation Based on Specialized DMPs 53
5.1 Adaptive Law-Based Parameter Estimation of Specialized DMPs . . 53
5.2 EKF-Based Parameter Estimation for Specialized DMPs 55
5.2.1 Classical EKF-Based State Estimation 55
5.2.2 Modified EKF-Based State Estimation 58
5.3 Discrete-Time Nonlinear Least-Squares Adaptive Law 60
5.3.1 Optimal Control Formulation 61
5.3.2 Implementation 63

6 Results 67
6.1 Evaluation of the Parameterizations 67
6.2 Parameter Estimation Performance 68
6.2.1 Original DMP 68
6.2.2 Specialized DMP 69
6.3 Parameter Estimation Performance Using Experimental Data 70
6.3.1 Qualitative Evaluation of the Parameter Estimators 71
6.3.2 Quantitative Evaluation of the EKF-Based Parameter Estimator Using a DMP 74

7 Conclusions and Future Work 81

Bibliography 85

A Appendix I
A.1 Derivations of Lipschitz Continuity for the EKF I
A.2 Additional Plots II
A.2.1 EKFs for the original DMP II
A.2.2 EKFs for the Specialized DMP III

List of Figures

2.1 Structure of the DMP representation of an n-DOF system with shared canonical system. 7
2.2 Trajectories produced with a DMP fitted to a minimum-jerk trajectory for different parameter values of timescale τ and goal g. 8

3.1 Overall structure of the proposed predictor. 20
3.2 Minimum jerk trajectory representing point-to-point motion of a human hand with position y, velocity $\dot{y}$ and acceleration $\ddot{y}$ in one dimension. 22
3.3 Distribution of the basis functions Ψ_i over time t. 23
3.4 Weights w_i resulting from off-line learning. 23
3.5 Phase variable and phase variable replacement of original and specialized DMP respectively. 24
3.6 Distribution of the basis functions $\Psi_{s,i}$ of the specialized DMP over t/τ. 27
3.7 Trajectories produced with the specialized DMP fitted to a minimum-jerk trajectory for different parameter values of goal g and timescale τ. 27
3.8 Fitting error for a minimum-jerk trajectory with $\tau = 1\,\mathrm{s}$ using $N = 30$ basis functions and a specialized DMP. 28

4.1 Spectral measure $S_y(\omega)$ of a minimum-jerk trajectory with $\tau = 10$, $y_0 = 0$ and $g = 2$. 31
4.2 Estimation of goal g for a known timescale of $\tau = 10\,\mathrm{s}$ using a least-squares adaptive law with forgetting factor $\beta = 0.1$, initial gain $\boldsymbol{P}_{0,lsq}$ and initial goal $\hat{g}_0 = 1\,\mathrm{m}$. 32
4.3 Estimation of g for known τ using an integral adaptive law with forgetting factor $\beta = 0.1$, $\boldsymbol{R}_0 = \boldsymbol{0}$, $\boldsymbol{Q}_0 = \boldsymbol{0}$ and $\boldsymbol{\Gamma} = \boldsymbol{P}_{0,lsq}$. The initial guess is $\hat{g}_0 = 1\,\mathrm{m}$. 33
4.4 On-line estimation of handover position $\hat{g}$ and handover time $\hat{\tau}$ with true values $g = 2\,\mathrm{m}$ and $\tau = 10\,\mathrm{s}$ and initial parameter values $\hat{g}_0 = 1\,\mathrm{m}$ and $\hat{\tau}_0 = 9\,\mathrm{s}$. 35
4.5 On-line estimation of handover position $\hat{g}$ and handover time $\hat{\tau}$ with true values $g = 2\,\mathrm{m}$, $\tau = 10\,\mathrm{s}$ and initial parameter estimates $\hat{g}_0 = 1\,\mathrm{m}$, $\hat{\tau}_0 = 9\,\mathrm{s}$ using explicit estimation of x and a least-squares adaptive law with $\beta = 0.1$ and $\boldsymbol{P}_{0,ee} = \mathrm{diag}([100, 5000, 1000])$. 37

4.6 Illustration of the boundedness of the basis functions Ψ_i and their sum $\sum_{i=1}^{N} \Psi(x)$ for $N = 30$ basis functions, width parameters h_i and exponentially spaced centers c_i. 40

4.7 On-line estimation of handover position $\hat{g}$ and handover time $\hat{\tau}$ with true values $g = 2\,\mathrm{m}$ and $\tau = 10\,\mathrm{s}$ and initial parameter estimates $\hat{g}_0 = 1\,\mathrm{m}$ and $\hat{\tau}_0 = 9\,\mathrm{s}$ using a classical EKF. 41

4.8 Estimated DMP states using a classical EKF. 42

4.9 Lower bound $\underline{p}_c(t)$ and upper bound $\overline{p}_c(t)$ of $\boldsymbol{P}(t)$ using a classical EKF to estimate the states of an original DMP. 43

4.10 On-line estimation of handover position $\hat{g}$ and handover time $\hat{\tau}$ with true values $g = 2\,\mathrm{m}$ and $\tau = 10\,\mathrm{s}$ and initial parameter values $\hat{g}_0 = 1\,\mathrm{m}$ and $\hat{\tau}_0 = 9\,\mathrm{s}$ using a modified EKF with $\alpha = 0.5$. 45

4.11 Estimated DMP states using a modified EKF. 46

4.12 On-line estimation of handover position and time with true values $g = 2\,\mathrm{m}$ and $\tau = 10\,\mathrm{s}$ and initial guesses $\hat{g}_0 = 1\,\mathrm{m}$ and $\hat{\tau}_0 = 9\,\mathrm{s}$ using an unfiltered modified EKF-based adaptive law. 48

4.13 On-line estimation of handover position and time with true values $g = 2\,\mathrm{m}$ and $\tau = 10\,\mathrm{s}$ and initial parameter values $\hat{g}_0 = 1\,\mathrm{m}$ and $\hat{\tau}_0 = 9\,\mathrm{s}$ using a modified EKF-based filtered adaptive law with filter parameter $\lambda_f = 5$. 50

4.14 On-line estimation of handover position time with true values $g = 2\,\mathrm{m}$, $\tau = 10\,\mathrm{s}$ and initial parameter values $\hat{g}_0 = 1\,\mathrm{m}$, $\hat{\tau}_0 = 9\,\mathrm{s}$ using a modified EKF-based filtered adaptive law with different filter parameters λ_f. 51

5.1 On-line estimation of handover position and time with true values $g = 2\,\mathrm{m}$, $\tau = 10\,\mathrm{s}$ and initial parameter values $\hat{g}_0 = 1\,\mathrm{m}$, $\hat{\tau}_0 = 9\,\mathrm{s}$ using a least-squares adaptive law with $\beta = 0$ and $\boldsymbol{P}_0 = 10^6 \mathrm{diag}([1, 50, 10])$ for a specialized DMP. 54

5.2 On-line estimation of handover position and time with true values $g = 2\,\mathrm{m}$, $\tau = 10\,\mathrm{s}$ and initial parameter estimates $\hat{g}_0 = 1\,\mathrm{m}$, $\hat{\tau}_0 = 9\,\mathrm{s}$ using a classical EKF with $\boldsymbol{P}_0 = 100\boldsymbol{I}$ and a specialized DMP. 58

5.3 On-line estimation of handover position and time with true values $g = 2\,\mathrm{m}$, $\tau = 10\,\mathrm{s}$ and initial parameter estimates $\hat{g}_0 = 1\,\mathrm{m}$, $\hat{\tau}_0 = 9\,\mathrm{s}$ using a classical EKF with $\boldsymbol{P}_0 = 10^5\boldsymbol{I}$ and a specialized DMP. 59

5.4 On-line estimation of handover position $\hat{g}$ and handover time $\hat{\tau}$ with true values $g = 2\,\mathrm{m}$ and $\tau = 10\,\mathrm{s}$ and initial parameter values $\hat{g}_0 = 1\,\mathrm{m}$ and $\hat{\tau}_0 = 9\,\mathrm{s}$ using a modified EKF with $\boldsymbol{P}_0 = 100\boldsymbol{I}$, convergence parameter $\alpha_s = 0.5$ and a specialized DMP. 60

5.5 On-line estimation of handover position and time with true values $g = 2\,\mathrm{m}$, $\tau = 10\,\mathrm{s}$ and initial parameter values $\hat{g}_0 = 1\,\mathrm{m}$, $\hat{\tau}_0 = 9\,\mathrm{s}$ using a discrete-time nonlinear least-squares adaptive law without forgetting with $T_c = 0.5\,\mathrm{s}$ and $T_m = 0.01\,\mathrm{s}$ for a specialized DMP. . . . 64

5.6 On-line estimation of handover position and time with true values $g = 2\,\mathrm{m}$, $\tau = 10\,\mathrm{s}$ and initial parameter values $\hat{g}_0 = 1\,\mathrm{m}$, $\hat{\tau}_0 = 9\,\mathrm{s}$ using discrete-time nonlinear least-squares adaptive law with forgetting factor $\gamma = 0.8$, $T_c = 0.5\,\mathrm{s}$ and $T_m = 0.01\,\mathrm{s}$ for a specialized DMP. . . . 65

6.1 Fitting errors ϵ_{fit} and squared fitting errors ϵ^2_{fit} for original and specialized DMP for a minimum-jerk trajectory with starting point $y_0 = 0\,\mathrm{m}$, endpoint $g = 2\,\mathrm{m}$ and duration $\tau = 1\,\mathrm{s}$. 67

6.2 Estimation errors $\tilde{g}_{se}$, $\tilde{\tau}_{se}$ using EKF-based state estimation and $\tilde{g}_{pe}$, $\tilde{\tau}_{pe}$ using EKF-based parameter estimation with initial guesses $\hat{g}_0 = 1\,\mathrm{m}$, $\hat{\tau}_0 = 4\,\mathrm{s}$ for true values $g = 2\,\mathrm{m}$, $\tau = 5\,\mathrm{s}$. 69

6.3 Estimation errors $\tilde{g}_{ekf}$, $\tilde{\tau}_{ekf}$ using EKF-based state estimation and $\tilde{g}_{nlsq}$, $\tilde{\tau}_{nlsq}$ using discrete-time nonlinear least-squares-based parameter estimation with initial guesses $\hat{g}_0 = 1\,\mathrm{m}$, $\hat{\tau}_0 = 4\,\mathrm{s}$ for true values $g = 2\,\mathrm{m}$, $\tau = 5\,\mathrm{s}$ of a specialized DMP. 70

6.4 Captured trajectories of the human hand during a human-human handover. 71

6.5 Estimation errors $\tilde{g}_{se}$, $\tilde{\tau}_{se}$ using EKF-based state estimation and estimation errors $\tilde{g}_{pe}$, $\tilde{\tau}_{pe}$ using EKF-based parameter estimation with initial guesses $\hat{g}_0 = -1.5\,\mathrm{m}$, $\hat{\tau}_0 = 2\,\mathrm{s}$ for a captured human handover with true values $g = -0.8920\,\mathrm{m}$, $\tau = 1.5667\,\mathrm{s}$ which was also used as training data. 72

6.6 Estimation errors $\tilde{g}_{se}$, $\tilde{\tau}_{se}$ using EKF-based state estimation and $\tilde{g}_{pe}$, $\tilde{\tau}_{pe}$ using EKF-based parameter estimation with initial guesses $\hat{g}_0 = -1.5\,\mathrm{m}$, $\hat{\tau}_0 = 2\,\mathrm{s}$ for a captured human handover with true values $g = -0.9451\,\mathrm{m}$, $\tau = 1.5250\,\mathrm{s}$. 73

6.7 Estimation errors $\tilde{g}_{ekf}$, $\tilde{\tau}_{ekf}$ using EKF-based state estimation for a specialized DMP and estimation errors $\tilde{g}_{nlsq}$, $\tilde{\tau}_{nlsq}$ using EKF-based parameter estimation for a specialized DMP. Initial guesses are $\hat{g}_0 = -1.5\,\mathrm{m}$, $\hat{\tau}_0 = 2\,\mathrm{s}$ for the training trajectory with true values $g = -0.8920\,\mathrm{m}$, $\tau = 1.5667\,\mathrm{s}$. 74

6.8 Estimation errors $\tilde{g}_{ekf}$, $\tilde{\tau}_{ekf}$ using a state estimation EKF for a specialized DMP and estimation errors $\tilde{g}_{nlsq}$, $\tilde{\tau}_{nlsq}$ using a parameter estimation EKF for a specialized DMP with initial guesses $\hat{g}_0 = -1.5\,\mathrm{m}$, $\hat{\tau}_0 = 2\,\mathrm{s}$ for the training trajectory with true values $g = -0.9451\,\mathrm{m}$, $\tau = 1.5250\,\mathrm{s}$. 75

6.9 Obtained goal estimation errors $\tilde{g}$ for the captured basic handover trajectories. 76

6.10 Close-up of the obtained estimation errors $\tilde{g}$ for the captured basic handover trajectories. 77

6.11 Obtained estimation errors $\tilde{\tau}$ for the captured basic handover trajectories. 78

6.12 Captured extended trajectories of the human hand during a human-human handover. 79

6.13 Estimation errors $\tilde{g}$ and $\tilde{\tau}$ for the captured extended handover trajectories. 79

A.1 Lower bound $\underline{p}_m(t)$ and upper bound $\overline{p}_m(t)$ of $\boldsymbol{P}(t)$ using a modified EKF to estimate the states of an original DMP. II
A.2 Lower bound $\underline{p}_m(t)$ and upper bound $\overline{p}_m(t)$ of $\boldsymbol{P}(t)$ using a modified EKF to estimate the parameters of an original DMP. II
A.3 Lower bound $\underline{p}_m(t)$ and upper bound $\overline{p}_m(t)$ of $\boldsymbol{P}(t)$ using a filtered version of the modified EKF to estimate the parameters of an original DMP. III
A.4 Estimates $\hat{y}$ and $\hat{z}$ using a classical EKF with $\boldsymbol{P}_{0,s} = 100\boldsymbol{I}$ and a specialized DMP. III
A.5 Estimates $\hat{y}$ and $\hat{z}$ using a classical EKF with $\boldsymbol{P}_{0,s} = 10^5\boldsymbol{I}$ and a specialized DMP. IV
A.6 Lower bound $\underline{p}_c(t)$ and upper bound $\overline{p}_c(t)$ of $\boldsymbol{P}(t)$ using a classical EKF with $\boldsymbol{P}_0 = 100\boldsymbol{I}$ to estimate the states of a specialized DMP. . . IV
A.7 Lower bound $\underline{p}_c(t)$ and upper bound $\overline{p}_c(t)$ of $\boldsymbol{P}(t)$ using a classical EKF with $\boldsymbol{P}_0 = 10^5\boldsymbol{I}$ to estimate the states of a specialized DMP. . . V
A.8 Estimates $\hat{y}$ and $\hat{z}$ using a modified EKF with $\boldsymbol{P}_{0,s} = 100\boldsymbol{I}$, convergence parameter $\alpha_s = 0.5$ and a specialized DMP. V
A.9 Lower bound $\underline{p}_m(t)$ and upper bound $\overline{p}_m(t)$ of $\boldsymbol{P}(t)$ using a modified EKF to estimate the states of a specialized DMP. VI

List of Tables

2.1 Notation conventions 5

3.1 Parameters of the transformation system of the original DMP. 21

6.1 Parameters of the minimum-jerk trajectory used to generate measurements. 69
6.2 Parameters of the modified EKF used for state estimation. 71
6.3 Parameters of the modified EKF used for parameter estimation. . . . 71
6.4 Parameters of the modified EKF designed for a specialized DMP used for state estimation. 73
6.5 Parameters of the discrete adaptive law designed for a specialized DMP. 73
6.6 Parameters of the filtered EKF-based parameter estimator using a DMP for the prediction of real human-human handovers. 74

1

Introduction

1.1 Context

In recent years, robots have come to provide an essential contribution to productivity in industrial settings. Usually, humans and robots working in production are separated by cages, leading to almost no collaboration between the two. Recent advancements on robotic technologies, however, foresee a strong collaboration between humans and robots in the near future. Higher efficiency in both industrial and domestic tasks is expected for humans and robots that work together. According to the European Strategic Agenda for Robotics, such collaboration relies on natural interaction between human and robot. Consequently a human-like behavior of the robot is desired in order for the collaboration to be efficient.

One basic scenario of human-robot collaboration is that of a human handing over an object to a robot. More specifically, this entails a human hand holding an object while reaching towards a robot to hand over that object to the end effector of a robot. A handover can be divided into a reaching phase, during which the human hand carries an object towards the handover point, and the phase where control of the object is transferred from the human hand to the robotic hand. In human-human handovers, the agents can anticipate each other's actions to some extend. This allows the receiving agent to already move towards an anticipated handover place while the giving agent reaches for that point.

For a human-robot handover to be done as seamlessly as between humans, the robot has to predict where and when the handover will take place and reach that point with its end effector sufficiently fast to receive the object in a human fashion. In order to make such a prediction, it needs to have some form of prior knowledge on how humans move during a handover. An approach is to use a dynamic movement primitive as a representation of possible and likely human trajectories and learn it from demonstration. The parameters of this nonlinear dynamical system describing handover place and time can then be estimated on-line. The estimation of these parameters allows the design of an adaptive controller controlling the robot in a human-robot handover.

1.2 Related Work

There exists a considerable array of research work in fields related to human-robot collaboration. Human-robot handovers as complex collaborations have been investigated by Strabala *et al.* [1]. They identify two processes that constitute the coordination of two actors handing over an object to one another: A physical process of moving and a cognitive process of exchanging information. In [2], Huber *et al.* focus on the physical process of a robot-human handover by analyzing the importance of human-like motion. Interaction was found to be smoother when the robot was following minimum-jerk trajectories. Work from Flash and Hogan confirms that human point-to-point motions, being an essential part of handovers, exhibit high smoothness originating from their minimum-jerk properties [3]. While the above works focus on the motion involved in handovers, Kim *et al.* consider grasp planning of the robot for handover operations between human and robot [4]. Taking into account several constraints like object shapes, functions, safety and social constraints, they propose an algorithm coping with different handover scenarios ranging from one-handed to two-handed handovers. Edsinger and Kemp have conducted experiments with robots and humans handing objects to one another from a more high-level perspective [5]. They show that both the human's as well as the robot's skills complement each other advantageously. While the human solves potentially difficult grasping problems for the robot by directly placing objects into its end effector in a favorable configuration, the robot simplifies the transfer by reaching towards the human.

To control a robot during a handover scenario, human motion has to be considered in the control design. The minimum-jerk properties observed in several papers can be exploited to find a parameterization of human motion. Different approaches to parameterize trajectories exist. Khansari-Zadeh and Billard present a method to learn point-to-point motions from a set of demonstrations. They use a nonlinear autonomous dynamical system to describe a movement and provide sufficient conditions to ensure global asymptotic stability at the endpoint of the movement trajectory [6]. The parameters of the nonlinear system are learned via a so called Stable Estimator of Dynamical Systems (SEDS), thus allowing for the dynamical system to be used for programming a robot to perform point-to-point motion and to respond to perturbations immediately and appropriately.

While SEDS rely on multiple demonstrations to learn system parameters to parameterize motion, a different concept only relying on one demonstration is the dynamic movement primitive (DMP) introduced by Schaal *et al.* [7]. Using a combination of linear and nonlinear autonomous differential equations, this formulation of movement primitives creates smooth motion of a shape that resembles that of a demonstration motion. They also suggest using DMPs with added coupling terms to do flexible and reactive motion planning and execution, e.g. for robot end effectors. Thanks to the linear parameterization of DMPs and certain invariance properties, DMPs can be learned from one demonstration via supervised learning and can also be used for movement recognition. Ijspeert *et al.* use DMPs to model attractor behaviors of autonomous nonlinear dynamical systems, which makes DMPs a parameterization of trajectories [8, 9]. Instead of a time-dependent function, a trajectory is then described by a dynamical system. Hoffmann *et al.* investigate a biologically inspired modification of the original DMP framework, extending a DMP to let a robot avoid obstacles in a human way. They also render this modified DMP more versatile as compared to the original DMP by solving scaling issues of the original DMP. DMPs have also been applied by Prada *et al.* to control a robot to perform a human-robot handover by directly feeding a measurement of the human hand position into a DMP as the current goal [10, 11]. The DMP is used as a control law to define a trajectory to a previously unknown handover trajectory. While the simplicity of the DMP based control law allows for relatively easy realization of their algorithm, the resulting robot trajectories clearly differ from human trajectories due to the constantly changing current position of the human hand that is being used as a goal of the DMP.

A different approach is to estimate unknown high-level parameters of a parameterization of human motion on-line to predict where and when a human-robot handover will take place and control the robot based on this prediction. This leads to the common combination of a parameter estimator and a control law, depending on the estimated parameters, used in adaptive control. Extensive theory on adaptive control and on-line estimation of mostly constant or slowly time-varying parameters was presented by Ioannou and Sun [12], Slotine [13] as well as Sastry and Bodson [14]. A robust adaptive observer design method for a class of uncertain nonlinear systems with time-varying unknown parameters and non-vanishing disturbances was presented by Stepanyan and Hovakimyan [15]. They use radial basis function neural networks and an adaptive bounding technique to achieve asymptotic convergence of the state estimation error to zero. However, only boundedness of parameter errors and not convergence to true parameters is guaranteed. While most adaptive control-based on-line parameter estimation algorithms can only be applied to systems linear in the unknown parameters, Tyukin *et al.* design adaptive observers and parameter estimators for systems that are nonlinear in the parameters [16]. Through combining an asymptotically converging observer with an exhaustive search algorithm, a method which is at least as good as general exhaustive search is obtained.

While their exhaustive search-based approach allows for global convergence, the slow convergence speed prevents its use for on-line parameter estimation. In contrast, extended Kalman filters (EKFs) are often used as nonlinear on-line state or parameter estimators with fast local convergence [17, 18]. The stability of the EKF has been investigated in numerous publications. Bonnabel and Slotine analyze the contraction properties of the EKF as a nonlinear observer and prove exponential convergence of the state estimation error under some conditions concerning the detectability and nonlinearity of the plant [19]. Ni and Zhang prove stability of the Kalman filter for output error systems [20], which implies no need for artificially introduced process noise in the filter design. Another modification of the EKF allowed Reif *et al.* to improve the speed and the domain of convergence of the estimation error for nonlinear systems with the help of a term of instability added to the classical EKF [21].

The states and parameters of a nonlinear system can also be estimated using moving horizon estimation (MHE) [22]. The relation between the EKF and MHE as well as a comparison of their performances was presented by Haseltine and Rawlings in [23].

Using a discrete-time recursive nonlinear least-squares algorithm closely related to an MHE, and a time-variant representation of a minimum-jerk trajectory to estimate the motion of a human hand, Maeda *et al.* conducted research on how to predict human motion during human-robot handover tasks [24]. While good results are obtained, their method is restricted to minimum-jerk like movements of the human agent during a handover. On the contrary, DMPs, being a parameterization of motion learned from a demonstration trajectory, can represent almost any form of point-to-point motion.

1.3 Approach and Structure

In the present thesis, we formulate the prediction of place and time of a human-robot handover as an on-line parameter estimation problem. Using DMPs, a parameterization of human motion is obtained via off-line learning by demonstration with one human training trajectory. Based on this learned parameterization, adaptive estimation laws, allowing for on-line estimation of the parameters of a DMP, are designed. Through estimating the parameters of the DMP on-line, prediction of place and time of a human-handover is achieved. In contrast to previous work, this poses a very versatile approach to predict human motion. It is not restricted to minimum-jerk trajectories or handover tasks, since DMPs can be fitted to trajectories of many different kinds. Additionally, by providing the high-level parameters of place and time of a handover, it facilitates sophisticated path planning, such as planning human-like trajectories for the robot end effector.

To present the conducted research, the following structure is used: In Chapter 2 we briefly introduce the theoretical background relevant for this thesis. The prediction problem and the parameterization approaches are formulated in Chapter 3. Subsequently, parameter estimation based on the original DMP is described in Chapter 4. In addition to this, parameter estimation based on a new, specialized DMP exploiting prior knowledge on human motion is presented in Chapter 5. The obtained estimation laws are compared and evaluated experimentally in Chapter 6. Conclusions are drawn and suggestions for future work are given in Chapter 7.

2

Background

In this section, we briefly introduce the theoretical background relevant for the algorithms presented in this thesis.

2.1 Notation Conventions

A number of notation conventions are shown in Table 2.1. Additionally, time-dependencies are generally dropped throughout the thesis whenever this enhances readability.

Symbol	Description
$\mathcal{R}_{\geq 0}$	$\{x : x \in \mathcal{R} \wedge x \geq 0\}$
$\lVert\cdot\rVert_*$	Tensor norm induced by the Euclidean norm on vectors
$\lVert\boldsymbol{x}\rVert_W$	W-norm: $\lVert\boldsymbol{x}\rVert_W = \boldsymbol{x}^\top \boldsymbol{W} \boldsymbol{x}$ with $\boldsymbol{x}$ a column vector
$\mathrm{diag}(\boldsymbol{A})$	If $\boldsymbol{A} \in \mathcal{R}^{n\times n}$ then $\mathrm{diag}(\boldsymbol{A}) \in \mathcal{R}^n$ is the vector of diagonal entries of $\boldsymbol{A}$. If $\boldsymbol{A} \in \mathcal{R}^n$, then $\mathrm{diag}(\boldsymbol{A}) \in \mathcal{R}^{n\times n}$ is a diagonal matrix with the elements of $\boldsymbol{A}$ as diagonal entries.
$\mathcal{L}_2$	The space of functions $\boldsymbol{u}$ for which $\lVert\boldsymbol{u}\rVert_{\mathcal{L}_2} = \sqrt{\int_0^\infty \boldsymbol{u}^\top(t)\boldsymbol{u}(t)dt} < \infty$
$\mathcal{L}_\infty$	The space of functions $\boldsymbol{u}$ for which $\lVert\boldsymbol{u}\rVert_{\mathcal{L}_\infty} = \sup\limits_{t\geq 0}\lVert\boldsymbol{u}(t)\rVert < \infty$
ℓ_2	The space of sequences $\boldsymbol{v}$ for which $\lVert\boldsymbol{v}\rVert_{\ell_2} = \sqrt{\sum_n \lVert\boldsymbol{v}_n\rVert^2} < \infty$
ℓ_∞	The space of sequences $\boldsymbol{v}$ for which $\lVert\boldsymbol{v}\rVert_{\ell_\infty} = \sup\limits_{n}\lVert\boldsymbol{v}_n\rVert < \infty$

Table 2.1: Notation conventions

2.2 Dynamic Movement Primitives

The concept of DMPs can be used to parameterize possible and likely trajectories of the human hand during a handover process [9, 7]. A DMP is a nonlinear dynamical system that can represent the attractor dynamics of an observed behavior. The essential idea is to transform a well-understood attractor system into an attractor system that exhibits a desired behavior by using a nonlinear forcing term that can be learned. With a DMP learned from a demonstrated trajectory, similar trajectories to the demonstrated one can then be generated.

2.2.1 Attractor System

Handover tasks mainly involve point-to-point trajectories, in literature also referred to as *discrete trajectories* [9]. Such trajectories can be produced by a dynamical system with a point attractor.

To begin with, a simple and well-understood attractor system with desirable stability properties is chosen as a so called *transformation system.* Following [9], one of the simplest systems having these properties is a linear spring-damper model. With an added forcing term f, this system is described by

$$\tau^2 \ddot{y} = G(g, y, \dot{y}) + f = \alpha_z(\beta_z(g - y) - \tau\dot{y}) + f. \tag{2.1}$$

In first-order notation, we have

$$\tau\dot{y} = z, \tag{2.2a}$$

$$\tau\dot{z} = \alpha_z(\beta_z(g - y) - z) + f, \tag{2.2b}$$

where τ is a positive time constant and α_z, β_z are positive constants of the transformation system. In the course of this thesis, DMPs are used to represent motion of a human hand. The human hand can be modeled as a point mass whose dynamics are usually described by a second-order dynamical system. Hence, a second order system is a reasonable choice to represent the attractor dynamics of human hand motion. To obtain exponential, non-oscillatory convergence towards a unique attractor point, the transformation system (2.1) can be rendered critically damped by choosing $\beta_z = \alpha_z/4$. For a vanishing forcing term $f = 0$, the system then has a globally asymptotically stable equilibrium at $(y, z) = (g, 0)$, which means, it has a unique point attractor at $(g, 0)$. Through the forcing term f, the transformation system (2.2) is enriched to exhibit a desired behavior. To achieve this enrichment, Ijspeert *et al.* introduce a so called *canonical system*

$$\tau\dot{x} = -\alpha_x x, \tag{2.3}$$

where α_x is a positive constant [9]. For some arbitrary initial state x_0, the state x converges monotonically to $x = 0$. Hence, x can be viewed as a phase variable that modulates the temporal evolution of a dynamical system without rendering it non-autonomous. This allows to simply guarantee some useful invariance properties of the DMP presented later on. Using x, a nonlinear forcing term $f(x)$ dependent on x can be formulated as

$$f(x) = \tilde{f}(x)(g - y_0), \tag{2.4}$$

with

$$\tilde{f}(x) = \frac{\sum_{i=1}^{N} \Psi_i(x) w_i}{\sum_{i=1}^{N} \Psi_i(x)} x, \tag{2.5}$$

where each of the N exponential basis functions Ψ_i is weighted with a w_i and the initial state is denoted by $y_0 = y(t = 0)$. The basis functions can be chosen as follows:

$$\Psi_i(x) = \exp\left(-h_i(x - c_i)^2\right), \tag{2.6}$$

with $h_i > 0$ and c_i being constants determining their widths and centers. The dynamical system described by the equations (2.2) and (2.3) forms a DMP for one degree of freedom (DOF).

2.2.2 Multiple DOF

To capture a multi-dimensional behavior with DMPs, Ijspeert *et al.* propose sharing one canonical system describing the evolution of a common phase variable x among all DOF [9], while using separate transformation systems for every DOF. As depicted in Figure 2.1, each DOF is assigned a transformation system of the form

$$\tau^2 \ddot{y}_i = G_i(g_i, y_i, \dot{y}_i) + f_i(x), \text{ with } i \in \{1, 2, .., N\},$$

where y_i and its derivative $\dot{y}_i$ constitute the state variable of the i-th DOF while G_i and the forcing term f_i compose the dynamics of the i-th transformation system. This is relevant when capturing human trajectories of reaching motion of the hand since up to three translational degrees of freedom can be considered when representing the position of a human hand during handover processes. The trajectories generated for the different DOFs of the human hand are temporally coupled, hence, one shared canonical system describing the temporal evolution of all the subsystems for each DOF as depicted in Figure 2.1, are a natural choice.

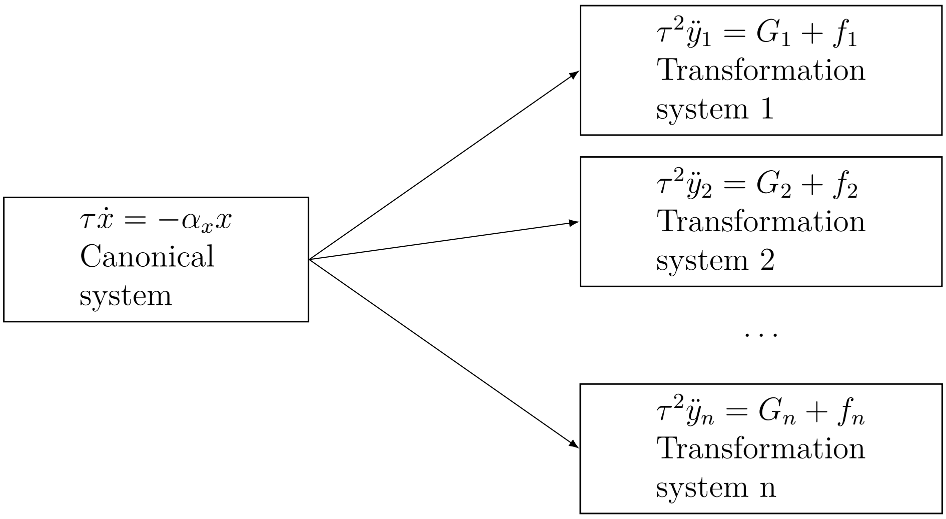
$\tau\dot{x} = -\alpha_x x$
Canonical system
$\tau^2\ddot{y}_1 = G_1 + f_1$
Transformation system 1
$\tau^2\ddot{y}_2 = G_2 + f_2$
Transformation system 2
...
$\tau^2\ddot{y}_n = G_n + f_n$
Transformation system n

Figure 2.1: Structure of the DMP representation of an n-DOF system with shared canonical system.

2.2.3 Stability and Invariance

The transformation systems are asymptotically stable by design. Therefore, bounded-input, bounded-output (BIBO) stability [25], of a 1-DOF DMP can easily be established by considering an input comprising the forcing term f from (2.4) and the goal g. For any finite goal g, bounded basis functions Ψ_i and bounded weights w_i in (2.6), BIBO stability of (2.1) can be proven. Consequently, the dynamical system (2.2), (2.3) is $\mathcal{L}_\infty$ stable [25]. Stability of the system of differential equations composing the DMP can also be shown using contraction theory [26]. According to it, any parallel or serial arrangement of contraction stable systems is contraction stable, which can be applied to DMPs. Following the same reasoning, contraction stability of the n-DOF DMP representation can be shown.

In addition to convenient stability properties, DMPs exhibit invariance properties. Ijspeert *et al.* show in [9] that DMPs are topologically equivalent. Hence, if the weights w_i are kept constant, both the timescale parameter τ and the goal parameter g can be changed without altering the attractor landscape of the DMP qualitatively. This qualifies DMPs as a model of a family of similar behaviors and thus poses a way to parameterize human motion. The invariance properties are illustrated in Figure 2.2, where a DMP was fitted to a minimum-jerk trajectory. Clearly, the qualitative behavior of the DMP does not change both for different timescales τ, shown in Figure 2.2b, and for different goals g, depicted in Figure 2.2a.

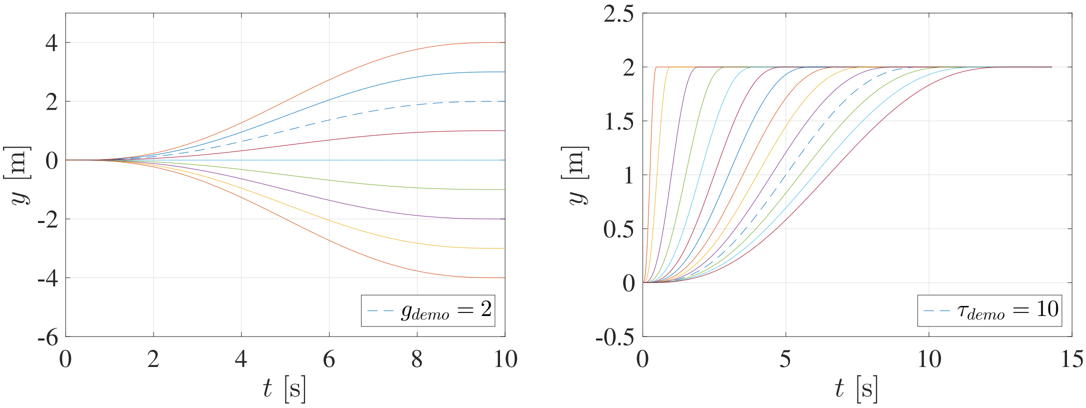

(a) Variation of g

(b) Variation of τ

Figure 2.2: Trajectories produced with a DMP fitted to a minimum-jerk trajectory for different parameter values of timescale τ and goal g.

2.2.4 Off-line Learning of Attractor Dynamics

To obtain a DMP that exhibits a demonstrated behavior given in terms of P data triples $(y_{demo,k}, \dot{y}_{demo,k}, \ddot{y}_{demo,k})$ obtained at times t_k, with $k \in [1, ..., P]$, its free parameters are calculated in two steps. First, the high-level parameters τ, y_0 and g are extracted. Second, the weights w_i of the basis functions (2.6) in the forcing term (2.4) are learned.

The parameter τ is set to the duration of the demonstrated movement, the initial value y_0 is set as $y_0 = y_{demo,1}$ and the goal is set to $g = y_{demo,P}$. With the high-level parameters set, the weights w_i of the forcing term (2.4) can be determined using a supervised learning method. A function approximation problem can be formulated by rearranging (2.1) to

$$\tau^2\ddot{y} + \tau\alpha_z\dot{y} - \alpha_z\beta_z(g - y) = f. \tag{2.7}$$

For a demonstrated behavior, (2.7) yields

$$f_{target,k} = \tau^2 \ddot{y}_{demo,k} + \tau \alpha_z \dot{y}_{demo,k} - \alpha_z \beta_z (g - y_{demo,k}), \tag{2.8}$$

which gives a target function value for each $k \in [1, ..., P]$. By introducing the vector of target function values

$$\boldsymbol{f}_{target} = \begin{bmatrix} f_{target,1} & f_{target,2} & \dots & f_{target,P} \end{bmatrix}^\top, \tag{2.9}$$

and the vector of weights

$$\boldsymbol{w} = \begin{bmatrix} w_1 & w_2 & \dots & w_N \end{bmatrix}^\top,$$

a linear regression problem, fitting the forcing term (2.4) to the target function f_{target} from (2.8) in a least-squares sense, can be formulated as in [27]. The function approximation problem with the parameterization of the forcing term (2.4) can be formulated in matrix form as

$$\boldsymbol{X}\boldsymbol{w} = \boldsymbol{f},$$

with

$$\boldsymbol{X} = \begin{bmatrix} \frac{\Psi_1(x_1)}{\sum_{i=1}^N \Psi_i(x_1)} x_1 & \dots & \frac{\Psi_N(x_1)}{\sum_{i=1}^N \Psi_i(x_1)} x_1 \\ \vdots & & \vdots \\ \frac{\Psi_1(x_P)}{\sum_{i=1}^N \Psi_i(x_P)} x_P & \dots & \frac{\Psi_N(x_P)}{\sum_{i=1}^N \Psi_i(x_P)} x_P \end{bmatrix} (g - y_0), \tag{2.10}$$

and the basis functions from (2.6). The values x_1, x_2, ..., x_P of the phase variable can be obtained using the solution of the canonical system (2.3),

$$x(t) = \exp\left(-\frac{\alpha_x}{\tau} t\right).$$

The initial condition can be chosen as $x_1 = 1$ for the phase variable x to evolve from $x(t_1) = x_1 = 1$ to $x(t_P) = 0$. Thus, we obtain $x_k = \exp(-\frac{\alpha_x}{\tau} t_k)$. The solution minimizing the cost function

$$\begin{aligned} J(\boldsymbol{w}) &= (\boldsymbol{f}_{target} - \boldsymbol{f})^\top (\boldsymbol{f}_{target} - \boldsymbol{f}) \\ &= (\boldsymbol{f}_{target} - \boldsymbol{X}\boldsymbol{w})^\top (\boldsymbol{f}_{target} - \boldsymbol{X}\boldsymbol{w}) \end{aligned}$$

is then given by

$$\boldsymbol{w} = (\boldsymbol{X}^\top \boldsymbol{X})^{-1} \boldsymbol{X}^\top \boldsymbol{f}. \tag{2.11}$$

Consequently, one single demonstration is enough to learn a DMP representation of the demonstrated behavior. Multiple demonstrations of a trajectory can easily be included in the least-squares approach by averaging over the f_{target} information obtained from the different data sets as suggested by Ijspeert *et al.* [8]. These demonstrations can even be of different spatial and temporal scales thanks to the invariance properties of the DMP. Note, that for goals g close to y_0, large weights w_i can result from the above described learning method. This issue has been addressed by Hoffmann *et al.* and can be eliminated by using an alternative DMP formulation [28].

2.2.5 Alternative Formulations

In literature, alternative DMP formulations exist. In [9] the formulation

$$\begin{aligned}\tau\ddot{y} &= \alpha_z(\beta_z(g-y)-\dot{y})+f(x),\\ \tau\dot{x} &= -\alpha_x x,\end{aligned}$$

is used to describe a DMP. It slightly differs from (2.7) and does not exhibit the above mentioned invariance properties.

Another formulation with better properties for goals g that are close to the initial state y_0 of the DMP has been proposed by Hoffmann *et al.* [28]. They introduce a bio-inspired model based on evidence obtained from studies on frogs. It reads

$$\begin{aligned}\tau\dot{z} &= xK\left(\frac{\tilde{f}(x)}{x}+y_0-y\right)+(1-x)K(g-y)-Dz,\\ \tau\dot{y} &= z,\\ \tau\dot{x} &= -\alpha_x x\end{aligned}$$

with the nonlinearity $\tilde{f}$ given by (2.5), spring constant $K > 0$ and damping constant $D > 0$.

Following a decoupling approach, Prada and Remazeilles introduce functions $f_w(x)$ and $w_g(x)$ to weight different terms of the transformation system (2.12), (2.13) independently, thus allowing for tuning of the transition between shape and goal attractor dynamics [10]. The resulting DMP is described by

$$\begin{aligned}\tau\dot{z} &= (1-w_g(x))(f_w(x)+y_0-y)+w_g(x)K(g-y)-Dz, && (2.12)\\ \tau\dot{y} &= z, && (2.13)\\ \tau\dot{x} &= -\alpha_x x,\end{aligned}$$

and is intended to be used with a time-varying goal g.

2.3 On-line Parameter Estimation

To estimate the trajectory of a human hand during a handover process, the parameters of an obtained parameterization of human motion have to be estimated on-line.

Following [12], a linear parametric representation of a plant can be given by

$$z = W(s)\boldsymbol{\theta}^\top\boldsymbol{\psi}, \tag{2.14}$$

where z is the scalar filtered output of the plant, $W(s)$ is a proper transfer function with stable poles, $\boldsymbol{\theta} \in \mathcal{R}^n$ is the vector of true parameters of the plant and $\boldsymbol{\psi} \in \mathcal{R}^n$ is the unfiltered information vector, containing known input and output signals of the plant. Taking into account that $\boldsymbol{\theta}$ is constant, the linear parametric model (2.14) can be written in the simple form

$$z = \boldsymbol{\theta}^\top\boldsymbol{\phi}, \tag{2.15}$$

where $\boldsymbol{\phi} = W(s)\boldsymbol{\psi}$ is the filtered information vector. According to [13], it is a common approach to substitute unmeasured derivatives in the unfiltered information vector $\boldsymbol{\psi}$ via a filtering operation. For an estimate $\hat{\boldsymbol{\theta}}(t)$ of the true parameter vector $\boldsymbol{\theta}$ at time t, an estimated filtered output $\hat{z}$ is obtained by using (2.15) to obtain

$$\hat{z} = \hat{\boldsymbol{\theta}}^\top \boldsymbol{\phi}. \tag{2.16}$$

The output error ϵ can be formulated as

$$\epsilon = \frac{z - \hat{z}}{m^2}, \tag{2.17}$$

where $m^2 = n_s^2 + 1$ is used to ensure

$$\frac{\boldsymbol{\phi}}{m} \in \mathcal{L}_\infty$$

by choosing $n_s^2 = \alpha \boldsymbol{\phi}^\top \boldsymbol{\phi}$ with $\alpha > 0$ [12]. Through introducing the parameter error $\tilde{\boldsymbol{\theta}} = \hat{\boldsymbol{\theta}} - \boldsymbol{\theta}$ and substituting z and $\hat{z}$ in (2.17) with (2.15) and (2.16),

$$\epsilon = -\frac{\tilde{\boldsymbol{\theta}}^\top \boldsymbol{\phi}}{m^2} \tag{2.18}$$

is obtained. Equation (2.18) relates the output error ϵ to the parameter error $\tilde{\boldsymbol{\theta}}$ and qualifies the signal

$$\epsilon m = -\tilde{\boldsymbol{\theta}}^\top \frac{\boldsymbol{\phi}}{m}$$

as a measure of the parameter error $\tilde{\boldsymbol{\theta}}$ [12]. For any piecewise continuous signal vector $\boldsymbol{\phi}$, ϵm has a high value if $\tilde{\boldsymbol{\theta}}$ is high. This property allows for different adaptive laws designed using the gradient algorithm from [12] to minimize cost functions of ϵ with respect to $\hat{\boldsymbol{\theta}}$.

2.3.1 Integral Adaptive Law

The integral adaptive law uses a cost function of the form

$$J(\hat{\boldsymbol{\theta}}) = \frac{1}{2} \int_0^t e^{-\beta(t-\tau)} \epsilon^2(t,\tau) m^2(\tau) d\tau, \tag{2.19}$$

with the normalized estimation error

$$\epsilon(t,\tau) = \frac{z(\tau) - \hat{\boldsymbol{\theta}}^\top(t)\boldsymbol{\phi}(\tau)}{m^2(\tau)}, \; \epsilon(t,t) = \epsilon$$

at time τ based on the parameter estimate $\hat{\boldsymbol{\theta}}(t)$ of $\boldsymbol{\theta}$ at time $t \geq \tau$. The cost function (2.19) penalizes the integral square of the estimation error over all past data. The forgetting factor $\beta > 0$ is used to discount past estimation error squares exponentially. As deduced in [12], $J(\hat{\boldsymbol{\theta}})$ is convex, hence, the gradient method can be applied to minimize $J(\hat{\boldsymbol{\theta}})$ with respect to $\hat{\boldsymbol{\theta}}$. The adaptive law

$$\dot{\hat{\boldsymbol{\theta}}} = -\boldsymbol{\Gamma}\nabla\boldsymbol{J} = \Gamma\int_0^t e^{-\beta(t-\tau)}\frac{z(\tau)-\hat{\boldsymbol{\theta}}^\top(t)\boldsymbol{\phi}(\tau)}{m^2(\tau)}\boldsymbol{\phi}(\tau)d\tau \tag{2.20}$$

with the scaling matrix $\boldsymbol{\Gamma} = \boldsymbol{\Gamma}^\top > 0$ is obtained. It is implemented as

$$\dot{\hat{\boldsymbol{\theta}}} = -\boldsymbol{\Gamma}(\boldsymbol{R}(t)\hat{\boldsymbol{\theta}} + \boldsymbol{Q}(t)), \tag{2.21a}$$

$$\dot{\boldsymbol{R}} = -\beta\boldsymbol{R} + \frac{\boldsymbol{\phi}\boldsymbol{\phi}^\top}{m^2},\ \boldsymbol{R}(0) = \boldsymbol{0}, \tag{2.21b}$$

$$\dot{\boldsymbol{Q}} = -\beta\boldsymbol{Q} - \frac{z\boldsymbol{\phi}}{m^2},\ \boldsymbol{Q}(0) = \boldsymbol{0}, \tag{2.21c}$$

where $\boldsymbol{R} \in \mathcal{R}^{n\times n}$ and $\boldsymbol{Q} \in \mathcal{R}^n$. Both (2.20) and (2.21) are called the *integral adaptive law* [12].

As shown in [12], the integral adaptive law guarantees that

(i) $\epsilon, \epsilon n_s, \hat{\boldsymbol{\theta}}, \dot{\hat{\boldsymbol{\theta}}} \in \mathcal{L}_\infty$
(ii) $\epsilon, \epsilon n_s, \dot{\hat{\boldsymbol{\theta}}} \in \mathcal{L}_2$
(iii) $\lim_{t\to\infty} \|\dot{\hat{\boldsymbol{\theta}}}(t)\| = \boldsymbol{0}$
(iv) if $n_s, \boldsymbol{\phi} \in \mathcal{L}_\infty$ and $\boldsymbol{\phi}$ is persistently excited (PE), then $\hat{\boldsymbol{\theta}}(t)$ converges to $\boldsymbol{\theta}$ exponentially. Additionally, the rate of convergence can be made arbitrarily large by increasing γ for $\boldsymbol{\Gamma} = \gamma\mathbf{I}$.

2.3.2 Least-Squares Adaptive Law

The cost function

$$J(\hat{\boldsymbol{\theta}}) = \frac{1}{2}\int_0^t e^{-\beta(t-\tau)}\frac{[z(\tau)-\hat{\boldsymbol{\theta}}^\top(t)\boldsymbol{\phi}(\tau)]^2}{m^2(\tau)}d\tau + \frac{1}{2}e^{-\beta t}(\hat{\boldsymbol{\theta}}-\hat{\boldsymbol{\theta}}_0)^\top\boldsymbol{Q}_0(\hat{\boldsymbol{\theta}}-\hat{\boldsymbol{\theta}}_0) \tag{2.22}$$

where $\boldsymbol{Q}_0 = \boldsymbol{Q}_0^\top > 0$, $\beta \geq 0$, $\hat{\boldsymbol{\theta}}_0 = \hat{\boldsymbol{\theta}}(0)$, is an extension of the integral cost function (2.19) by a penalty on the initial parameter error $\hat{\boldsymbol{\theta}} - \hat{\boldsymbol{\theta}}_0$ as given in [12, 13]. It can be shown that the so-called *continuous-time recursive least-squares algorithm with forgetting factor*, minimizing $J(\hat{\boldsymbol{\theta}})$ from (2.22), is given by the differential equations

$$\dot{\hat{\boldsymbol{\theta}}} = \boldsymbol{P}\epsilon\boldsymbol{\phi}, \tag{2.23a}$$

$$\dot{\boldsymbol{P}} = \beta\boldsymbol{P} - \boldsymbol{P}\frac{\boldsymbol{\phi}\boldsymbol{\phi}^\top}{m^2}\boldsymbol{P},\ \boldsymbol{P}(0) = \boldsymbol{P}_0 = \boldsymbol{Q}_0^{-1}. \tag{2.23b}$$

Given that $n_s, \boldsymbol{\phi} \in \mathcal{L}_\infty$ and $\boldsymbol{\phi}$ is PE, the recursive least-squares algorithm (2.23) with forgetting factor $\beta > 0$ guarantees

(i) $\boldsymbol{P}, \boldsymbol{P}^{-1} \in \mathcal{L}_\infty$
(ii) exponential convergence of $\hat{\boldsymbol{\theta}}(t)$ to $\boldsymbol{\theta}$

for an output error ϵ from (2.17) [12]. If $\beta = 0$ is chosen, (2.23) becomes the pure least-squares adaptive law [12]. If $n_s, \boldsymbol{\phi} \in \mathcal{L}_\infty$ and $\boldsymbol{\phi}$ is PE, the pure least-squares adaptive law guarantees asymptotic convergence of $\hat{\boldsymbol{\theta}}(t)$ to $\boldsymbol{\theta}$.

2.3.3 Persistence of Excitation and Parameter Identification

The notion of persistence of excitation plays a key role in the convergence of the parameter vector $\hat{\boldsymbol{\theta}}$ to its true value $\boldsymbol{\theta}$. In [12] a piecewise continuous signal vector $\boldsymbol{\phi} : \mathcal{R}_{\geq 0} \mapsto \mathcal{R}^n$ is defined to be persistently excited in $\mathcal{R}^n$ with excitation level $\alpha_0 > 0$ if there exist constants α_1, $T_0 > 0$, such that

$$\alpha_1 \mathbf{I} \geq \frac{1}{T_0} \int_t^{t+T_0} \boldsymbol{\phi}(\tau)\boldsymbol{\phi}(\tau)^\top d\tau \geq \alpha_0 \mathbf{I}, \qquad \forall t \geq 0. \tag{2.24}$$

In other words, (2.24) requires the signal vector $\boldsymbol{\phi}(t)$ to vary in such a way that the integral of the matrix $\boldsymbol{\phi}(\tau)\boldsymbol{\phi}(\tau)^\top$ is uniformly positive definite over any time interval $[t, t + T_0]$.

If the estimates of a parameter vector $\boldsymbol{\theta}$ converge to the true parameter values, identification of the parameters is performed. True parameters can only be identified using one of the above adaptive laws (2.21) and (2.23) if boundedness of n_s and $\boldsymbol{\phi}$ is ensured and the PE property (2.24) is satisfied for $\boldsymbol{\phi}$.

2.3.4 Hybrid Adaptive Law

In addition to the adaptive laws presented above, Ioannou and Sun introduce hybrid adaptive laws to perform on-line parameter estimation [12]. Instead of computing a new parameter estimate $\hat{\boldsymbol{\theta}}(t)$ for every time instance t, a hybrid adaptive law can improve robustness and reduce computational cost by only updating the parameter estimate at specific instances of time t_k. Setting $t_k = kT_s$ with sampling time T_s and $\hat{\boldsymbol{\theta}}_k = \hat{\boldsymbol{\theta}}(t_k)$, we have the update law

$$\hat{\boldsymbol{\theta}}_{k+1} = \hat{\boldsymbol{\theta}}_k + \Gamma \int_{t_k}^{t_{k+1}} \epsilon(\tau)\boldsymbol{\phi}(\tau) d\tau, \tag{2.25}$$

with $\hat{\boldsymbol{\theta}}(0) = \boldsymbol{\theta}_0$, $k = 0, 1, 2, \ldots$ and the output error

$$\epsilon(t) = \frac{z(t) - \hat{z}(t)}{m^2(t)} = \frac{z(t) - \hat{\boldsymbol{\theta}}_k^\top \boldsymbol{\phi}(t)}{m^2(t)} \qquad \forall t \in [t_k, t_{k+1}]. \tag{2.26}$$

The following stability properties of the hybrid adaptive law consisting of (2.25) and (2.26) can be established [12]. Assume $m, T_s, \boldsymbol{\Gamma}$ can be chosen such that

(a) $\frac{\boldsymbol{\phi}^\top \boldsymbol{\phi}}{m^2} \leq 1, \ m \geq 1$
(b) $2 - T_s \lambda_m \geq \gamma$ for some $\gamma > 0$

and $\lambda_m = \lambda_{max}(\boldsymbol{\Gamma})$. Then the hybrid adaptive law guarantees:

(i) $\hat{\boldsymbol{\theta}}_k \in l_\infty$
(ii) $\Delta\hat{\boldsymbol{\theta}}_k = \hat{\boldsymbol{\theta}}_{k+1} - \hat{\boldsymbol{\theta}}_k \in l_2 \ \epsilon m \in \mathcal{L}_\infty \bigcap \mathcal{L}_2$
(iii) If $m, \boldsymbol{\phi} \in \mathcal{L}_\infty$ and $\boldsymbol{\phi}$ is PE, then $\hat{\boldsymbol{\theta}}_k \to \boldsymbol{\theta}$ as $k \to \infty$ exponentially fast.

2.4 The Continuous Extended Kalman filter

While on-line parameter estimators only estimate the unknown parameters of a plant, observers estimate the whole state of a plant. Unknown parameters can be viewed as part of this state. Consequently, estimation of unknown parameters of a plant can be treated as a state estimation problem. For nonlinear plants, nonlinear observers are often required to solve the state estimation problem.

The extended Kalman filter (EKF) is a commonly used nonlinear observer, which belongs to the class of empirical observers [17]. Empirical observers are based on approximations of nonlinearities and therefore often require sufficiently good initial estimates to converge. The EKF estimates the states of a nonlinear system by linearization and is therefore only a locally converging observer. Originating from the Kalman filter, which is a globally converging linear optimal observer with respect to a quadratic cost function, the EKF is almost optimal. In the following we first introduce the classical EKF and then present a modified version of it.

2.4.1 Classical Extended Kalman Filter

Definition

Consider a nonlinear system represented by

$$\dot{\boldsymbol{x}} = \boldsymbol{f}(\boldsymbol{x}, t), \tag{2.27}$$

$$\boldsymbol{y} = \boldsymbol{h}(\boldsymbol{x}, t), \tag{2.28}$$

where $\boldsymbol{x} \in \mathcal{R}^n$ is the state vector, $t \geq t_0 \in \mathcal{R}_{\geq 0}$ the time and $\boldsymbol{y} \in \mathcal{R}^p$ the measured output. We assume that both the nonlinear functions $\boldsymbol{f}$ and $\boldsymbol{h}$ are $\mathcal{C}^1$-functions. As presented in [17, 19], an observer for the nonlinear system (2.27), (2.28) is given by

$$\dot{\hat{\boldsymbol{x}}} = \boldsymbol{f}(\hat{\boldsymbol{x}}, t) + \boldsymbol{K}(t)(\boldsymbol{y} - \boldsymbol{h}(\hat{\boldsymbol{x}}, t)), \tag{2.29}$$

with $\hat{\boldsymbol{x}} \in \mathcal{R}^n$ being the estimated state with initial estimate $\hat{\boldsymbol{x}}(0) = \hat{\boldsymbol{x}}_0$ and $\boldsymbol{K}(t) \in \mathcal{R}^{n\times p}$ being the time-variant observer gain. In the classical setup of the EKF [17, 19], the observer gain $\boldsymbol{K}(t)$ is calculated through

$$\boldsymbol{K}(t) = \boldsymbol{P}(t)\boldsymbol{C}(\hat{\boldsymbol{x}}, t)^\top \boldsymbol{R}^{-1}, \tag{2.30}$$

where $\boldsymbol{P}(t) \in \mathcal{R}^{n\times n}$ is obtained by solving the Riccati differential equation

$$\begin{aligned}\dot{\boldsymbol{P}}(t) =& \boldsymbol{A}(\hat{\boldsymbol{x}}, t)\boldsymbol{P}(t) + \boldsymbol{P}(t)\boldsymbol{A}(\hat{\boldsymbol{x}}, t)^\top + \boldsymbol{Q} \\ &- \boldsymbol{P}(t)\boldsymbol{C}(\hat{\boldsymbol{x}}, t)^\top \boldsymbol{R}^{-1}\boldsymbol{C}(\hat{\boldsymbol{x}}, t)\boldsymbol{P}(t),\end{aligned} \tag{2.31}$$

with initial condition $\boldsymbol{P}(0) = \boldsymbol{P}_0$. The equations

$$\boldsymbol{A}(\hat{\boldsymbol{x}}, t) = \left.\frac{\partial \boldsymbol{f}}{\partial \boldsymbol{x}}(\boldsymbol{x}, t)\right|_{\boldsymbol{x}=\hat{\boldsymbol{x}}} \tag{2.32}$$

and

$$\boldsymbol{C}(\hat{\boldsymbol{x}}, t) = \left.\frac{\partial \boldsymbol{h}}{\partial \boldsymbol{x}}(\boldsymbol{x}, t)\right|_{\boldsymbol{x}=\hat{\boldsymbol{x}}}, \tag{2.33}$$

form the linearization of (2.27), (2.28) around the current state estimate $\hat{\boldsymbol{x}}$. While from a stochastic point of view, the positive definite matrices $\boldsymbol{Q}$ and $\boldsymbol{R}$ represent the covariances of process noise and measurement noise respectively, Bonnabel and Slotine suggest they can be seen as design parameters in the deterministic and nonlinear setting that we have introduced above [19]. Confidence in the model (2.27) can be set by $\boldsymbol{Q}^{-1}$, whereas $\boldsymbol{R}^{-1}$ can be interpreted as the confidence in the measurements from (2.28).

Stability

In order for the state estimate $\hat{\boldsymbol{x}}$ provided by the EKF to converge to the true state $\boldsymbol{x}$ for sufficiently good initial estimates $\hat{\boldsymbol{x}}_0$, as presented in [19], two main assumptions have to hold in the classical setup.

Assumption 1. *There exist* $\underline{p}_c, \overline{p}_c > 0$ *such that*

$$\underline{p}_c \mathbf{I} \leq \boldsymbol{P}(t) \leq \overline{p}_c \mathbf{I},\ \forall t \in \mathcal{R}_{\geq 0}. \tag{2.34}$$

This is verified when the linearized system

$$\begin{aligned} \dot{\boldsymbol{\xi}}_c &= \boldsymbol{A}(\hat{\boldsymbol{x}}, t)\boldsymbol{\xi}_c \\ \boldsymbol{\eta} &= \boldsymbol{C}(\hat{\boldsymbol{x}}, t)\boldsymbol{\xi}_c \end{aligned}$$

is uniformly detectable.

Assumption 2. *The matrices,* $\partial \boldsymbol{f}/\partial \boldsymbol{x}$ *and* $\partial \boldsymbol{h}/\partial \boldsymbol{x}$ *satisfy Lipschitz properties, i.e., positive numbers* κ_z, κ_A *and* κ_C *exist, such that for all* $\boldsymbol{x}$ *satisfying* $\|\hat{\boldsymbol{x}} - \boldsymbol{x}\| \leq \kappa_z$ *and all* $t \geq 0$ *the following inequalities hold:*

$$\left\| \frac{\partial^2 \boldsymbol{f}}{\partial^2 \boldsymbol{x}}(\boldsymbol{x}, t) \right\|_* \leq \kappa_A, \tag{2.35}$$

$$\left\| \frac{\partial^2 \boldsymbol{h}}{\partial^2 \boldsymbol{x}}(\boldsymbol{x}, t) \right\|_* \leq \kappa_C. \tag{2.36}$$

2.4.2 Modified Extended Kalman Filter with prescribed Degree of Stability

In [21] a modified version of the EKF, having a prescribed degree of stability, is investigated.

Definition

The methodology of the modified extended Kalman filter from [21] can be based on the general nonlinear system

$$\dot{\boldsymbol{x}} = \boldsymbol{f}(\boldsymbol{x}, t), \tag{2.37}$$

$$\boldsymbol{y} = \boldsymbol{h}(\boldsymbol{x}, t), \tag{2.38}$$

where, as before, $\boldsymbol{x} \in \mathcal{R}^n$ is the state vector, $t \geq t_0 \in \mathcal{R}_{\geq 0}$ the time and $\boldsymbol{y} \in \mathcal{R}^p$ the measured output.

We assume that both the nonlinear functions $\boldsymbol{f}$ and $\boldsymbol{h}$ are $\mathcal{C}^1$-functions. As presented in [21], an observer for the nonlinear system (2.37), (2.38) is given by

$$\dot{\hat{\boldsymbol{x}}} = \boldsymbol{f}(\hat{\boldsymbol{x}}, t) + \boldsymbol{K}(t)(\boldsymbol{y} - \boldsymbol{h}(\hat{\boldsymbol{x}}, t)), \tag{2.39}$$

with $\hat{\boldsymbol{x}} \in \mathcal{R}^n$ being the time-dependent estimated state with initial estimate $\hat{\boldsymbol{x}}(0) = \hat{\boldsymbol{x}}_0$ and the time-variant observer gain $\boldsymbol{K}(t) \in \mathcal{R}^{n \times p}$. Clearly, the structure of the differential equation producing the estimate has not changed compared to the classical EKF in (2.29).

However, to calculate the observation gain $\boldsymbol{K}(t)$ in (2.29), we use the slightly different Riccati equation

$$\begin{aligned} \dot{\boldsymbol{P}}(t) = (\boldsymbol{A}(\hat{\boldsymbol{x}}, t) + \alpha \mathbf{I})\boldsymbol{P}(t) + \boldsymbol{P}(t)(\boldsymbol{A}(\hat{\boldsymbol{x}}, t)^\top + \alpha \mathbf{I}) + \boldsymbol{Q} \\ - \boldsymbol{P}(t)\boldsymbol{C}(\hat{\boldsymbol{x}}, t)^\top \boldsymbol{R}^{-1} \boldsymbol{C}(\hat{\boldsymbol{x}}, t)\boldsymbol{P}(t), \end{aligned} \tag{2.40}$$

with $\boldsymbol{P}(0) = \boldsymbol{P}_0$ where $\alpha > 0$ and $\boldsymbol{Q}$ and $\boldsymbol{R}$ are positive definite matrices. The matrices $\boldsymbol{A}(\hat{\boldsymbol{x}}, t)$ and $\boldsymbol{C}(\hat{\boldsymbol{x}}, t)$ are obtained using (2.32) and (2.33). The observer gain is then calculated using (2.30) as in the classical case.

Stability

In order to guarantee local convergence of the estimate obtained using the modified extended Kalman filter, a number of assumptions, given in [21], have to hold.

Firstly, extension of the nonlinearities into power series yields

$$\begin{aligned} \boldsymbol{f}(\boldsymbol{x}, t) - \boldsymbol{f}(\hat{\boldsymbol{x}}, t) &= \boldsymbol{A}(\hat{\boldsymbol{x}}, t)(\boldsymbol{x} - \hat{\boldsymbol{x}}) + \boldsymbol{\Phi}(\boldsymbol{x}, \hat{\boldsymbol{x}}), \\ \boldsymbol{h}(\boldsymbol{x}, t) - \boldsymbol{h}(\hat{\boldsymbol{x}}, t) &= \boldsymbol{C}(\hat{\boldsymbol{x}}, t)(\boldsymbol{x} - \hat{\boldsymbol{x}}) + \boldsymbol{\Psi}(\boldsymbol{x}, \hat{\boldsymbol{x}}), \end{aligned}$$

where $\boldsymbol{\Phi}$ and $\boldsymbol{\Psi}$ are the terms of second and higher order. To ensure stability of the dynamics of the estimation error $\boldsymbol{\xi}_m = \boldsymbol{x} - \hat{\boldsymbol{x}}$,

$$\dot{\boldsymbol{\xi}}_m = (\boldsymbol{A}(\hat{\boldsymbol{x}}, t) - \boldsymbol{K}(t)\boldsymbol{C}(\hat{\boldsymbol{x}}, t))\boldsymbol{\xi}_m + \boldsymbol{\Phi}(\boldsymbol{x}, \hat{\boldsymbol{x}}) - \boldsymbol{K}(t)\boldsymbol{\Psi}(\boldsymbol{x}, \hat{\boldsymbol{x}}),$$

for sufficiently good initial estimates $\hat{\boldsymbol{x}}_0$, the following assumptions have to hold in addition to Assumption 1:

Assumption 3. *There exist* $\kappa_\Phi, \kappa_\Psi, \epsilon_\Phi, \epsilon_\Psi > 0$*, such that the nonlinearities* $\boldsymbol{\Phi}$*,* $\boldsymbol{\Psi}$ *are bounded via*

$$\|\boldsymbol{\Phi}(\boldsymbol{x}, \hat{\boldsymbol{x}})\| \leq \kappa_\Phi \|\boldsymbol{x} - \hat{\boldsymbol{x}}\|^2, \tag{2.41}$$

$$\|\boldsymbol{\Psi}(\boldsymbol{x}, \hat{\boldsymbol{x}})\| \leq \kappa_\Psi \|\boldsymbol{x} - \hat{\boldsymbol{x}}\|^2, \tag{2.42}$$

for $\|\boldsymbol{x} - \hat{\boldsymbol{x}}\| \leq \epsilon_\Phi$*,* $\|\boldsymbol{x} - \hat{\boldsymbol{x}}\| \leq \epsilon_\Psi$ *respectively.*

Assumption 4. *The time-varying matrix* $\boldsymbol{C}(\hat{\boldsymbol{x}}, t)$ *is bounded by*

$$\|\boldsymbol{C}(\hat{\boldsymbol{x}}, t)\| \leq \bar{c}, \tag{2.43}$$

for all $t \geq t_0$ *for a* $\bar{c} \in \mathcal{R}_{>0}$*.*

Under Assumptions 1, 3 and 4, the observer given by (2.39), (2.30) and the Riccati equation (2.40) is an exponential observer for the nonlinear system (2.27), (2.28) and the estimation error $\boldsymbol{\xi}_m$ decays exponentially with a time constant $\tau_\xi > \alpha$ [21].

2.4.3 Adaptive Laws as EKFs

The adaptive control framework is closely connected to extended Kalman filters. While the parameter estimators from Section 2.3 were all presented in an adaptive control context, it is possible to show that the least-squares adaptive law is actually a continuous extended Kalman filter.

For the linear parametric model (2.15) we can introduce the parameter vector $\boldsymbol{\theta}$ and derive the state space representation

$$\dot{\boldsymbol{\theta}} = \mathbf{0}, \tag{2.44}$$

$$z = \boldsymbol{\theta}^\top \boldsymbol{\phi}, \tag{2.45}$$

with a random-walk process model and the linear parametric measurement model from (2.15). For the system (2.44), (2.45) we can design an EKF as described in Section 2.4. The update law of the extended Kalman filter is given by

$$\dot{\hat{\boldsymbol{\theta}}} = \boldsymbol{K}(z - \hat{\boldsymbol{\theta}}^\top \boldsymbol{\phi}). \tag{2.46}$$

Since (2.44) is a random-walk process model, the prediction term in (2.46) is zero. The update law (2.46) thus only contains a correction term dependent on the observer gain $\boldsymbol{K}$ and the output error

$$e_o = z - \hat{\boldsymbol{\theta}}^\top \boldsymbol{\phi}.$$

In the Kalman filter framework, the observer gain is calculated as

$$\boldsymbol{K} = \boldsymbol{P}\boldsymbol{\phi}\boldsymbol{R}^{-1}, \tag{2.47}$$

where $\boldsymbol{P}$ is the solution of the Riccati equation

$$\dot{\boldsymbol{P}} = \boldsymbol{Q} - \boldsymbol{P}\boldsymbol{\phi}\boldsymbol{R}^{-1}\boldsymbol{\phi}^\top\boldsymbol{P} + 2\alpha_r\boldsymbol{P}.$$

Plugging (2.47) into (2.46) and setting the measurement noise covariance matrix to $\boldsymbol{R} = \boldsymbol{I}$ and the process noise covariance to $\boldsymbol{Q} = \mathbf{0}$ yields,

$$\dot{\hat{\boldsymbol{\theta}}} = \boldsymbol{P}\boldsymbol{\phi}(z - \hat{\boldsymbol{\theta}}^\top \boldsymbol{\phi}), \tag{2.48}$$

$$\dot{\boldsymbol{P}} = 2\alpha_r\boldsymbol{P} - \boldsymbol{P}\boldsymbol{\phi}\boldsymbol{\phi}^\top\boldsymbol{P}. \tag{2.49}$$

When choosing $\beta = 2\alpha_r$ the EKF given by (2.48) and (2.49) is identical to the least-squares adaptive law from (2.23). Note that for $\alpha = 0$ we have a classical EKF which consequently is the same as a least-squares adaptive law with forgetting factor $\beta = 0$. For $\alpha > 0$, (2.48) and (2.49) form a modified EKF, coinciding with a least-squares adaptive law with forgetting factor.

3

Problem Description

Generally, many ways to control a robot in a human-robot handover exist. A challenge is to move the robot towards the handover point in a way that allows for a seamless human-robot handover. In view of this, it is essential to know where the handover point is and when the human hand will be there to hand over an object as soon as possible. In this chapter we introduce the overall structure of the predictor used to predict handover place and time. After limiting the scope of the considered prediction problem, two different approaches to parameterize human motion are considered.

3.1 Problem Formulation: Predictor Structure

A human-robot handover can be viewed as consisting of different phases. It starts with the human hand holding an object and beginning to move towards the handover place. This can be considered as the reaching phase. At the end of the reaching phase, the human and the robot hand meet at the handover place and the control of the object is transferred from the human to the robot, resulting in a completed handover. Our main objective is to predict the place g and time τ of an upcoming human-robot handover during the reaching phase.

Focusing on the reaching phase of the handover, the handover place can be viewed as the endpoint of the reaching trajectory of the human hand. Similarly, the handover time can be seen as the duration of the reaching trajectory. Observations of the reaching trajectory can be obtained using measurements of the position y, the velocity $\dot{y}$ and, if necessary, the acceleration $\ddot{y}$ of the human hand. Generally, it is advantageous to rely on as little measurements as possible to limit the number of necessary sensors and thus broaden the scope of possible applications. Obtaining the required measurements of the human hand is possible, e.g. by using vision based measurements that could be supplemented with velocity and acceleration measurements obtained by the human wearing a special glove with sensors.

To solve the prediction problem, we can use prior knowledge on human motion to parameterize human motion with a DMP that is learned off-line by demonstration. This DMP has a point attractor at the goal g, representing the handover place, and a certain timescale τ, representing the handover time. Treating these two parameters as unknown, an on-line estimation scheme can be designed to estimate the point attractor g and the timescale τ of a DMP using the available measurements. Hence, the prediction of handover place and time can be reduced to parameter estimation of the goal and timescale of a DMP. The structure of the resulting predictor, consisting of a mathematical model parameterizing human motion, and an estimator estimating its parameters on-line based on measurements of the human hand, is illustrated in Figure 3.1.

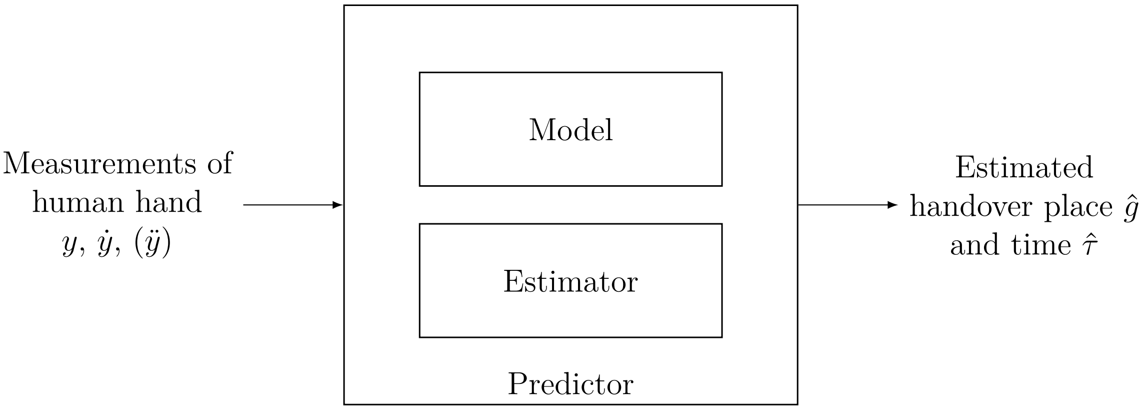

Figure 3.1: Overall structure of the proposed predictor.

3.2 Limitations

For simplicity, we only consider the motion of the human hand in one dimension. Once goal and timescale of a one-dimensional human motion can be predicted, extension to multiple dimensions is straight forward, e.g. by extending the state vectors of the EKFs with the additional positions, velocities and parameters of other dimensions. Furthermore, we do not take the orientation of the human hand during the handover process into account. Note also that any parameterization of human motion during a handover is probably restricted to a certain phase of the handover process. Therefore, decision-making is necessary to determine when this phase begins in order to conduct the model-based estimation of the handover place and time while the parameterization of the human motion is valid. In this thesis, we assume to know this by only considering the phase for which our parameterization is valid.

3.3 Parameterization of Human Motion Using a DMP

One way to parameterize human motion is to use the original methodology of DMPs presented in Section 2.2. An advantage of DMPs is that only one human trajectory, a so called training trajectory, is necessary to obtain a DMP via demonstration learning. Thanks to the invariance properties of DMPs explained in Section 2.2.3, this learned DMP embodies a dynamical system that can produce trajectories of different timescales and endpoints, all being of the same shape as the demonstrated training trajectory. In the DMP framework, endpoints of trajectories are referred to as goals. At what time a human-robot handover takes place is described by the timescale of the DMP representation of the human motion. Both timescale and goal appear as high-level parameters of the learned DMP. Our approach is to learn a DMP as a parameterization of human motion during human-robot handovers with a training trajectory. Subsequently, the two high-level parameters, goal and timescale, are treated as unknown and we try to estimate their values for different handovers using measurements of the human motion. In the course of this thesis, we focus on the motion of the human hand since it is the most relevant body part during the handover of an object.

Applying a DMP as parameterization of human motion, we have the nonlinear forcing term introduced in Section 2.2,

$$f(x,g) = (g - y_0)\tilde{f}(x), \tag{3.1}$$

with

$$\tilde{f}(x) = \frac{\sum_{i=1}^{N} \Psi_i(x) w_i}{\sum_{i=1}^{N} \Psi_i(x)} x, \tag{3.2}$$

where the dependency of f on the goal g was added, since the goal, representing the handover place, is now considered as unknown. As part of the DMP representation, we have the second order transformation system (2.7), which can be reordered to

$$\ddot{y} = \frac{1}{\tau^2}(-\alpha_z\beta_z y - \alpha_z\tau\dot{y} + \alpha_z\beta_z g + f(x,g)) \tag{3.3}$$

and with (3.1), we obtain

$$\ddot{y} = \frac{1}{\tau^2}(-\alpha_z\beta_z y - y_0\tilde{f}(x)) - \frac{\alpha_z}{\tau}\dot{y} + \frac{g}{\tau^2}(\alpha_z\beta_z + \tilde{f}(x)). \tag{3.4}$$

The parameters α_z, β_z, α_x are chosen to obtain a critically damped transformation system, as done in [9] and given in Table 3.1. Following Section 2.2.4, the attractor dynamics of the DMP are learned off-line via learning from demonstration. Results presented in [3] suggest human point-to-point motion can be described by minimum-jerk trajectories. The process of a human-robot handover typically involves a human point-to-point motion, whose endpoint and transition time are to be estimated by the robot. Consequently, we use the minimum-jerk trajectory

Parameter	**Value**
α_z	25
β_z	$\alpha_z/4$
α_x	$\alpha_z/3$

Table 3.1: Parameters of the transformation system of the original DMP.

$$y(t) = y_0 + (g - y_0)\left(10\left(\frac{t}{\tau}\right)^3 - 15\left(\frac{t}{\tau}\right)^4 + 6\left(\frac{t}{\tau}\right)^5\right) \tag{3.5}$$

and its first two time derivatives with starting point $y_0 = 0\,\mathrm{m}$, endpoint $g = 2\,\mathrm{m}$ and transition time $\tau = 10\,\mathrm{s}$ to learn a DMP which represents human motion in form of

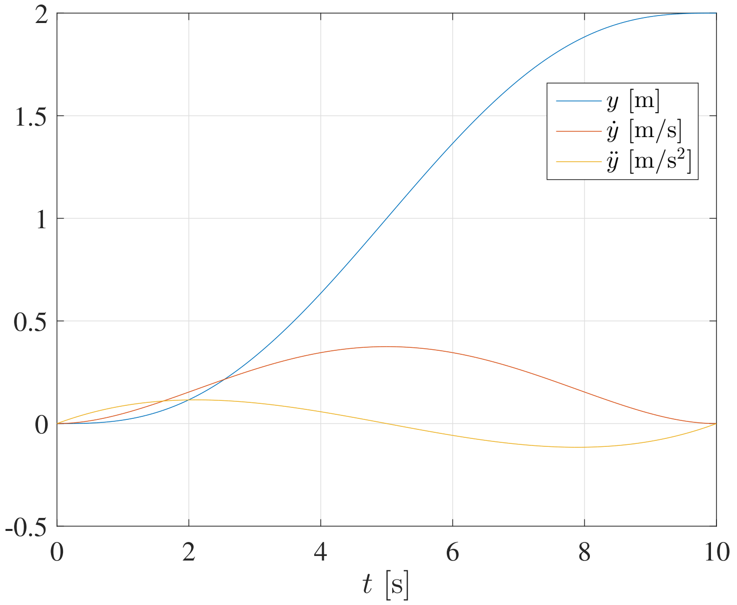

Figure 3.2: Minimum jerk trajectory representing point-to-point motion of a human hand with position y, velocity $\dot{y}$ and acceleration $\ddot{y}$ in one dimension.

a dynamical system. The trajectories of y, $\dot{y}$ and $\ddot{y}$ are shown in Figure 3.2.

Using (2.8), (2.9), (2.10) and (2.11) for the off-line learning, $N = 30$ basis functions are chosen. As the phase variable x exhibits an exponential decay from one to zero, an exponential distribution of the centers c_i, $i = 1, \ldots, N$ of the basis functions (2.6) results in a uniform spacing in time [9]. For a spacing

$$\Delta_t = \frac{\tau}{N-1} \tag{3.6}$$

of the basis functions in time, the centers are set to

$$c_i = \exp\left(-\frac{\alpha_x}{\tau}\Delta_t(i-1)\right) x_0. \tag{3.7}$$

Similarly, the widths are set via h_i to

$$h_i = 10 \exp\left(\frac{\alpha_x}{\tau}\Delta_t\right)^2 x_0. \tag{3.8}$$

The distribution of the basis functions (2.6),

$$\Psi_i(x) = \exp\left(-h_i(x-c_i)^2\right),$$

resulting from (3.7) and (3.8) is shown in Figure 3.3. Clearly, the centers of the basis functions are uniformly distributed over time thanks to the exponential spacing of the c_i in x. However, due to the exponential relation between t and x, the shape of the basis functions in the time space is that of a distorted Gaussian.

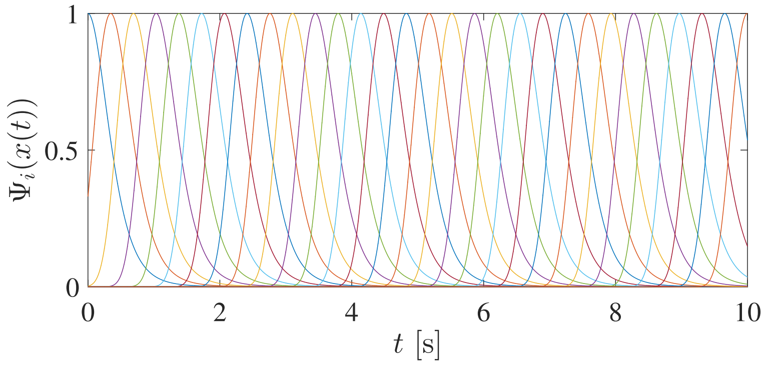

Figure 3.3: Distribution of the basis functions Ψ_i over time t.

Based on the Ψ_i, the weights are calculated as in (2.11),

$$\boldsymbol{w} = (\boldsymbol{X}^\top \boldsymbol{X})^{-1} \boldsymbol{X}^\top \boldsymbol{f}.$$

The weights and their associated basis function centers c_i are illustrated in Figure 3.4. While the absolute values of the weights for small basis function center values c_i are large, they decrease with increasing c_i values. Considering that the basis functions are functions of the phase variable x, which modulates the temporal evolution of the forcing term, we can observe the following relation: Basis functions with a large c_i influence the forcing term in the beginning of motion of the human hand, whereas small c_i belong to basis functions influencing the forcing term towards the end of motion. Correspondingly, Figure 3.4 shows rather high weights for small c_i which effectively means large weights towards the end of motion.

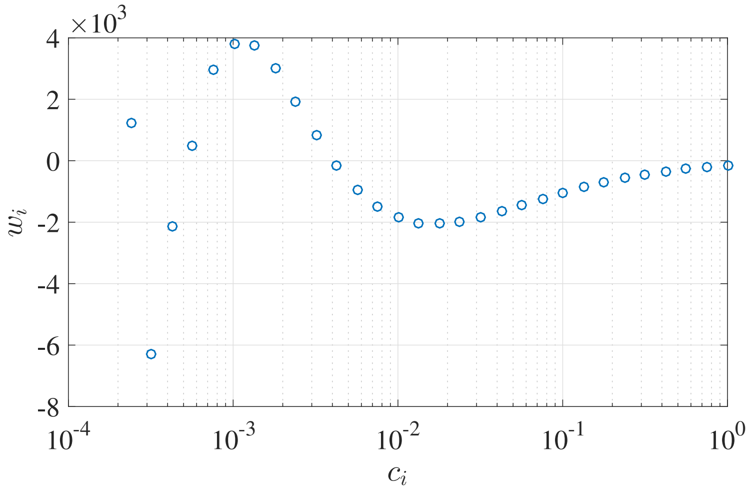

Figure 3.4: Weights w_i resulting from off-line learning.

3.4 Parameterization of Human Motion Using a Specialized DMP

The phase variable x of the original DMP formulation is a result of the canonical system (2.3) describing the temporal evolution of the nonlinear forcing term (2.4) and therefore the temporal evolution of the DMP. For a known timescale τ, the explicit solution of the canonical system (2.3),

$$x(t, \tau) = \exp\left(-\frac{\alpha_x}{\tau} t\right), \tag{3.9}$$

is a bijective mapping $x : D_t \to D_x$ for $t \in D_t = [0, \tau]$ and $x \in D_x = [0, 1]$. In the following, we suggest a new way of describing the temporal evolution of the nonlinearity by exploiting prior knowledge on human motion. As justified by the findings of Flash and Hogan [3], we consider minimum-jerk trajectories to represent human point-to-point motion. The functional representation $y : D_t \to D_y$ with $D_y = [y_0, g]$ of the minimum-jerk trajectory from (3.5) is also bijective for a known goal $g \neq y_0$ and timescale $\tau > 0$. Consequently, it is possible to substitute x in (2.4) with the bijective relation,

$$x(t, g) = 1 - \frac{y(t) - y_0}{g - y_0}, \tag{3.10}$$

for $t \geq 0$ and a known, fixed $g > 0$. This replacement of the phase variable x is shown in Figure 3.5b. Clearly, it goes from one to zero monotonically within the time τ, as does the phase variable of the original DMP from Figure 3.5a, while also assigning each $t \in D_t$ exactly one unique $x \in D_x$. Note that it is possible to use the specialized DMP to represent any point-to-point trajectory that is monotone since this will always yield a feasible phase variable replacement.

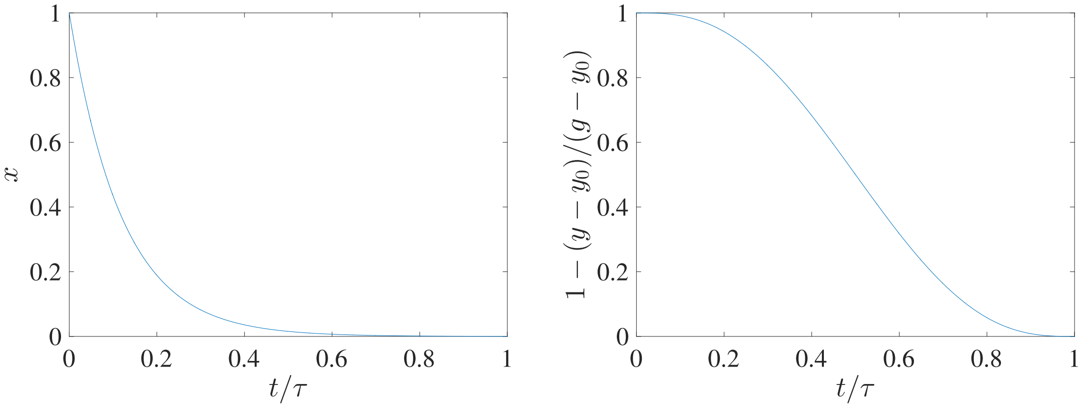

(a) Original DMP **(b)** Specialized DMP

Figure 3.5: Phase variable and phase variable replacement of original and specialized DMP respectively.

While the nonlinear forcing term $f(x, g)$ given by (3.1) used to be a function of the phase variable x and the goal g in the original DMP framework, for the specialized DMP it now reads

$$f(y, g) = \tilde{f}_s(y, g)(g - y_0), \tag{3.11}$$

with

$$\tilde{f}_s(y, g) = \underbrace{\frac{\sum_{i=1}^{N} \Psi_{s,i}(y, g) w_i}{\sum_{i=1}^{N} \Psi_{s,i}(y, g)}}_{\tilde{g}(y,g)} \left(1 - \frac{y - y_0}{g - y_0}\right), \tag{3.12}$$

and it is therefore no longer dependent on x. Plugging (3.9) into (2.6) yields the new basis functions for the specialized DMP,

$$\Psi_{s,i}(y, g) = \exp\left(-h_{s,i}\left(1 - \frac{y - y_0}{g - y_0}\right) - c_{s,i}\right)^2,$$

with width parameters $h_{s,i}$ and centers $c_{s,i}$. The second order representation of the specialized DMP is then given by

$$\tau^2 \ddot{y} = \alpha_z \left(\beta_z \left(g - y\right) - \tau \dot{y}\right) + f(y, g). \tag{3.13}$$

In contrast to the original DMP formulation from Ijspeert *et al.*, this specialized DMP does not need a phase variable and therefore no canonical system.

One of the greatest advantages of using the original DMP formulation are the invariance properties, which allow parameterization of minimum-jerk trajectories of different timescales and goals, since a change of τ and g does not qualitatively change the attractor landscape of the original DMP. For this specialized DMP to be applicable to the presented human-robot handover scenario, these invariance properties have to be ensured as well.

To show spatial invariance, we can apply the concept of topological equivalence [29]. Two dynamical systems $\dot{\boldsymbol{x}} = \boldsymbol{f}_o(\boldsymbol{x})$ and $\dot{\boldsymbol{y}} = \boldsymbol{g}_o(\boldsymbol{y})$ are considered topologically invariant, if there exists an orientation preserving homeomorphism $\boldsymbol{h}_o : [\boldsymbol{x}, \dot{\boldsymbol{x}}] \rightarrow [\boldsymbol{y}, \dot{\boldsymbol{y}}]$ with inverse $\boldsymbol{h}_o^{-1} : [\boldsymbol{y}, \dot{\boldsymbol{y}}] \rightarrow [\boldsymbol{x}, \dot{\boldsymbol{x}}]$, mapping the state spaces of the two dynamical systems into each other [9]. We now consider an unscaled and a scaled version of the specialized DMP (3.13) as the two dynamical systems which we want to be topologically equivalent. We denote the states of the scaled DMP with $\tilde{y}$, $\dot{\tilde{y}}$, $\ddot{\tilde{y}}$ and the initial value of $\tilde{y}$ by $\tilde{y}(0) = \tilde{y}_0$. Scaling the movement amplitude with $(g - \tilde{y}_0) \rightarrow k_s(g - \tilde{y}_0)$ for a $k_s > 0$ yields the scaled DMP

$$\tau^2 \ddot{\tilde{y}} = \alpha_z \left(\beta_z \left(k_s(g - \tilde{y}_0) + \tilde{y}_0 - \tilde{y}\right) - \tau \dot{\tilde{y}}\right) + f_{scaled}(\tilde{y}, g) \tag{3.14}$$

where we used $g = g - \tilde{y}_0 + \tilde{y}_0$. With the scaled nonlinear forcing term

$$f_{scaled}(\tilde{y}, g) = \frac{\sum_{i=1}^{N} \Psi_{scaled,i}(\tilde{y}, g) w_i}{\sum_{i=1}^{N} \Psi_{scaled,i}(\tilde{y}, g)} \left(1 - \frac{\tilde{y} - \tilde{y}_0}{k_s(g - \tilde{y}_0)}\right) k_s(g - \tilde{y}_0), \tag{3.15}$$

and the scaled basis functions

$$\Psi_{scaled,i}(\tilde{y}, g) = \exp\left(-h_{s,i}\left(1 - \frac{(\tilde{y} - \tilde{y}_0)}{k_s(g - \tilde{y}_0)}\right) - c_{s,i}\right)^2. \tag{3.16}$$

Since the bijection

$$\begin{bmatrix} \tilde{y} - \tilde{y}_0 \\ \dot{\tilde{y}} \\ \ddot{\tilde{y}} \end{bmatrix} = \boldsymbol{h}_g(y, \dot{y}, \ddot{y}) = \begin{bmatrix} k_s(y - y_0) \\ k_s\dot{y} \\ k_s\ddot{y} \end{bmatrix} \tag{3.17}$$

and its inverse $\boldsymbol{h}_g^{-1}$ are continuous thanks to their linearity, $\boldsymbol{h}_g$ is a homeomorphism. It is also orientation preserving as the determinant of its Jacobian is positive for $k_s > 0$. Plugging (3.17) into the scaled system (3.14), (3.15), (3.16) yields the unscaled specialized DMP from (3.13), showing that the unscaled and the scaled system are topologically equivalent. Consequently, the specialized DMP is spatially invariant.

Similarly, the temporal invariance of the specialized DMP can be shown via the orientation preserving homeomorphism

$$\begin{bmatrix} \tilde{y} \\ \dot{\tilde{y}} \\ \ddot{\tilde{y}} \end{bmatrix} = \boldsymbol{h}_\tau(y, \dot{y}, \ddot{y}) = \begin{bmatrix} y \\ k_s\dot{y} \\ k_s^2\ddot{y} \end{bmatrix},$$

using the same reasoning as for spatial invariance.

To achieve a uniform spacing of the N basis functions, we use the minimum-jerk representation (3.5) and choose centers

$$c_{s,i} = 1 - \left(10\left(\frac{\Delta_t(i-1)}{\tau}\right)^3 - 15\left(\frac{\Delta_t(i-1)}{\tau}\right)^4 + 6\left(\frac{\Delta_t(i-1)}{\tau}\right)^5\right), \tag{3.18}$$

for $i = 1, \ldots, N$ with time steps (3.6),

$$\Delta_t = \frac{\tau}{N-1},$$

and transition time τ. Due to the shape of the minimum-jerk trajectory, the replacement of the phase variable (3.10) only exhibits a slow change in value at the beginning and at the end of motion. This can also be observed in Figure 3.5b. To account for this, the basis function width parameters $h_{s,i}$ are chosen to be

$$h_{s,i} = 10 + 10\left(\Delta_t(i-1) - \frac{\tau}{2}\right)^4 \tag{3.19}$$

for $i = 1, \ldots, N$. The distribution of the basis functions for the specialized DMP with $N = 30$ are depicted in Figure 3.6. While the centers are uniformly spaced over t, the widths of the kernels still become larger towards the beginning and the end of motion despite the larger values of the $h_{s,i}$ in (3.19) at the beginning and the end of motion.

Using training data generated by (3.5) with $\tau = 1$ and $g = 1$, a specialized DMP is learned to represent the minimum-jerk trajectory. Using this specialized DMP, minimum-jerk trajectories for different timescales τ and goals g are illustrated in Figure 3.7. The invariance properties shown above are verified, as the trajectories do not appear to change qualitatively. However, in Figure 3.7a it can be observed

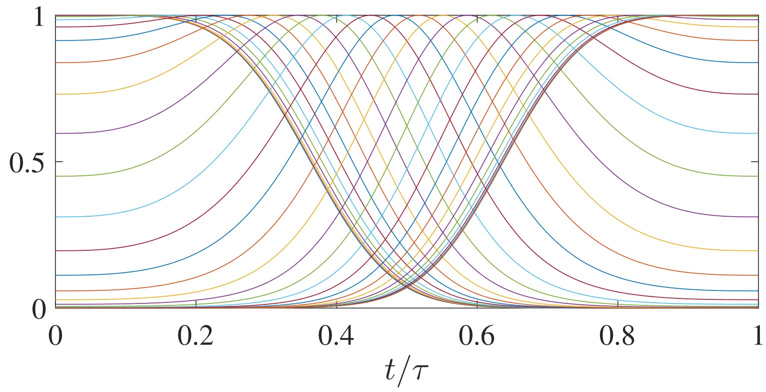

Figure 3.6: Distribution of the basis functions $\Psi_{s,i}$ of the specialized DMP over t/τ.

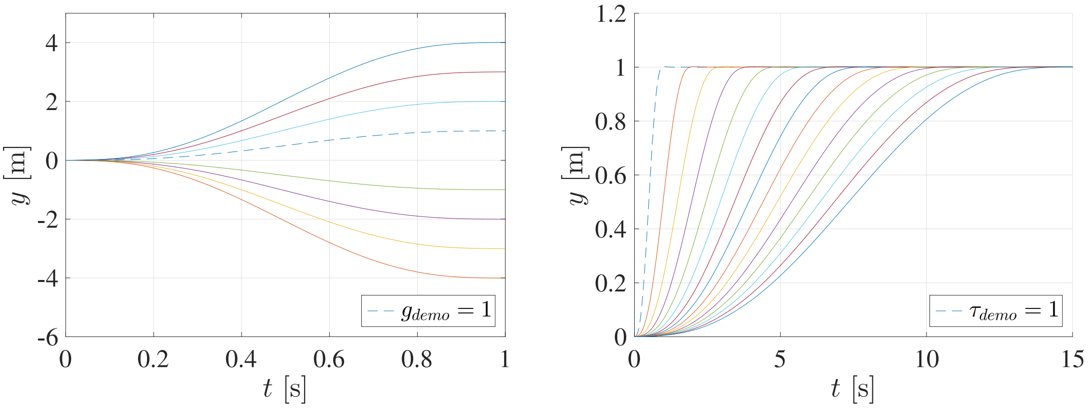

(a) Variation of goal g **(b)** Variation of timescale τ

Figure 3.7: Trajectories produced with the specialized DMP fitted to a minimum-jerk trajectory for different parameter values of goal g and timescale τ.

that there is a slight overshoot at the end of some minimum-jerk trajectories. This can be explained by investigating the fitting error $\epsilon_{fit}(t_k) = f_{target,k} - f(y(t_k), g)$ which is obtained using (2.8) at time instances t_k with $k = 1, \ldots, P$, as defined in Section 2.2.4. For very large P, we can consider $\epsilon_{fit}(t)$. Figure 3.8 shows the fitting error $\epsilon_{fit}(t)$. Relatively large fitting errors in the beginning and end of the motion occur. Given the large widths of the basis functions in these regions of t, we can observe that the fitting of the nonlinear forcing term $f(y, g)$ is difficult when using the specialized DMP, since the shape of the replacement of the phase variable (3.10) makes a proper choice of basis function width parameters $h_{s,i}$ difficult.

It can be concluded, that while the specialized DMP allows for elimination of the phase variable x as compared to the original DMP, thus having a lower number of DMP states, it becomes harder to fit the specialized DMP to given trajectories. Note that the positions $y(t)$ produced by the learned specialized DMP in Figure 3.7 are still very close to the demonstrated positions since the fitting error from Figure 3.8 only affects the acceleration $\ddot{y}$. Also, increasing the number of basis functions N for the fitting of the specialized DMP allows to somewhat compensate for the bad fitting

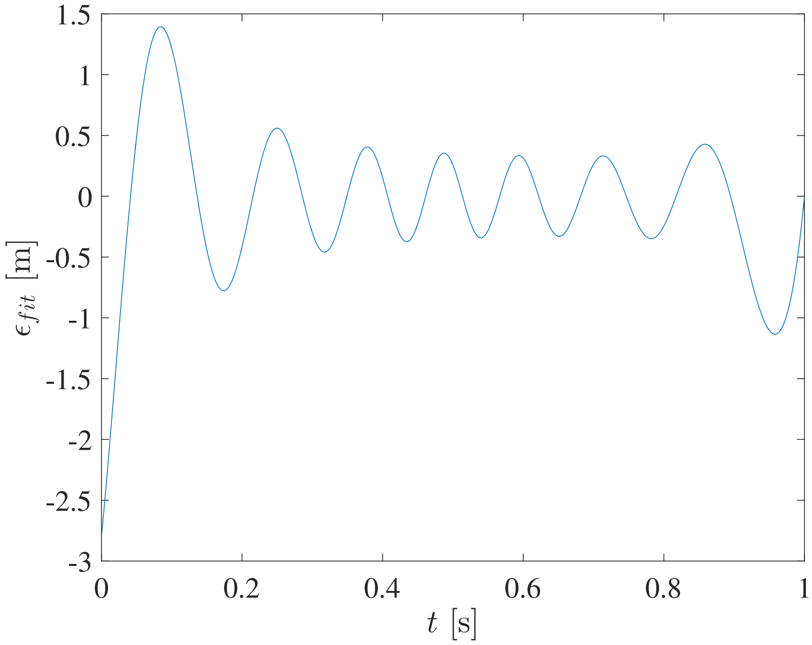

Figure 3.8: Fitting error for a minimum-jerk trajectory with $\tau = 1\,\mathrm{s}$ using $N = 30$ basis functions and a specialized DMP.

properties of the specialized DMP. Hence, it is of interest to use the specialized DMP as a parameterization of human motion and estimate time and place of a human-robot handover based on it.

4

Parameter Estimation Based on DMPs

By using a DMP as a parameterization for human motion, the problem of predicting place and time of a human-robot handover can be formulated as a parameter estimation problem. Different parameter estimation schemes can be designed to estimate goal and timescale of the DMP.

4.1 Adaptive Law-Based Parameter Estimation of DMPs

Assuming both position y and speed $\dot{y}$ of the human hand can be measured, we filter both sides of (3.4) with

$$H(s) = \frac{1}{\Lambda(s)} = \frac{1}{(s + \lambda_f)} \tag{4.1}$$

to eliminate $\ddot{y}$ [13]. Consequently, (3.4) can be written as the linear parametric model from (2.15),

$$z = \frac{s}{\Lambda(s)}\dot{y} = \underbrace{\begin{bmatrix} \frac{1}{\tau^2} & \frac{1}{\tau} & \frac{g}{\tau^2} \end{bmatrix}}_{\boldsymbol{\theta}^\top} \underbrace{\begin{bmatrix} (-\alpha_z\beta_z y - y_0\tilde{f}(x))\frac{1}{\Lambda(s)} \\ -\alpha_z\dot{y}\frac{1}{\Lambda(s)} \\ (\alpha_z\beta_z + \tilde{f}(x))\frac{1}{\Lambda(s)} \end{bmatrix}}_{\boldsymbol{\phi}}, \tag{4.2}$$

where z is the filtered system output and the timescale τ and the goal g are treated as unknown parameters. Note that different linear parameterizations for the given DMP can be chosen dependent on the available measurements. As fast parameter convergence is desired, a filter of the lowest order possible is advantageous. The pole $-\lambda_f$ of the filter from (4.1) also affects the convergence rate. A trade-off between desirable differentiating behavior for large λ_f and measurement noise suppression through a low-pass property for small λ_f has to be done.

Based on the linear parametric representation (4.2) of the DMP, an attempt to estimate goal and timescale of the DMP, representing place and time of a human-robot handover can be made. A common approach is to use adaptive laws to estimate these parameters on-line [12]. As opposed to the usual case in the adaptive control framework presented in Section 2.3, in (4.2) the information vector $\boldsymbol{\phi}$ is dependent on the signals y, $\dot{y}$ and x. While y and $\dot{y}$ are available measurements and thus known signals, the phase variable x constitutes an auxiliary state modulating the temporal evolution of the nonlinear forcing term f of the DMP and cannot be measured. To be able to use established adaptive laws from Section 2.3, different approaches to substitute x with a known signal in the information vector $\boldsymbol{\phi}$ are possible.

4.1.1 Continuous Goal Estimation for Known Timescales

As a first step, we consider a case where the timescale τ of the human motion is known in advance. This allows to use the explicit solution of the canonical system (2.3),

$$x(t) = \exp\left(-\frac{\alpha_x}{\tau}t\right), \tag{4.3}$$

with initial condition $x(0) = x_0 = 1$, as is part of the DMP formulation from Section 2.2, to substitute x in $\boldsymbol{\phi}$. This yields a fully known information vector $\boldsymbol{\phi}$ in (4.2). Using a rather slow filter (4.1) with $\lambda_f = 3$, position and speed measurements of the human hand are obtained and fed into the adaptive laws from Section 2.3.

Since we consider human point-to-point motion, both position y and velocity $\dot{y}$ of the human hand are bounded functions of time. Furthermore, $\tilde{f}$ is bounded thanks to the boundedness of the basis functions Ψ_i and weights w_i. Hence, no normalization is needed to guarantee $\boldsymbol{\phi} \in \mathcal{L}_\infty$, which is the first requirement for stability of the adaptive laws from Section 2.3.

For convergence of the adaptive laws, it remains to show that $\boldsymbol{\phi}$ is PE. We can relate

$$\boldsymbol{\phi} = \boldsymbol{H}(s)y$$

by using $y_0 = 0$, eliminating $\dot{y}$ with a filtering operation and pulling y out of $\boldsymbol{\phi}$ in (4.2). The vector $\boldsymbol{H}(s)$ is a proper stable transfer matrix with $\boldsymbol{\phi} \in \mathcal{R}^3$ and y being the position measurement signal. According to Ioannou and Sun [12], the information vector $\boldsymbol{\phi}$ is PE if, and only if, y is stationary, sufficiently rich of order n with $\boldsymbol{\theta} \in \mathcal{R}^n$ and if there exist n different frequencies $\omega_1, \dots, \omega_n \in \mathcal{R}$ such that $\boldsymbol{H}(j\omega_1), \dots, \boldsymbol{H}(j\omega_n)$ are linearly independent on $\mathcal{C}^n$.

If y is stationary, then it is sufficiently rich of order n if the support of the spectral measure $S_y(\omega)$ of y contains at least n points [12]. The spectral measure is given by

$$S_y(\omega) = \int_{-\infty}^{\infty} e^{-j\omega\tau} R_y(\tau) d\tau,$$

which is the Fourier transform of the auto-covariance $R_y(t) \in \mathcal{R}$. For a minimum-jerk trajectory with $\tau = 10$, $y_0 = 0$ and $g = 2$ the spectral measure is shown in Figure 4.1. The support of $S_y(\omega)$ clearly contains more than $n = 3$ points. Since the auto-covariance $R_y(t)$ exists and is finite uniformly in t and the minimum-jerk trajectory $y(t)$ from (3.5) always has the same shape, y is stationary. Consequently, y is also sufficiently rich of order 3. As we can find at least three different frequencies $\omega_1, \dots, \omega_3 \in \mathcal{R}$ such that $\boldsymbol{H}(j\omega_1), \dots, \boldsymbol{H}(j\omega_3)$ are linearly independent on $\mathcal{C}^n$, and because y is sufficiently rich of order 3, $\boldsymbol{\phi}$ is PE [12]. Since the spectral measure will not change qualitatively for different transition times τ of the minimum-jerk trajectory, $\boldsymbol{\phi}$ is PE for all minimum-jerk trajectories with $g \neq y_0$.

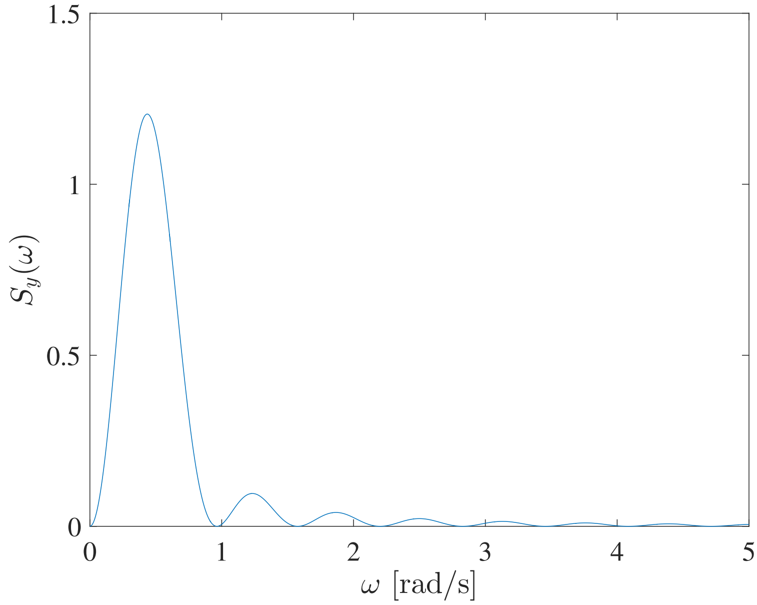

Figure 4.1: Spectral measure $S_y(\omega)$ of a minimum-jerk trajectory with $\tau = 10$, $y_0 = 0$ and $g = 2$.

Least-Squares Adaptive Law

First, we use the least-squares adaptive law from (2.23),

$$\dot{\hat{\boldsymbol{\theta}}} = \boldsymbol{P}\epsilon\boldsymbol{\phi},$$
$$\dot{\boldsymbol{P}} = \beta\boldsymbol{P} - \boldsymbol{P}\boldsymbol{\phi}\boldsymbol{\phi}^\top\boldsymbol{P}, \;\; \boldsymbol{P}(0) = \boldsymbol{P}_{0,lsq},$$

with the output error ϵ from (2.17) and an empirically obtained initial gain of

$$\boldsymbol{P}_{0,lsq} = \mathrm{diag}(100, 5000, 100). \tag{4.5}$$

As no normalization is needed, we set $m = 1$. The elements of the true parameter vector $\boldsymbol{\theta}$ from (4.2) only depend on the timescale τ and the goal g. We already know the constant timescale τ and assume the goal g is constant for one specific motion of the human hand. Consequently, $\boldsymbol{\theta}$ is a constant vector as well. As discussed in [12], this allows for a small forgetting factor of $\beta = 0.1$, meaning that measurement data collected in the past is only slightly discounted and used to obtain an estimate $\hat{\boldsymbol{\theta}}$. Figure 4.2 shows how the estimated goal $\hat{g}$, obtained by the presented least-squares based adaptive law, converges to the true g. The simulation is conducted using the initial guess $\hat{g}_0 = 1$ while the true goal is $g = 2$. Obviously, the goal estimate $\hat{g}$ converges to the true value g. After one second, the parameter error is already less than 0.1 m.

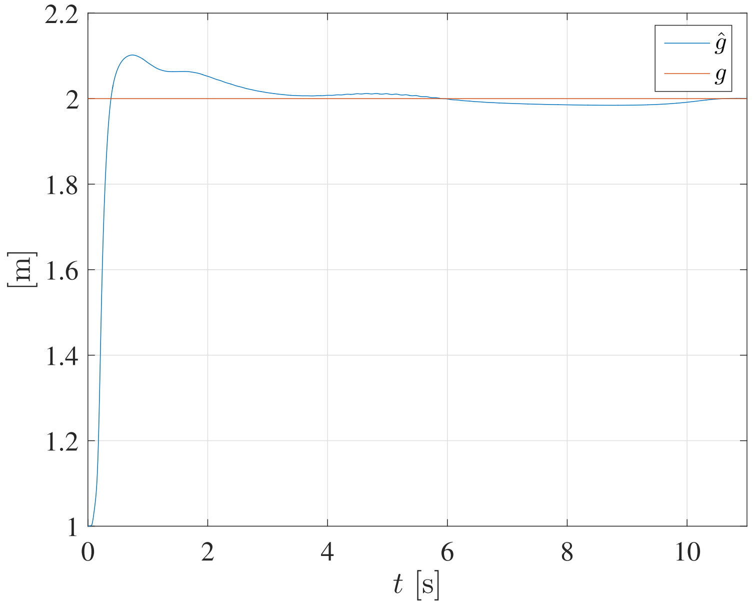

Figure 4.2: Estimation of goal g for a known timescale of $\tau = 10\,\mathrm{s}$ using a least-squares adaptive law with forgetting factor $\beta = 0.1$, initial gain $\boldsymbol{P}_{0,lsq}$ and initial goal $\hat{g}_0 = 1\,\mathrm{m}$.

Integral Adaptive Law

The integral adaptive law introduced in Section 2.3 poses another possible approach to estimate the parameters of a DMP. Choosing a forgetting factor $\beta = 0.1$, the general version of the integral adaptive law (2.21) simplifies to

$$\begin{aligned}\dot{\hat{\boldsymbol{\theta}}} &= -\boldsymbol{\Gamma}(\boldsymbol{R}(t)\hat{\boldsymbol{\theta}} + \boldsymbol{Q}(t)),\\ \dot{\boldsymbol{R}} &= -\beta\boldsymbol{R} + \boldsymbol{\phi}\boldsymbol{\phi}^\top,\\ \dot{\boldsymbol{Q}} &= -\beta\boldsymbol{Q} - z\boldsymbol{\phi},\end{aligned}$$

with the initial values $\boldsymbol{R}(0) = \boldsymbol{0}$, $\boldsymbol{Q}(0) = \boldsymbol{0}$ and $\hat{\boldsymbol{\theta}}(0) = \hat{\boldsymbol{\theta}}_0$ and the filtered output z from (4.2). For comparability we use (4.5) and choose $\boldsymbol{\Gamma} = \boldsymbol{P}_{0,lsq}$. Simulation is conducted using initial guesses $\hat{g}_0 = 1\,\mathrm{m}$ and $\hat{\tau}_0 = 10\,\mathrm{s}$ while the true values are $g = 2\,\mathrm{m}$ and $\tau = 10\,\mathrm{s}$. Figure 4.3 shows the fast convergence of the goal estimate. Reasonable estimates are already available after about a second. By comparing Figure 4.3 to Figure 4.2, it can be seen that the integral adaptive law gives slightly faster convergence speed. The reason for this observation is, that it allows for tuning of the rate of exponential convergence through the gain $\boldsymbol{\Gamma}$, whereas the least-squares adaptive law only guarantees exponential convergence. However, through tuning of $\boldsymbol{P}(0)$ of the least-squares based adaptive law, similar performance of both adaptive laws could be achieved.

We can see that classically designed adaptive laws can be applied to estimate the goal of human point-to-point motion. A clear weakness of the presented least-squares and integral cost estimation laws from this section is the fact, that the known timescale τ also appears in the parameter vector $\boldsymbol{\theta}$ of the used parameterization

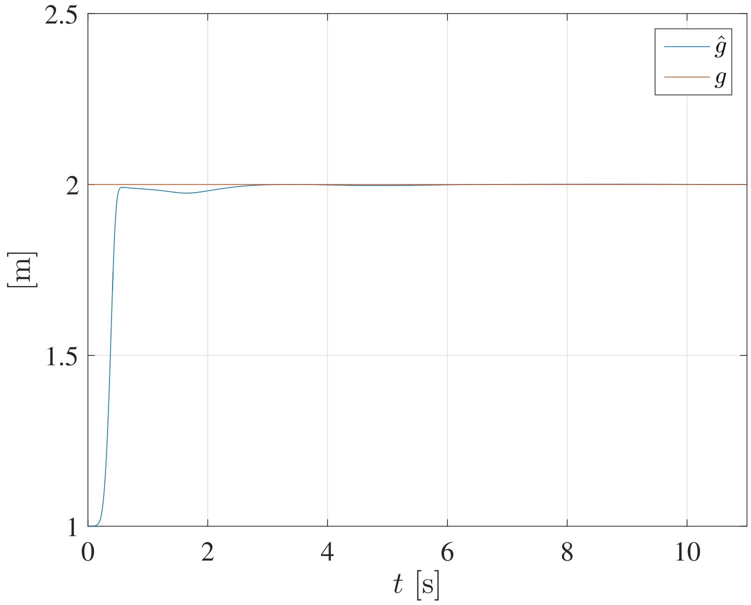

Figure 4.3: Estimation of g for known τ using an integral adaptive law with forgetting factor $\beta = 0.1$, $\boldsymbol{R}_0 = \boldsymbol{0}$, $\boldsymbol{Q}_0 = \boldsymbol{0}$ and $\boldsymbol{\Gamma} = \boldsymbol{P}_{0,lsq}$. The initial guess is $\hat{g}_0 = 1\,\mathrm{m}$.

(4.2). Due to a lower dimension of the parameter vector, faster convergence might be achieved for a linear parametric parameterization of the DMP where only the goal g appears in the parameter vector, as the PE property (2.24) is satisfied more easily for a smaller parameter vector.

A disadvantage of continuous goal estimation based on a known timescale τ is the fact, that in a realistic scenario, it is unlikely that a robot would initially know the duration of a human handover motion. Therefore, it is sensible to treat the timescale τ as an unknown parameter and to try to estimate it alongside the goal g.

4.1.2 Continuous Goal and Timescale Estimation

Treating both goal g and timescale τ as unknown implies that the phase variable x can no longer be produced using the explicit solution (4.3) of the canonical system (2.3). For simplicity, we assume position, velocity and acceleration measurements of the human hand are available in the following. Hence, the linear parametric model from (2.14) simplifies to the unfiltered version

$$\begin{aligned} z = \ddot{y} &= \boldsymbol{\theta}^\top \boldsymbol{\phi}(x) \\ &= \underbrace{\begin{bmatrix} \frac{1}{\tau^2} & \frac{1}{\tau} & \frac{g}{\tau^2} \end{bmatrix}}_{\boldsymbol{\theta}^\top} \underbrace{\begin{bmatrix} -\alpha_z\beta_z y - y_0\tilde{f}(x) \\ -\alpha_z\dot{y} \\ \alpha_z\beta_z + \tilde{f}(x) \end{bmatrix}}_{\boldsymbol{\phi}}, \end{aligned} \tag{4.6}$$

where the information vector $\boldsymbol{\phi}$ is now dependent on the unknown phase variable x.

Dynamical Approximation of the Phase Variable

One approach to estimate the true parameter vector $\boldsymbol{\theta}$ is to combine an adaptive law designed based on the model (4.6) with a simple dynamical system approximating x. Being a simple approach to parameter estimation, the least-squares adaptive law from (2.23) is implemented using a forgetting factor of $\beta = 0.1$. As in Section 4.1.1, we can establish $\boldsymbol{\phi} \in \mathcal{L}_\infty$ and thus choose $m = 1$. Consequently, the least-squares adaptive law simplifies to

$$\dot{\hat{\boldsymbol{\theta}}} = \boldsymbol{P}\epsilon\boldsymbol{\phi}, \tag{4.7}$$

$$\dot{\boldsymbol{P}} = \beta\boldsymbol{P} - \boldsymbol{P}\boldsymbol{\phi}\boldsymbol{\phi}^\top\boldsymbol{P}, \tag{4.8}$$

where

$$\epsilon = z - \hat{z} = \ddot{y} - \hat{\boldsymbol{\theta}}^\top\boldsymbol{\phi} \tag{4.9}$$

is the output error and the initial conditions are $\boldsymbol{P}(0) = \boldsymbol{P}_{0,da}$ and $\hat{\boldsymbol{\theta}}(0) = \hat{\boldsymbol{\theta}}_0$.

A key property of the nonlinear forcing term (2.4) of the DMP formulation from [9] is that it vanishes with time. Hence, the influence of x on the DMP vanishes with time as well. This motivates using a simple and rather rough approximation $\hat{x}$ of x, which can be obtained using the dynamical system

$$\dot{\hat{x}} = -\frac{\alpha_x}{\hat{\tau}}\hat{x} \tag{4.10}$$

with the known initial condition $\hat{x}(0) = x(0) = 1$. System (4.10) can be found by replacing all unknowns in the canonical system (2.3) with their estimates. The estimated timescale $\hat{\tau}$ of the DMP is extracted from the first component $\hat{\theta}_1$ of the current estimate of the parameter vector $\hat{\boldsymbol{\theta}} = [\hat{\theta}_1, \hat{\theta}_2, \hat{\theta}_3]^\top$ from (4.6) through

$$\hat{\tau} = \frac{1}{\sqrt{\hat{\theta}_1}}.$$

Due to the redundancy of $\hat{\tau}$ information in $\hat{\boldsymbol{\theta}}$, both $\hat{\theta}_1$ and $\hat{\theta}_2$ can be used to extract a current estimate of the timescale. Simulations have proven $\hat{\theta}_1$ to converge faster, which makes it better suited for use in (4.10). Note that many ways to exploit this redundancy exist, of which the one chosen here is just a simple one. The approximation $\hat{x}$ of x obtained by (4.10) is fed into the adaptive law (4.7), (4.8) through the information vector $\boldsymbol{\phi}$, whose dependency on $\hat{x}$ is depicted as $\boldsymbol{\phi}(\hat{x})$. The overall dynamical system estimating the parameters $\boldsymbol{\theta}$ is therefore given by (4.10) and the adaptive law from (4.7) and (4.8), with the dependency on the approximation $\hat{x}$ of the phase variable reading,

$$\dot{\hat{\boldsymbol{\theta}}} = \boldsymbol{P}\epsilon\boldsymbol{\phi}(\hat{x}),$$

$$\dot{\boldsymbol{P}} = \beta\boldsymbol{P} - \boldsymbol{P}\boldsymbol{\phi}(\hat{x})\boldsymbol{\phi}(\hat{x})^\top\boldsymbol{P},$$

with the output error ϵ given by (4.9) and initial conditions $\boldsymbol{P}(0) = \boldsymbol{P}_{0,da}$ and

$$\hat{\boldsymbol{\theta}}(0) = \hat{\boldsymbol{\theta}}_0 = \begin{bmatrix} \frac{1}{\hat{\tau}_0^2} & \frac{1}{\hat{\tau}_0} & \frac{\hat{g}_0}{\hat{\tau}_0^2} \end{bmatrix}.$$

The least-squares adaptive law is simulated using $\boldsymbol{P}_{0,da} = \mathrm{diag}([1, 50, 10])$, $\beta = 0.1$ and initial parameter values $\hat{g}_0 = 1\,\mathrm{m}$ and $\hat{\tau}_0 = 9\,\mathrm{s}$, where the measurements y, $\dot{y}$ and $\ddot{y}$ are generated using the training minimum-jerk trajectory (3.5) with true timescale $\tau = 10\,\mathrm{s}$, goal $g = 2\,\mathrm{m}$ and starting point $y_0 = 0\,\mathrm{m}$. The goal and timescale estimates are extracted from the estimated parameter vector $\hat{\boldsymbol{\theta}} = [\hat{\theta}_1, \hat{\theta}_2, \hat{\theta}_3]^\top$ via

$$\hat{\tau}_1 = \frac{1}{\sqrt{\hat{\theta}_1}}, \quad \hat{\tau}_2 = \tfrac{1}{\hat{\theta}_2}, \quad \text{and } \hat{g} = \frac{\hat{\theta}_3}{\hat{\theta}_2^2}.$$

The trajectories of the estimates $\hat{g}$ and $\hat{\tau}_1, \hat{\tau}_2$ are depicted in Figure 4.4. Clearly, neither of the estimates converges to a constant value. However, while $\hat{g}$ stays within $0.2\,\mathrm{m}$ of the true value g after about 4 seconds, $\hat{\tau}_1, \hat{\tau}_2$ do not provide a useful estimate of the timescale of the human motion.

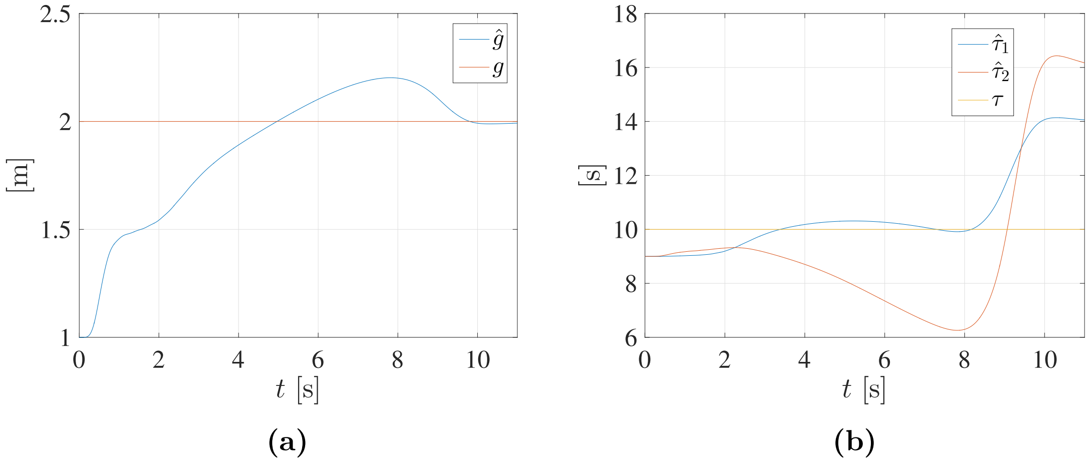

Figure 4.4: On-line estimation of handover position $\hat{g}$ and handover time $\hat{\tau}$ with true values $g = 2\,\mathrm{m}$ and $\tau = 10\,\mathrm{s}$ and initial parameter values $\hat{g}_0 = 1\,\mathrm{m}$ and $\hat{\tau}_0 = 9\,\mathrm{s}$.

A reason for the observed unsatisfying performance is the fact that the information vector $\boldsymbol{\phi}(\hat{x})$ depends on a possibly erroneous estimate $\hat{x}$. The adaptive law then updates the parameter vector $\hat{\boldsymbol{\theta}}$ in a way that minimizes the estimation error based on a wrong information vector. Hence it is not well-suited for large errors in the estimate $\hat{x}$.

As mentioned above, dynamical approximation is a rather rough estimation of the phase variable x. The main cause for this is the fact that, while a dynamical approximation provides relatively smooth estimates $\hat{x}$, errors in the estimated timescale $\hat{\tau}$ accumulate over time due to the dynamical approximation.

Explicit Estimation of the Phase Variable

Another approach to deal with the dependency of the information vector $\boldsymbol{\phi}$ on x is to use the explicit solution of the canonical system (4.3) and by using the current estimate $\hat{\tau}$, produce an estimate $\hat{x}$ through

$$\hat{x}(t) = e^{-\frac{\alpha_x}{\hat{\tau}}t}. \tag{4.12}$$

The benefit of this approach, as opposed to the dynamical approximation, is that a correct estimate $\hat{\tau}$ would yield a correct estimate of the phase variable $\hat{x}$ since (4.12) is an algebraic relation between $\hat{x}$ and $\hat{\tau}$. Hence, past errors in $\hat{\tau}$ do not affect the current estimate $\hat{x}$.

Substituting x with its estimate $\hat{x}$ and $\boldsymbol{\theta}$ with its estimate $\hat{\boldsymbol{\theta}}$ in (4.6) yields

$$\begin{aligned} \hat{z} &= \hat{\boldsymbol{\theta}}^\top \boldsymbol{\phi}(\hat{x}) \\ &= \begin{bmatrix} \frac{1}{\hat{\tau}^2} & \frac{1}{\hat{\tau}} & \frac{\hat{g}}{\hat{\tau}^2} \end{bmatrix} \begin{bmatrix} -\alpha_z \beta_z y - y_0 \tilde{f}(\hat{x}) \\ -\alpha_z \dot{y} \\ \alpha_z \beta_z + \tilde{f}(\hat{x}) \end{bmatrix}. \end{aligned} \tag{4.13}$$

Plugging relation (4.12) into (4.13) yields the measurement model producing the estimated output

$$\hat{z}(t) = \hat{\boldsymbol{\theta}}^\top \boldsymbol{\phi}(t, \hat{\boldsymbol{\theta}}).$$

Clearly, this measurement model is nonlinear in the parameters. A quite simple and straightforward approach to change (4.13) in a way that renders it linear in the parameters is to neglect the dependency of $\boldsymbol{\phi}$ on the parameter estimate $\hat{\boldsymbol{\theta}}$. Even though this clearly is a very rough approximation, the forcing term f vanishes with time and hence the dependency of $\boldsymbol{\phi}$ on $\hat{\boldsymbol{\theta}}$ recedes with time as well. While estimates will probably be bad in the beginning, convergence to the true parameters is expected over time.

We apply the least-squares based adaptive law from (2.23) designed for a linear parametric model using $\beta = 0.1$, initial gain $\boldsymbol{P}_{0,ee} =$ diag$([100, 5000, 1000])$, true values $g = 2\,\mathrm{m}$, $\tau = 10\,\mathrm{s}$ and initial parameter values $\hat{g}_0 = 1\,\mathrm{m}$, $\hat{\tau}_0 = 9\,\mathrm{s}$ as before. The resulting trajectories are shown in Figure 4.5. The parameter estimates clearly do not converge at all. Neglecting the dependency of $\boldsymbol{\phi}$ on $\hat{\boldsymbol{\theta}}$ proofs to be a heavy assumption. As before, the vanishing influence of the forcing term is not enough to obtain a converging parameter estimation scheme through the presented simplifications of the model.

The adaptive laws presented in this section clearly have not proven to be able to cope with the nonlinearities in the parameters. Instead of neglecting the dependency of the information vector on the parameters, a different approach is to linearize the nonlinearities around the current estimate, as it is done in extended Kalman filters.

4.2 EKF-Based Parameter Estimation of DMPs

The estimation of the parameters of a DMP can be put into a state estimation context by simply including the unknown parameters in the state vector of an observer. In the presence of nonlinear models, a common approach for state estimation is to use EKFs. EKFs are popular due to their relatively easy implementation, their optimality for linear systems and their efficiency in a lot of practical problems [17]. Different versions of EKFs can be found in literature. In this thesis we present the application of both the classical EKF and a modified EKF with enhanced convergence speed.

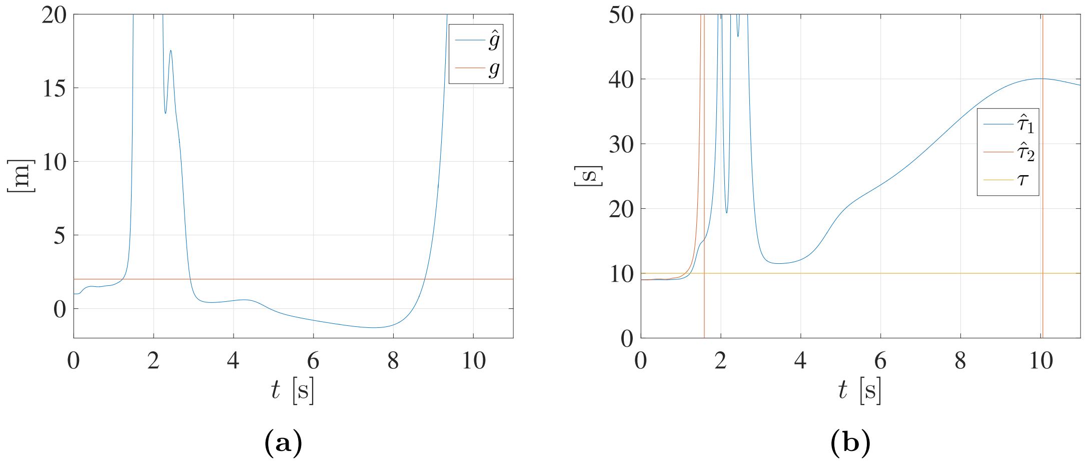

(a) **(b)**

Figure 4.5: On-line estimation of handover position $\hat{g}$ and handover time $\hat{\tau}$ with true values $g = 2\,\mathrm{m}$, $\tau = 10\,\mathrm{s}$ and initial parameter estimates $\hat{g}_0 = 1\,\mathrm{m}$, $\hat{\tau}_0 = 9\,\mathrm{s}$ using explicit estimation of x and a least-squares adaptive law with $\beta = 0.1$ and $\boldsymbol{P}_{0,ee} =$ diag$([100, 5000, 1000])$.

4.2.1 Classical EKF-Based State Estimation

Initially, we use a classical EKF state estimation approach to estimate the unknown parameters of the DMP.

Observer Formulation

To estimate the unknown goal g and timescale τ of the DMP formulation (3.3) and deal with the nonlinearities in the parameters g and τ, we introduce the state vector

$$\boldsymbol{x} = \begin{bmatrix} x & y & z & g & \tau \end{bmatrix}^\top \tag{4.14}$$

and write the nonlinear system consisting of the DMP dynamics and the parameter dynamics as

$$\begin{aligned} \dot{\boldsymbol{x}} &= \boldsymbol{f}(\boldsymbol{x}) \\ \Leftrightarrow \begin{bmatrix} \dot{x} \\ \dot{y} \\ \dot{z} \\ \dot{g} \\ \dot{\tau} \end{bmatrix} &= \begin{bmatrix} -\frac{\alpha_x}{\tau} x \\ z \\ \alpha_z \left(\frac{\beta_z}{\tau^2}(g - y) - \frac{z}{\tau} \right) + \frac{f(x,g)}{\tau^2} \\ 0 \\ 0 \end{bmatrix}. \end{aligned} \tag{4.15}$$

Assuming position y and velocity $\dot{y}$ are measurable, we obtain the linear measurement model

$$\boldsymbol{y} = \boldsymbol{h}(\boldsymbol{x}) = \boldsymbol{C}\boldsymbol{x}, \tag{4.16}$$

with

$$\boldsymbol{C} = \begin{bmatrix} 0 & 1 & 0 & 0 & 0 \\ 0 & 0 & 1 & 0 & 0 \end{bmatrix}. \tag{4.17}$$

Plugging the process model (4.15) and the measurement model (4.16) into the update law (2.29) from the EKF formulation yields the update equation

$$\dot{\hat{\boldsymbol{x}}} = \boldsymbol{f}(\hat{\boldsymbol{x}}) + \boldsymbol{K}(t)(\boldsymbol{y} - \boldsymbol{C}\boldsymbol{x}), \tag{4.18}$$

where

$$\hat{\boldsymbol{x}} = \begin{bmatrix} \hat{x} & \hat{y} & \hat{z} & \hat{g} & \hat{\tau} \end{bmatrix}^\top \tag{4.19}$$

is the estimate of the state vector $\boldsymbol{x}$. The initial condition $x(0) = 1$ is known by construction of the DMP. As we consider human point-to-point motion, the trajectories of the human hand can be assumed to start at $y(0) = y_0 = 0$ with zero velocity $z(0) = 0$. Consequently, the initial estimate is set to

$$\begin{aligned} \hat{\boldsymbol{x}}(0) &= \begin{bmatrix} x(0) & y(0) & z(0) & \hat{g}(0) & \hat{\tau}(0) \end{bmatrix}^\top \\ &= \begin{bmatrix} 1 & 0 & 0 & \hat{g}_0 & \hat{\tau}_0 \end{bmatrix}^\top, \end{aligned} \tag{4.20}$$

where $\hat{g}_0$ and $\hat{\tau}_0$ are initial estimates for goal g and timescale τ. In the classical EKF, the time-variant Kalman gain is set to

$$\boldsymbol{K}(t) = \boldsymbol{P}(t)\boldsymbol{C}^\top \boldsymbol{R}^{-1}, \tag{4.21}$$

where $\boldsymbol{P}(t)$ is the solution of the Riccati differential equation

$$\dot{\boldsymbol{P}}(t) = \boldsymbol{A}(\hat{\boldsymbol{x}})\boldsymbol{P}(t) + \boldsymbol{P}(t)\boldsymbol{A}(\hat{\boldsymbol{x}})^\top + \boldsymbol{Q} - \boldsymbol{P}(t)\boldsymbol{C}^\top \boldsymbol{R}^{-1}\boldsymbol{C}\boldsymbol{P}(t), \tag{4.22}$$

with positive definite covariance matrices $\boldsymbol{Q}$ and $\boldsymbol{R}$ for process and measurement noise respectively. The initial condition of the Riccati differential equation (4.22) is set to $\boldsymbol{P}(0) = \boldsymbol{P}_0$, with $\boldsymbol{P}_0$ being a positive definite matrix ensuring (2.34). The linearized system matrix $\boldsymbol{A}(\hat{\boldsymbol{x}})$ is obtained through linearization of $\boldsymbol{f}$ around the current estimate $\hat{\boldsymbol{x}}$,

$$\begin{aligned} \boldsymbol{A}(\hat{\boldsymbol{x}}) &= \left.\frac{\partial \boldsymbol{f}(\boldsymbol{x})}{\partial \boldsymbol{x}}\right|_{\boldsymbol{x}=\hat{\boldsymbol{x}}} \\ &= \left.\begin{bmatrix} -\frac{\alpha_x}{\tau} & 0 & 0 & 0 & \frac{\alpha_x}{\tau^2}x \\ 0 & 0 & 1 & 0 & 0 \\ \frac{1}{\tau^2}\frac{\partial f(x,g)}{\partial x} & -\frac{\alpha_z\beta_z}{\tau^2} & -\frac{\alpha_z}{\tau} & \frac{1}{\tau^2}(\alpha_z\beta_z + \frac{\partial f(x,g)}{\partial g}) & A_{35} \\ 0 & 0 & 0 & 0 & 0 \\ 0 & 0 & 0 & 0 & 0 \end{bmatrix}\right|_{\boldsymbol{x}=\hat{\boldsymbol{x}}}, \end{aligned} \tag{4.23}$$

with

$$A_{35} = \frac{\alpha_z z}{\tau^2} - \frac{2}{\tau^3}\left(\alpha_z\beta_z(g-y) + f(x,g)\right),$$

where for $y_0 = 0$ from (4.20), by using (3.2) we obtain

$$\frac{\partial f}{\partial g}(x,g) = \tilde{f}(x) = \frac{\sum_{i=1}^N \Psi_i(x)w_i}{\sum_{i=1}^N \Psi_i(x)}x$$

and

$$\frac{\partial f}{\partial x}(x, g) = g\tilde{f}'(x) \tag{4.24}$$

with

$$\begin{aligned}\tilde{f}'(x) = & \frac{\sum_{i=1}^{N} \Psi_i(x) w_i}{\sum_{i=1}^{N} \Psi_i(x)} \\ & + x \frac{\left(\sum_{i=1}^{N} \Psi_i'(x) w_i\right)\left(\sum_{i=1}^{N} \Psi_i(x)\right) - \left(\sum_{i=1}^{N} \Psi_i(x) w_i\right)\left(\sum_{i=1}^{N} \Psi_i'(x)\right)}{\left(\sum_{i=1}^{N} \Psi_i(x)\right)^2},\end{aligned} \tag{4.25}$$

and

$$\Psi_i'(x) = -2h_i(x - c_i)\Psi_i(x),$$

where c_i are the centers (3.7) and h_i set the widths (3.8) of the basis functions Ψ_i.

Stability

To ensure convergence, a number of assumptions for the stability of the classical EKF have to hold. For simplicity we initially assume that Assumption 1 holds. Additionally, the nonlinearities have to satisfy the Lipschitz properties from Assumption 2. As the measurement model (4.16) is linear, the inequality (2.36),

$$\left\| \frac{\partial^2 \boldsymbol{h}}{\partial^2 \boldsymbol{x}}(\boldsymbol{x}, t) \right\|_* \leq \kappa_C,$$

with $\|\hat{\boldsymbol{x}} - \boldsymbol{x}\| \leq \kappa_z$, holds for arbitrary $\kappa_z > 0$ and $\kappa_C = 0$ for all $t \geq 0$.

For the right-hand side $\boldsymbol{f}(\boldsymbol{x})$ of the nonlinear DMP model (4.15), inequality (2.35),

$$\left\| \frac{\partial^2 \boldsymbol{f}}{\partial^2 \boldsymbol{x}}(\boldsymbol{x}, t) \right\|_* \leq \kappa_A, \tag{4.26}$$

has to hold for some positive κ_z, κ_A with $\|\hat{\boldsymbol{x}} - \boldsymbol{x}\| \leq \kappa_z$. Inequality (4.26) holds locally if all elements of $\partial \boldsymbol{f}/\partial \boldsymbol{x} = \boldsymbol{A}(\boldsymbol{x})$ are locally Lipschitz continuous. Clearly, all linear terms in (4.23) are Lipschitz. It remains to check the appearing nonlinear terms f, $\partial f/\partial x$ and $\partial f/\partial g$ for local Lipschitz continuity. According to Lemma 3.1 from [25], a function $f : [a, b] \times D \to \mathcal{R}^m$, with $D \subset \mathcal{R}^m$, whose derivative $\partial f/\partial x$ exists and is continuous on $[a, b] \times D$ is locally Lipschitz on $I = [a, b] \times W$ where W is a convex subset of D, if its derivative $\partial f/\partial x$ is bounded by some Lipschitz constant $L \geq 0$ on I. To check Lipschitz continuity of $\partial f/\partial x$, using (4.24), we calculate

$$\frac{\partial}{\partial \boldsymbol{x}}\left(\frac{\partial f}{\partial x}\right) = \begin{bmatrix} g\tilde{f}'' & 0 & 0 & \tilde{f}' & 0 \end{bmatrix}. \tag{4.27}$$

The basis functions Ψ_i from (2.6) are Gaussians and thus bounded functions for all x. In other words $\Psi_i \in \mathcal{L}_\infty$. Additionally, the weights w_i are also bounded by construction. Moreover, as Ψ_i are Gaussians, the derivatives Ψ_i' and Ψ_i'' exist, are continuous and it is also $\Psi_i', \Psi_i'' \in \mathcal{L}_\infty$. Hence, we have

$$\left(\sum_{i=1}^{N} \Psi_i^{(n_d)} w_i\right) \in \mathcal{L}_\infty, \tag{4.28}$$

$$\left(\sum_{i=1}^{N} \Psi_i^{(n_d)}\right) \in \mathcal{L}_\infty \text{ for } n_d = 0, 1, 2. \tag{4.29}$$

Consequently, the numerators in (4.25) are all bounded. To ensure boundedness of $\tilde{f}'$, it remains to show that the denominators are lower bounded by some constant. As x is the phase variable and it is $x \in [0, 1] = I_x$, we can ensure a lower bound $\kappa_\Psi > 0$ for

$$\sum_{i=1}^{N} \Psi_i(\hat{x}) \geq \kappa_\Psi \tag{4.30}$$

on a convex set I_{lb} with $I_x \subseteq I_{lb}$ for estimates $\hat{x}$ close to x by choosing a sufficiently large number of basis functions N as well as basis function parameters h_i and c_i that ensure overlap between the basis functions and a large enough I_{lb}.

To illustrate this argumentation, the boundedness properties are shown in Figure 4.6 for $N = 30$ basis functions, width settings h_i from (3.8) and centers c_i from (3.7). We see that for the presented case, we can choose $\kappa_\Psi = 0.5$ and $I_{lb} = [0, 1.1]$ such that (4.30) is satisfied. Therefore, we can conclude local boundedness of $\tilde{f}'$. To show that $\partial/\partial \boldsymbol{x}\,(\partial f/\partial x)$ given by (4.27) is bounded, we continue by computing

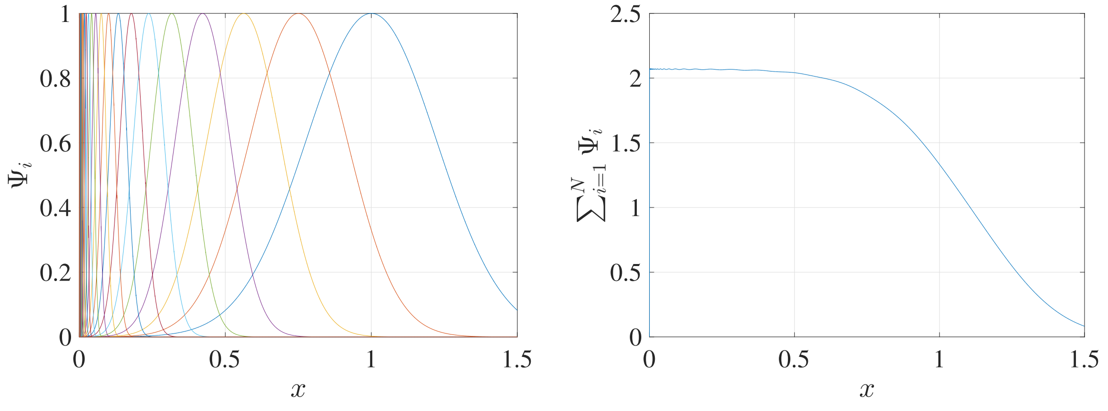

(a) Spacing of basis functions Ψ_i in x **(b)** Sum of basis functions Ψ_i

Figure 4.6: Illustration of the boundedness of the basis functions Ψ_i and their sum $\sum_{i=1}^{N} \Psi(x)$ for $N = 30$ basis functions, width parameters h_i and exponentially spaced centers c_i.

$$\tilde{f}''(x) = \tilde{h}(x) + x\tilde{g}(x), \tag{4.31}$$

where the lengthy expressions $\tilde{h}(x)$ and $\tilde{g}(x)$ are given Section A.1. Again, we can use (4.28), (4.29) and (4.30) to establish local boundedness of $\tilde{h}$ and $\tilde{g}$ and thus conclude local boundedness of $\tilde{f}''$ via (4.31). With that and (4.27), it is

$$\left\| \frac{\partial}{\partial \boldsymbol{x}} \left(\frac{\partial f}{\partial x} \right) \right\| = \left\| \begin{bmatrix} g\tilde{f}'' & 0 & 0 & \tilde{f}' & 0 \end{bmatrix} \right\| \leq L_x$$

for some $L_x > 0$ in a neighborhood of $\boldsymbol{x}$. Thus, $\partial f / \partial x$ is locally Lipschitz, which also implies that f is locally Lipschitz.

Similarly, thanks to the local boundedness of $\tilde{f}'$ shown above, we get

$$\left\| \frac{\partial}{\partial \boldsymbol{x}} \left(\frac{\partial f}{\partial g} \right) \right\| = \left\| \begin{bmatrix} \tilde{f}' & 0 & 0 & 0 & 0 \end{bmatrix} \right\| \leq L_g$$

for some $L_g > 0$ in a neighborhood of $\boldsymbol{x}$. Consequently, $\partial f / \partial g$ is locally Lipschitz as well, which means that Assumption 2 holds. Hence the assumptions ensuring local stability of the EKF are satisfied.

Implementation

The EKF consisting of (4.18), (4.21) and (4.22) is implemented using the initial guess (4.20) with $\hat{g}_0 = 1\,\mathrm{m}$ and $\hat{\tau}_0 = 9\,\mathrm{s}$ for the true values $g = 2\,\mathrm{m}$ and $\tau = 10\,\mathrm{s}$. Choosing an initial covariance of $\boldsymbol{P}_0 = 10^6 \boldsymbol{I}$ as well as matrices $\boldsymbol{R} = \boldsymbol{I}$ and $\boldsymbol{Q} = \mathrm{diag}([0.1, 0.1, 0.1, 10^4, 10^4])$ yields the convergence results shown in Figure 4.7. The measurements y and $\dot{y}$ are produced using the minimum-jerk trajectory (3.5) and its first derivative.

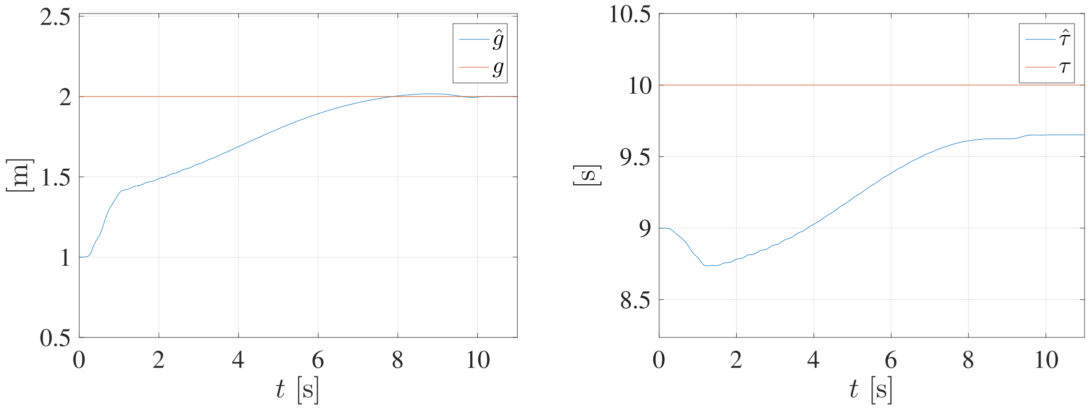

(a) **(b)**

Figure 4.7: On-line estimation of handover position $\hat{g}$ and handover time $\hat{\tau}$ with true values $g = 2\,\mathrm{m}$ and $\tau = 10\,\mathrm{s}$ and initial parameter estimates $\hat{g}_0 = 1\,\mathrm{m}$ and $\hat{\tau}_0 = 9\,\mathrm{s}$ using a classical EKF.

We observe, that while the estimate $\hat{g}$ slowly converges to the true g, the estimated timescale $\hat{\tau}$ does not completely converge to the true τ. This error can be decreased by increasing $\boldsymbol{P}_0$ even more. Since we use the same minimum-jerk trajectory as in Section 4.1, the measurements still have the same level of excitation as before. However, we now estimate a five-dimensional state vector, as opposed to the three-dimensional parameter vector from (4.6) in Section 4.1. Consequently, the observed slow convergence is expected for larger estimation problems since more unknowns have to be estimated using the same amount of information. Generally, it can be observed that the estimates mostly improve towards the end of the motion as the effect of the nonlinearity vanishes. In Figure 4.8 the remaining elements of $\hat{\boldsymbol{x}}$ can be seen. As y and $z = \dot{y}$ are measured, their estimates $\hat{y}$ and $\hat{z}$ coincide. The estimate of the phase variable, however, deviates from the true value x during the first few seconds of motion.

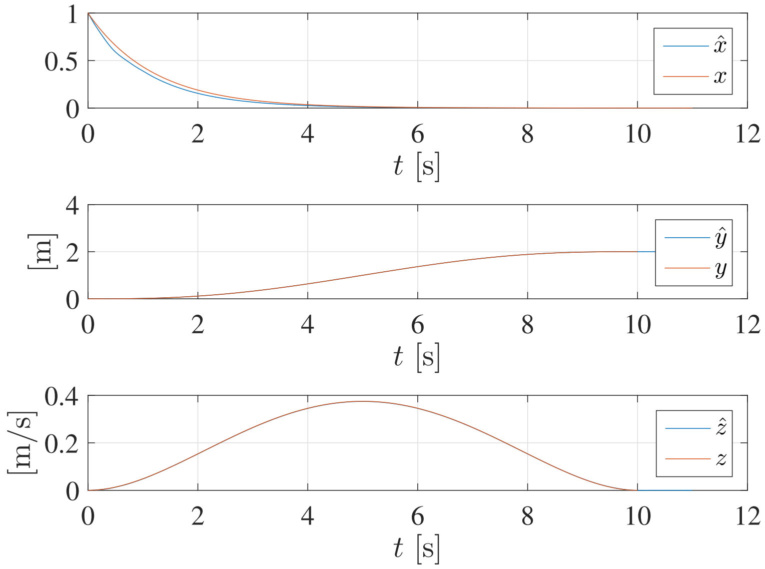

Figure 4.8: Estimated DMP states using a classical EKF.

Following the recommendation from [19], the lower and upper bounds $\underline{p}_c$ and $\overline{p}_c$ of $\boldsymbol{P}(t)$ are illustrated in Figure 4.9. Clearly, Assumption 1 holds for the time interval of the present case, meaning stability of the EKF was ensured for this case. While it might seem inconvenient to not be able to ensure the detectability-related Assumption 1 in advance, it is at least possible to use the bounds $\underline{p}_c$ and $\overline{p}_c$ as a measure of how reliable the estimations of goal and timescale are at time t. If the bounds ensure that Assumption 1 holds, the robot can treat the estimations as reliable.

In order to allow a robot to receive an object in a human-like manner, it is important that the estimation of the handover place and time converge fast enough to make sure there is enough time left for the robot to move to the estimated handover position. The estimation scheme based on a classical EKF presented in this section however is rather slow to converge for the convergence parameters chosen. For faster convergence either a higher initial covariance $\boldsymbol{P}_0$ or a different observer design has to be chosen.

4.2.2 Modified EKF-Based State Estimation

A modified version of the EKF was presented by [21]. It allows to design an EKF with prescribed degree of stability, meaning that the convergence speed can be tuned

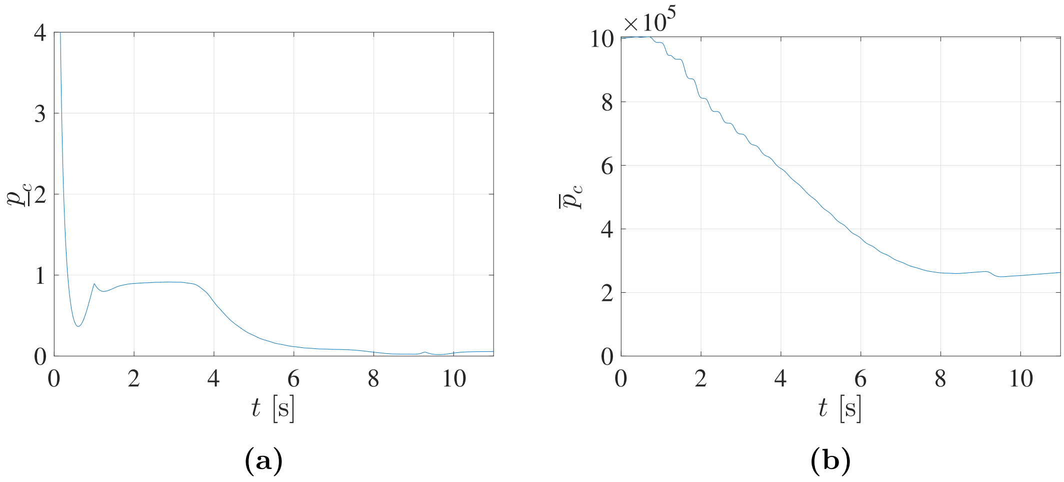

Figure 4.9: Lower bound $\underline{p}_c(t)$ and upper bound $\overline{p}_c(t)$ of $\boldsymbol{P}(t)$ using a classical EKF to estimate the states of an original DMP.

via a special parameter.

Observer Formulation

Similar to the classical EKF above, we use the estimated state vector (4.19) and the DMP model (4.15) with the measurement model (4.16). Following [21], the modified EKF is given by the update law (4.18), the Kalman gain (4.21) and the modified Riccati equation

$$\begin{aligned}\dot{\boldsymbol{P}}(t) = (\boldsymbol{A}(\hat{\boldsymbol{x}}) + \alpha\boldsymbol{I})\boldsymbol{P}(t) + \boldsymbol{P}(t)(\boldsymbol{A}(\hat{\boldsymbol{x}})^\top + \alpha\boldsymbol{I}) + \boldsymbol{Q}\\ -\boldsymbol{P}(t)\boldsymbol{C}^\top\boldsymbol{R}^{-1}\boldsymbol{C}\boldsymbol{P}(t),\end{aligned} \tag{4.32}$$

which is obtained by plugging (4.17) and (4.23) into (2.40). Compared to the Riccati equation (4.22) of the classical EKF, equation (4.32) features the added term of instability $\alpha\boldsymbol{I}$. It is $\alpha > 0$, and $\boldsymbol{Q}$, $\boldsymbol{R}$ are positive definite matrices, as explained in Section 2.4.2. Again the linearization $\boldsymbol{A}(\hat{\boldsymbol{x}})$ around the current estimate (4.23) is used. As in the classical case, we use (4.20) as an initial estimate and the initial condition $\boldsymbol{P}(0) = \boldsymbol{P}_0$ for the Riccati equation (4.32).

Stability

For the modified version of the EKF to be stable, we initially assume that Assumption 1, related to uniform detectability properties of the system, holds.

It can easily be seen that the output matrix $\boldsymbol{C}$ from (4.17) satisfies the boundedness condition (2.43) since $\boldsymbol{C}$ is constant. Consequently, Assumption 4 holds.

The nonlinearities

$$\boldsymbol{\Phi}(\boldsymbol{x}, \hat{\boldsymbol{x}}) = \boldsymbol{f}(\boldsymbol{x}) - \boldsymbol{f}(\hat{\boldsymbol{x}}) - \boldsymbol{A}(\hat{\boldsymbol{x}})(\boldsymbol{x} - \hat{\boldsymbol{x}}), \tag{4.33}$$

$$\boldsymbol{\Psi}(\boldsymbol{x}, \hat{\boldsymbol{x}}) = \boldsymbol{h}(\boldsymbol{x}) - \boldsymbol{h}(\hat{\boldsymbol{x}}) - \boldsymbol{C}(\boldsymbol{x} - \hat{\boldsymbol{x}}) = \boldsymbol{0}, \tag{4.34}$$

have to satisfy Assumption 3. As the measurement model (4.16) is linear, (4.34) is zero and thus,

$$\|\boldsymbol{\Psi}(\boldsymbol{x}, \hat{\boldsymbol{x}})\| \leq \kappa_{\Psi} \|\boldsymbol{x} - \hat{\boldsymbol{x}}\|^2,$$

from (2.41) holds for all $\epsilon_{\Psi} > 0$ with $\|\boldsymbol{x} - \hat{\boldsymbol{x}}\| \leq \epsilon_{\Psi}$. To show that (4.33) satisfies

$$\|\boldsymbol{\Phi}(\boldsymbol{x}, \hat{\boldsymbol{x}})\| \leq \kappa_{\Phi} \|\boldsymbol{x} - \hat{\boldsymbol{x}}\|^2,$$

from (2.41) for some $\epsilon_{\Phi} > 0$ and $\|\boldsymbol{x} - \hat{\boldsymbol{x}}\| \leq \epsilon_{\Phi}$, we simply use the fact that $\partial \boldsymbol{f} / \partial \boldsymbol{x}$ is locally Lipschitz as shown in Section 4.2.1. Reordering (4.33) yields

$$\boldsymbol{f}(\boldsymbol{x}) = \boldsymbol{f}(\hat{\boldsymbol{x}}) + \boldsymbol{A}(\hat{\boldsymbol{x}})(\boldsymbol{x} - \hat{\boldsymbol{x}}) + \boldsymbol{\Phi}(\boldsymbol{x}, \hat{\boldsymbol{x}}). \tag{4.35}$$

Considering the norm of the second derivative of (4.35) with respect to $\boldsymbol{x}$, we use (4.26) and obtain

$$\left\| \frac{\partial^2}{\partial \boldsymbol{x}^2} \boldsymbol{f}(\boldsymbol{x}) \right\| = \left\| \frac{\partial^2}{\partial \boldsymbol{x}^2} \boldsymbol{\Phi}(\boldsymbol{x}, \hat{\boldsymbol{x}}) \right\| \leq \kappa_A. \tag{4.36}$$

Thus, using the monotony of the integral, integration of (4.36) yields

$$\|\boldsymbol{\Phi}(\boldsymbol{x}, \hat{\boldsymbol{x}})\| \leq \kappa_A \|\boldsymbol{x} - \hat{\boldsymbol{x}}\|^2$$

for some $\epsilon_{\Phi} > 0$ and $\|\boldsymbol{x} - \hat{\boldsymbol{x}}\| \leq \epsilon_{\Phi}$ and consequently Assumption 3 is satisfied.

Implementation

Implementation of the modified EKF is similar to the classical version of the EKF. As before, the EKF consists of the update law (4.18) and the gain (4.21). However, now the matrix $\boldsymbol{P}(t)$ is the solution of the modified Riccati differential equation (4.32).

As with the classical EKF from above, we use $\hat{g}_0 = 1\,\mathrm{m}$, $\hat{\tau}_0 = 9\,\mathrm{s}$ and $g = 2\,\mathrm{m}$, $\tau = 10\,\mathrm{s}$. Simulation results using $\alpha = 0.5$, an initial covariance of $\boldsymbol{P}_0 = 10^6 \boldsymbol{I}$ as well as matrices $\boldsymbol{R} = \boldsymbol{I}$ and $\boldsymbol{Q} = \mathrm{diag}([0.1, 0.1, 0.1, 10^4, 10^4])$ are plotted in Figure 4.10. As before, the measurements y and $\dot{y}$ are obtained from (3.5) and its first derivative, which can be seen in Figure 3.2. Convergence to the true values after about 5 s can be observed. While the goal estimate $\hat{g}$ reaches the true value very precisely as seen in Figure 4.10a, the timescale estimate $\hat{\tau}$ in Figure 4.10b exhibits some small deviation from the true τ. Figure 4.11 depicts the remaining elements of the state estimate $\hat{\boldsymbol{x}}$. While the measured signals y and z coincide with their respective estimates $\hat{y}$ and $\hat{z}$, there is a vanishing estimation error for $\hat{x}$ present for the first 4 seconds.

Similar to the classical EKF case, the lower and upper bounds $\underline{p}_c$ and $\overline{p}_c$ of $\boldsymbol{P}(t)$ are illustrated in Figure A.1. Clearly, Assumption 1 holds for the time-instances of the present case, meaning stability of the EKF was ensured.

The obtained simulation results verify that the presented modified EKF is able to provide good estimates for the goal g and the timescale τ. After slightly more than half the duration of motion, $\hat{g}$ and $\hat{\tau}$ are close enough to their true values for

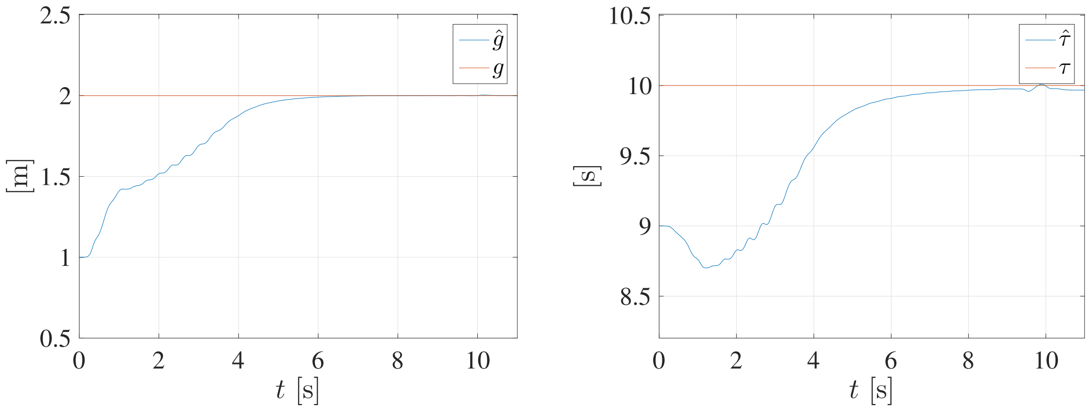

(a) **(b)**

Figure 4.10: On-line estimation of handover position $\hat{g}$ and handover time $\hat{\tau}$ with true values $g = 2\,\mathrm{m}$ and $\tau = 10\,\mathrm{s}$ and initial parameter values $\hat{g}_0 = 1\,\mathrm{m}$ and $\hat{\tau}_0 = 9\,\mathrm{s}$ using a modified EKF with $\alpha = 0.5$.

the robot to start moving towards the predicted handover position at a speed fitting the predicted handover time. Faster convergence can be obtained by choosing larger α and $\boldsymbol{P}_0$. However, it is important to note that excessively large values of α can introduce significant oscillation to the system, possibly resulting in poor accuracy of the estimates. Similar behaviors have also been observed by [21].

4.2.3 Modified EKF-Based Parameter Estimation

As the main objective is to estimate place and time of a human-robot handover action, we are actually only interested in estimating the goal g and the timescale τ. To deal with the nonlinearity in the DMP model, it is possible to obtain an EKF-based adaptive law similar to those presented in [12] by using the methodology of the modified EKF from [21].

Unfiltered Adaptive Law

To begin with, we assume y, $\dot{y}$, $\ddot{y}$ are measurable. Plugging the explicit solution of the canonical system (2.3),

$$x(t) = e^{-\frac{\alpha_x}{\tau}t}, \tag{4.37}$$

into the DMP representation (3.3), we obtain

$$\begin{aligned}\ddot{y}(t) &= h(\boldsymbol{\theta}, y(t), \dot{y}(t), t)\\ &= \frac{1}{\tau^2}(-\alpha_z\beta_z y(t) - \alpha_z\tau\dot{y}(t) + \alpha_z\beta_z g + f_t(g,\tau,t)),\end{aligned} \tag{4.38}$$

where f_t is an expression of the nonlinear forcing term that explicitly depends on time rather than the phase variable x and is obtained by plugging (4.37) into the nonlinear forcing term (2.4). We introduce the state vector

$$\boldsymbol{\theta} = \begin{bmatrix} g & \tau \end{bmatrix}^\top,$$

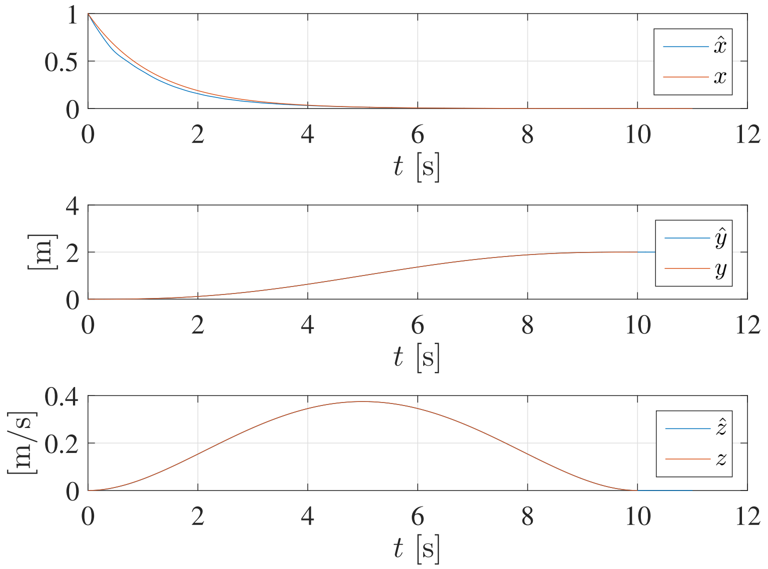

Figure 4.11: Estimated DMP states using a modified EKF.

which only consists of desired parameters and is thus smaller than in (4.14) where all states of the DMP are estimated. As both g and τ can be assumed constant, we can design a modified EKF for the random-walk process model

$$\dot{\boldsymbol{\theta}} = \mathbf{0} \tag{4.39}$$

and (4.38) as a nonlinear measurement model. Following Section 2.4 and using the estimate

$$\hat{\boldsymbol{\theta}} = \begin{bmatrix} \hat{g} & \hat{\tau} \end{bmatrix}$$

we therefore get

$$\boldsymbol{A}(\hat{\boldsymbol{\theta}}) = \mathbf{0}$$

and

$$\begin{aligned} \boldsymbol{C}(\hat{\boldsymbol{\theta}}, t) &= \frac{\partial h}{\partial \boldsymbol{\theta}}(\boldsymbol{\theta}, t)\bigg|_{\boldsymbol{\theta}=\hat{\boldsymbol{\theta}}} \\ &= \begin{bmatrix} \frac{\partial h}{\partial g} & \frac{\partial h}{\partial \tau} \end{bmatrix}\bigg|_{\boldsymbol{\theta}=\hat{\boldsymbol{\theta}}}, \end{aligned} \tag{4.40}$$

where the partial derivatives are

$$\frac{\partial h}{\partial g} = \frac{\alpha_z \beta_z}{\tau^2} + \frac{1}{\tau^2} \frac{\partial f_t(g, \tau, t)}{\partial g} \tag{4.41}$$

and

$$\frac{\partial h}{\partial \tau} = -\frac{2}{\tau^3} \left(\alpha_z \left(\beta_z (g - y)\right) + f_t(g, \tau, t)\right) + \frac{1}{\tau^2} \left(\dot{y} + \frac{\partial f_t(g, \tau, t)}{\partial \tau}\right), \tag{4.42}$$

with the partial derivatives of the forcing term

$$\frac{\partial f_t(g,\tau,t)}{\partial g} = \tilde{f}_t(\tau,t) = \tilde{g}_t(\tau,t)e^{-\frac{\alpha_x}{\tau}t}$$

and

$$\frac{\partial f_t(g,\tau,t)}{\partial \tau} = \tilde{g}_t(\tau,t)\frac{\alpha_x}{\tau^2}te^{-\frac{\alpha_x}{\tau}t} + \frac{\partial \tilde{g}_t(\tau,t)}{\partial \tau}e^{-\frac{\alpha_x}{\tau}t},$$

where

$$\tilde{g}_t(\tau,t) = \frac{\sum_{i=1}^{N}\Psi_i(\tau,t)w_i}{\sum_{i=1}^{N}\Psi_i(\tau,t)},$$

$$\frac{\partial \tilde{g}_t(\tau,t)}{\partial \tau} = \frac{\left(\sum_{i=1}^{N}\partial_\tau\Psi_i(\tau,t)w_i\right)\left(\sum_{i=1}^{N}\Psi_i(\tau,t)\right) - \left(\sum_{i=1}^{N}\Psi_i(\tau,t)w_i\right)\left(\sum_{i=1}^{N}\partial_\tau\Psi_i(\tau,t)\right)}{\left(\sum_{i=1}^{N}\Psi_i(\tau,t)\right)^2}.$$

The basis functions are

$$\Psi_i(\tau,t) = \exp\left(-h_i(e^{-\frac{\alpha_x}{\tau}t} - c_i)^2\right),$$

and their partial derivatives read

$$\partial_\tau\Psi_i(\tau,t) = \frac{\partial \Psi_i(\tau,t)}{\partial \tau} = \Psi_i(\tau,t)(-2h_i)\left(e^{-\frac{\alpha_x}{\tau}t} - c_i\right)e^{-\frac{\alpha_x}{\tau}t}\frac{\alpha_x}{\tau^2}t.$$

Using (2.39) and (2.40) the parameter estimator is then given by

$$\dot{\hat{\boldsymbol{\theta}}} = \boldsymbol{P}\boldsymbol{C}(\hat{\boldsymbol{\theta}},t)\epsilon_{uf}\boldsymbol{R}^{-1}, \tag{4.43}$$

$$\dot{\boldsymbol{P}} = \boldsymbol{Q} - \boldsymbol{P}\boldsymbol{C}(\hat{\boldsymbol{\theta}},t)^\top\boldsymbol{R}^{-1}\boldsymbol{C}(\hat{\boldsymbol{\theta}},t)\boldsymbol{P} + 2\alpha\boldsymbol{P}, \tag{4.44}$$

with the unfiltered scalar output error

$$\epsilon_{uf} = \left(\ddot{y} - h(\hat{\boldsymbol{\theta}}, y(t), \dot{y}(t), t)\right), \tag{4.45}$$

initial guess

$$\hat{\boldsymbol{\theta}}(0) = \begin{bmatrix} g_0 & \tau_0 \end{bmatrix}^\top, \tag{4.46}$$

measurement and process noise covariance matrices $\boldsymbol{R}, \boldsymbol{Q} > 0$ and initial covariance matrix

$$\boldsymbol{P}(0) = \boldsymbol{P}_0. \tag{4.47}$$

To guarantee stability, the assumptions made in the modified EKF case from Section 2.4.2 have to hold. Firstly, we assume that Assumption 1 concerning the detectability of the plant holds.

Again Assumption 3 ensuring Lipschitz properties has to hold. As (4.39) is linear, (2.41) is satisfied. Similar to the state estimation case, (2.42) holds if $\partial h/\partial \boldsymbol{\theta}$ is locally Lipschitz. As before, $\partial h/\partial \boldsymbol{\theta}$ is locally Lipschitz if all appearing nonlinear terms f_t, $\partial f_t/\partial g$, $\partial f_t/\partial \tau$ in (4.40), (4.41) and (4.42) are locally Lipschitz. In Section 4.2.1 we showed that f, $\partial f/\partial g$, $\partial f/\partial x$ are locally Lipschitz. According to [30], the composition of locally Lipschitz functions is also locally Lipschitz. Since the explicit solution $x(t, \tau)$ given by (4.37) is continuously differentiable, it is locally Lipschitz and hence, f_t, $\partial f_t/\partial g$, $\partial f_t/\partial \tau$, being compositions of locally Lipschitz (4.37) and f, $\partial f/\partial g$, $\partial f/\partial x$, are also locally Lipschitz. Consequently, $\partial h/\partial \boldsymbol{\theta}$ is locally Lipschitz and inequality (2.42) and with that Assumption 1 holds.

In addition to the Lipschitz properties of the model, following Assumption 4, $\boldsymbol{C}(\hat{\boldsymbol{\theta}}, t)$ given by (4.40) has to be bounded. If h from (4.38) is locally Lipschitz, then $\partial h/\partial \boldsymbol{\theta}$ and hence $\boldsymbol{C}(\hat{\boldsymbol{\theta}}, t)$, are locally bounded. Because f_t is locally Lipschitz, h is locally Lipschitz if the measurement signals $y(t)$ and $\dot{y}(t)$ are Lipschitz on a sufficiently large domain. For measurements produced using the minimum-jerk trajectory this is satisfied, as can directly be seen in Figure 3.2. Hence, Assumption 4 is satisfied, if all Lipschitz properties hold for a large enough domain which contains all appearing estimates $\hat{\boldsymbol{\theta}}$. Roughly speaking, this is the case if the estimates $\hat{\boldsymbol{\theta}}$ are close to the real parameter vector $\boldsymbol{\theta}$.

Note, that the modified EKF given by (4.43), (4.44) and (4.45) can also be viewed as nonlinear version of the least-squares adaptive law (2.23) from [12], where $\boldsymbol{Q} = \boldsymbol{0}$ and $\boldsymbol{R} = \boldsymbol{I}$.

We implement the parameter estimator given by (4.43), (4.44) and (4.45) and use $\boldsymbol{P}_0 = 10^2\boldsymbol{I}$, $\boldsymbol{R} = \boldsymbol{I}$, $\boldsymbol{Q} = 10\boldsymbol{I}$ and $\alpha = 1$. With initial guess (4.46) of $\hat{g}_0 = 1\,\mathrm{m}$ and $\hat{\tau}_0 = 9\,\mathrm{s}$ and true values $g = 2\,\mathrm{m}$ and $\tau = 10\,\mathrm{s}$ simulation shows the convergence of the estimates to the true values in Figure 4.12. Clearly, the estimates $\hat{g}$ and $\hat{\tau}$ converge to their true values g and τ. The qualitative behavior of the presented modified EKF-based adaptive law (4.43), (4.44) which only estimates the unknown

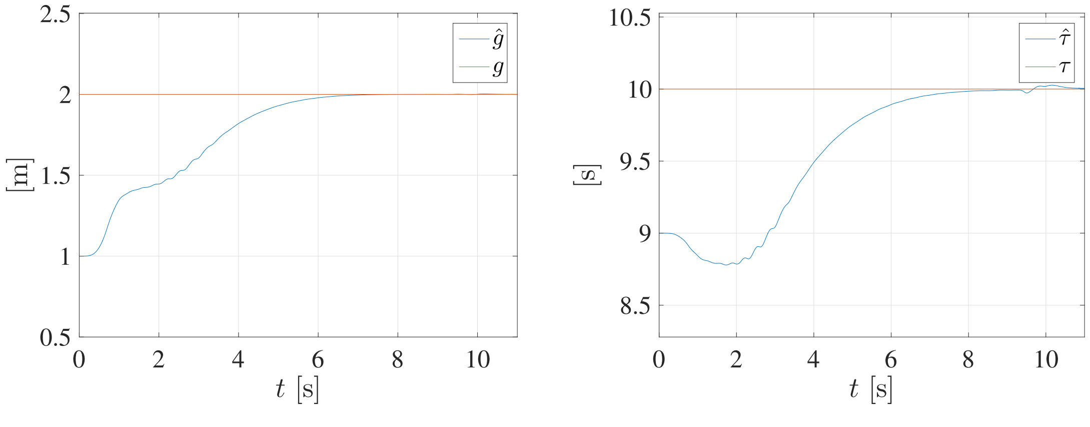

(a) (b)

Figure 4.12: On-line estimation of handover position and time with true values $g = 2\,\mathrm{m}$ and $\tau = 10\,\mathrm{s}$ and initial guesses $\hat{g}_0 = 1\,\mathrm{m}$ and $\hat{\tau}_0 = 9\,\mathrm{s}$ using an unfiltered modified EKF-based adaptive law.

parameters, resembles that of the modified EKF presented in Section 4.2.2, that estimates both unknown parameters as well as states of the DMP. In contrast to the rather large initial covariance in the state estimation case of Figure 4.10, $\boldsymbol{P}_0$ and $\boldsymbol{Q}$ were chosen relatively small in the parameter estimation case from Figure 4.12, whereas the convergence parameter α was set to values of similar scale.

The lower and upper bounds $\underline{p}_m$ and $\overline{p}_m$ of $\boldsymbol{P}(t)$ are illustrated in Figure A.3. Clearly, Assumption 1 holds for the time-instances of the present case, meaning stability of the EKF was ensured.

Since we are only interested in goal g and timescale τ for the considered human-robot handover, the modified EKF-based adaptive law presented in this section poses a solution to predict human motion. Additionally, as can be seen in Figure 4.12, relatively conservative values for the tuning parameters $\boldsymbol{P}_0$, $\boldsymbol{Q}$ and α already allow estimation of both place and time of the human-robot object handover within about seven seconds.

A disadvantage of the modified EKF-based adaptive law presented in this section is the fact, that in addition to position and velocity measurements also needed for the modified EKF-based state estimation, an acceleration measurement $\ddot{y}$ is required to estimate the unknown parameters.

Filtered Adaptive Law

A common approach to eliminate signals that cannot be measured in a parameter estimator, is to perform a filtering operation. Multiplying both sides of the measurement model (4.38) with a normalized first order filter with pole $-\lambda_f$ yields the filtered estimated output

$$\hat{z} = \frac{\lambda_f}{\Lambda(s)} h(\hat{\boldsymbol{\theta}}, y(t), \dot{y}(t), t) \tag{4.48}$$

and the filtered, measured output

$$z = \frac{\lambda_f s}{\Lambda(s)} \dot{y}, \tag{4.49}$$

where $\Lambda(s) = s + \lambda_f$. The purpose of using a normalized filter is to prevent λ_f from affecting the gain of the adaptive law and to thereby simplify tuning of the filtered adaptive law. Introducing the filtered output error

$$\epsilon_f = z - \hat{z} \tag{4.50}$$

and replacing the unfiltered output error in the parameter estimator from (4.43), (4.44) with the filtered output error from (4.50), we have the filtered adaptive law

$$\begin{aligned} \dot{\hat{\boldsymbol{\theta}}} &= \boldsymbol{P}\boldsymbol{C}(\hat{\boldsymbol{\theta}}, t)\boldsymbol{R}^{-1}\epsilon_f, \\ \dot{\boldsymbol{P}} &= \boldsymbol{Q} - \boldsymbol{P}\boldsymbol{C}(\hat{\boldsymbol{\theta}}, t)^\top \boldsymbol{R}^{-1}\boldsymbol{C}(\hat{\boldsymbol{\theta}}, t)\boldsymbol{P} + 2\alpha\boldsymbol{P}, \end{aligned}$$

with the initial conditions (4.46) and (4.47) from the unfiltered case.

Viewing the filters as part of the obtained measurements, it is sensible to assume that the stability of the filtered EKF-based adaptive law is not affected for sufficiently large λ_f. We therefore again assume Assumption 1 holds. Apart from that, the filtering operations do not change the fact that Assumptions 3 and 4 hold.

As in the unfiltered case, we use $\boldsymbol{P}_0 = 10^2\boldsymbol{I}$, $\boldsymbol{R} = \boldsymbol{I}$, $\boldsymbol{Q} = 10\boldsymbol{I}$ and $\alpha = 1$. With an initial guess (4.46) of $\hat{g}_0 = 1\,\mathrm{m}$ and $\hat{\tau}_0 = 9\,\mathrm{s}$ and true values $g = 2\,\mathrm{m}$ and $\tau = 10\,\mathrm{s}$ we simulate the parameter estimation performance of the filtered adaptive law. The results for a first order filter with $\lambda_f = 5$ are plotted in Figure 4.13. Convergence to the true values can be observed for both goal and timescale estimate. The speed of convergence seems similar to the unfiltered case from Figure 4.12 even though the filtered adaptive law no longer requires measurements of the accelerations $\ddot{y}$.

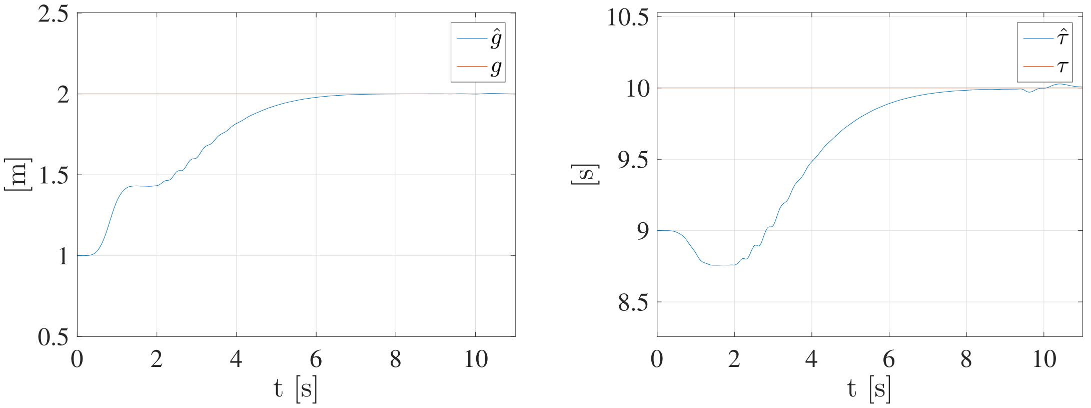

(a) **(b)**

Figure 4.13: On-line estimation of handover position and time with true values $g = 2\,\mathrm{m}$ and $\tau = 10\,\mathrm{s}$ and initial parameter values $\hat{g}_0 = 1\,\mathrm{m}$ and $\hat{\tau}_0 = 9\,\mathrm{s}$ using a modified EKF-based filtered adaptive law with filter parameter $\lambda_f = 5$.

Convergence can also be observed because detectability Assumption 1 can be ensured during the human motion as the bounds $\underline{p}_m(t)$ and $\overline{p}_m(t)$ from Figure A.3 satisfy inequality (2.34).

It was found that the tuning of the filtering parameter λ_f plays a key role in the performance of the filtered adaptive law presented in this section. In Figure 4.14 the convergence behavior of the presented adaptive law is depicted for different values of λ_f. The reason for the different performances of the adaptive law for different values of λ_f is that the speed of convergence depends on the amount of information obtained by the measurements. For convergence of the estimates to their true values, sufficiently rich measurements, meaning signals containing sufficiently many different frequencies, and thus enough information, are needed. For large λ_f, the filter $\lambda_f s/\Lambda(s)$ for the system output (4.49) is the causal version of a differentiator. As can be seen in Figure 4.14, values of $\lambda_f = 3$ or larger already allow for good convergence of the estimates for minimum-jerk trajectories. The larger λ_f is chosen, the closer the trajectories resemble the ones from the unfiltered adaptive law in Figure 4.12 since more frequencies and thus more information passes the filter from (4.48) and the filter $\lambda_f s/\Lambda(s)$ for the system output (4.49) tends towards a differentiator. Note that, in this case, the measurement signals are not subject to noise. Otherwise, the numerical differentiation with $\lambda_f s/\Lambda(s)$ would lead to estimation errors for large λ_f in case the measurements are subject to noise.

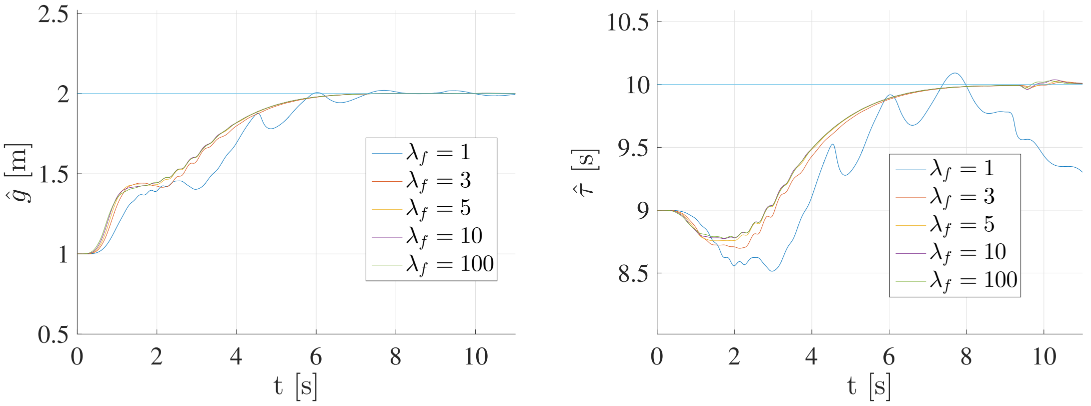

(a) **(b)**

Figure 4.14: On-line estimation of handover position time with true values $g = 2\,\text{m}$, $\tau = 10\,\text{s}$ and initial parameter values $\hat{g}_0 = 1\,\text{m}$, $\hat{\tau}_0 = 9\,\text{s}$ using a modified EKF-based filtered adaptive law with different filter parameters λ_f.

5

Parameter Estimation Based on Specialized DMPs

When using the original DMP as a parameterization of human motion, the canonical system adds an unmeasurable phase variable to the plant model, consequently making the estimation of goal and timescale harder or often at least slow to converge. An attempt to simplify and thereby improve estimation performance is to use a specialized DMP incorporating prior knowledge on the considered human motion.

5.1 Adaptive Law-Based Parameter Estimation of Specialized DMPs

Assuming that position y, velocity $\dot{y}$ and acceleration $\ddot{y}$ of the human hand are measurable, the specialized DMP from (3.13) can be written as

$$\begin{aligned}\ddot{y} &= \boldsymbol{\theta}^\top \boldsymbol{\phi}(\boldsymbol{\theta}) \\ &= \underbrace{\begin{bmatrix} \frac{1}{\tau^2} & \frac{1}{\tau} & \frac{g}{\tau^2} \end{bmatrix}}_{\boldsymbol{\theta}^\top} \underbrace{\begin{bmatrix} -\alpha_z \beta_z y - y_0 \tilde{f}_s(y,g) \\ -\alpha_z \dot{y} \\ \alpha_z \beta_z + \tilde{f}_s(y,g) \end{bmatrix}}_{\boldsymbol{\phi}},\end{aligned} \tag{5.1}$$

with $\tilde{f}_s$ from (3.12). This system is clearly nonlinear in the parameters. In order to be able to design an adaptive law from Section 2.3 and [12], we again neglect the dependence of $\boldsymbol{\phi}$ on $\boldsymbol{\theta}$ and thereby render (5.1) linear parametric. The least-squares adaptive law from (2.23) is implemented using a forgetting factor of $\beta = 0$. Since we consider human point-to-point motion, y, $\dot{y}$ and $\ddot{y}$ are bounded functions of time. Furthermore, $\tilde{f}_s(y,g)$ is bounded thanks to the boundedness of basis functions $\Psi_{s,i}$ and weights w_i. Hence, no normalization is needed to guarantee $\boldsymbol{\phi} \in \mathcal{L}_\infty$ for a constant $\boldsymbol{\theta}$ and $m = 1$ can be chosen. The least-squares adaptive law reads

$$\dot{\hat{\boldsymbol{\theta}}} = \boldsymbol{P} \epsilon \boldsymbol{\phi}(\hat{\boldsymbol{\theta}}), \tag{5.2}$$

$$\dot{\boldsymbol{P}} = -\boldsymbol{P} \boldsymbol{\phi}(\hat{\boldsymbol{\theta}}) \boldsymbol{\phi}^\top(\hat{\boldsymbol{\theta}}) \boldsymbol{P}, \tag{5.3}$$

where

$$\hat{\boldsymbol{\theta}} = \begin{bmatrix} \hat{\theta}_1 & \hat{\theta}_2 & \hat{\theta}_3 \end{bmatrix}^\top = \begin{bmatrix} \frac{1}{\hat{\tau}^2} & \frac{1}{\hat{\tau}} & \frac{\hat{g}}{\hat{\tau}^2} \end{bmatrix}^\top \tag{5.4}$$

is the estimated parameter vector and

$$\epsilon = z - \hat{z} = \ddot{y} - \hat{\boldsymbol{\theta}}^\top \boldsymbol{\phi}(\hat{\boldsymbol{\theta}})$$

is the output error. The initial conditions are $\boldsymbol{P}(0) = \boldsymbol{P}_0$ and

$$\hat{\boldsymbol{\theta}}(0) = \hat{\boldsymbol{\theta}}_0 = \begin{bmatrix} \frac{1}{\hat{\tau}_0{}^2} & \frac{1}{\hat{\tau}_0} & \frac{\hat{g}_0}{\hat{\tau}_0{}^2} \end{bmatrix}^\top .$$

In the case for a known timescale τ and an original DMP from Section 4.1.1, the PE property was shown for $\boldsymbol{\phi}$. As our approach here is to neglect the dependency of $\boldsymbol{\phi}$ on $\boldsymbol{\theta}$, we have PE as before and thus expect convergence of the estimate if the modeling error resulting from neglecting the nonlinearity in the parameters is small enough.

Simulation for $\boldsymbol{P}_0 = 10^6 \mathrm{diag}([1, 50, 10])$ and initial estimates $\hat{g}_0 = 1\,\mathrm{m}$ and $\hat{\tau}_0 = 9\,\mathrm{s}$ for true parameters $g = 2\,\mathrm{m}$ and $\tau = 10\,\mathrm{s}$ yields the trajectories depicted in Figure 5.1. Since we are interested in the estimated timescale $\hat{\tau}$ and the estimated goal $\hat{g}$ of the human motion, these two parameters are extracted from the parameter vector (5.4) via

$$\hat{\tau}_1 = \frac{1}{\sqrt{\hat{\theta}_1}}, \quad \hat{\tau}_2 = \frac{1}{\hat{\theta}_2}, \quad \text{and } \hat{g} = \frac{\hat{\theta}_3}{\hat{\theta}_2^2}.$$

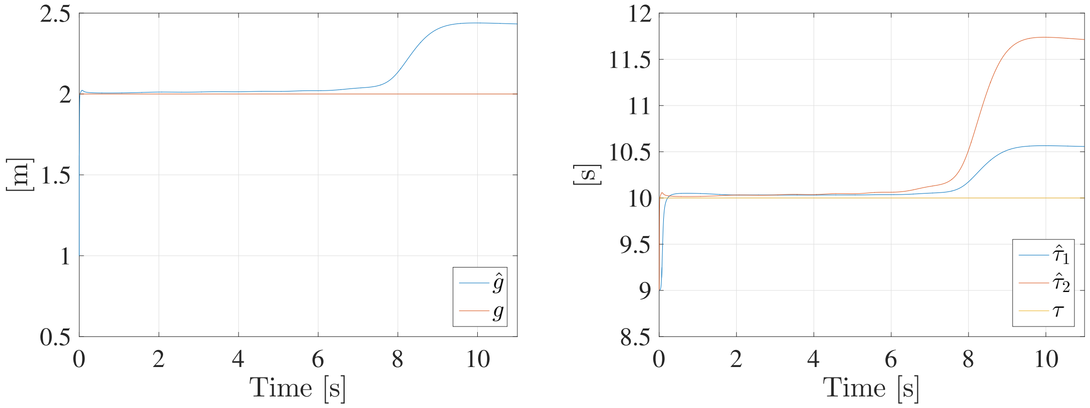

(a) **(b)**

Figure 5.1: On-line estimation of handover position and time with true values $g = 2\,\mathrm{m}$, $\tau = 10\,\mathrm{s}$ and initial parameter values $\hat{g}_0 = 1\,\mathrm{m}$, $\hat{\tau}_0 = 9\,\mathrm{s}$ using a least-squares adaptive law with $\beta = 0$ and $\boldsymbol{P}_0 = 10^6 \mathrm{diag}([1, 50, 10])$ for a specialized DMP.

It can be observed, that both the timescale estimates and the goal estimate rapidly converge to their true values thanks to the very high values for $\boldsymbol{P}_0$. However, after slightly more than six seconds, the estimates become erroneous. The rather large fitting error from Figure 3.8 towards the end of motion gives rise to an oscillating and hence highly nonlinear forcing term. Consequently, the fact that the nonlinearity $\tilde{f}_s$ is vanishing is not sufficient to just neglect the dependency of the information vector $\boldsymbol{\phi}$ on the parameter estimate $\hat{\boldsymbol{\theta}}$.

In the considered case, the measurement data was generated using the specialized DMP fitted to a minimum-jerk trajectory. The large $\boldsymbol{P}_0$ introduces high stiffness to the system comprising the specialized DMP (3.13) as a plant and the high-gain adaptive law (5.2), (5.3) as a parameter estimator. For the large $\boldsymbol{P}_0$ successfully used to estimate parameters in Figure 5.1 with measurements generated by the specialized DMP, numerical simulations became unstable when generating measurement data using the functional representation of the minimum-jerk trajectory from (3.5). For lower values of $\boldsymbol{P}_0$, no convergence to the true timescale and goal could be observed for both the case where measurement data was generated using a specialized DMP and when using the functional representation of a minimum-jerk trajectory (3.5) to generate measurement data.

5.2 EKF-Based Parameter Estimation for Specialized DMPs

Estimating the unknown parameters of the specialized DMP is also possible by applying an EKF. For the original DMP this approach has worked well, hence, it is expected that good performance in face of the nonlinearities (5.1) can be achieved when using the specialized DMP as well. We consider both classical and modified versions of the EKF to perform state estimation of a state containing the unknown parameters of timescale and goal.

5.2.1 Classical EKF-Based State Estimation

To perform state estimation for the specialized DMP, an EKF can be designed as a nonlinear observer.

Observer Formulation

In a state estimation context, the states of the specialized DMP (3.13) and the unknown parameters can be viewed as elements of the state vector

$$\boldsymbol{x}_s = \begin{bmatrix} y & z & g & \tau \end{bmatrix}^\top$$

with $z = \dot{y}$. Following the definition of the classical EKF from Section 2.4, the state space representation of the nonlinear plant, describing human motion via a specialized DMP, is thus given by

$$\begin{aligned} \dot{\boldsymbol{x}}_s &= \boldsymbol{f}(\boldsymbol{x}_s) \\ \Leftrightarrow \begin{bmatrix} \dot{y} \\ \dot{z} \\ \dot{g} \\ \dot{\tau} \end{bmatrix} &= \begin{bmatrix} z \\ \frac{1}{\tau^2}\left(\alpha_z\left(\beta_z\left(g-y\right)-\tau\dot{y}\right)+f(y,g)\right) \\ 0 \\ 0 \end{bmatrix}. \end{aligned} \tag{5.6}$$

Since the parameters g and τ represent goal and timescale of a specific human motion, it is sensible to assume they are constants and therefore use a random walk model as their process model. Assuming both position y and velocity $\dot{y} = z$ of the human hand are measurable, we have the linear measurement model

$$\boldsymbol{y} = \boldsymbol{h}_s(\boldsymbol{x}_s) = \boldsymbol{C}\boldsymbol{x}_s \tag{5.7}$$

with $\boldsymbol{C}$ from (4.17). Using the estimated state vector

$$\hat{\boldsymbol{x}}_s = \begin{bmatrix} \hat{y} & \hat{z} & \hat{g} & \hat{\tau} \end{bmatrix}^\top \tag{5.8}$$

we can calculate the linearization of the nonlinear parameterization $\boldsymbol{f}$ around the current estimate $\hat{\boldsymbol{x}}_s$,

$$\begin{aligned} \boldsymbol{A}(\hat{\boldsymbol{x}}_s) &= \left.\frac{\partial \boldsymbol{f}(\boldsymbol{x}_s)}{\partial \boldsymbol{x}}\right|_{\boldsymbol{x}_s = \hat{\boldsymbol{x}}_s} \qquad (5.9) \\ &= \left.\begin{bmatrix} 0 & 1 & 0 & 0 \\ -\frac{\alpha_z\beta_z}{\tau^2} + \frac{1}{\tau^2}\frac{\partial f(y,g)}{\partial y} & -\frac{\alpha_z}{\tau} & A_{23} & \frac{1}{\tau^2}\left(\alpha_z\beta_z + \frac{\partial f(y,g)}{\partial g}\right) \\ 0 & 0 & 0 & 0 \\ 0 & 0 & 0 & 0 \end{bmatrix}\right|_{\boldsymbol{x}_s = \hat{\boldsymbol{x}}_s}, \end{aligned}$$

with

$$A_{23} = -\frac{2}{\tau^3}\left(\alpha_z\beta_z(g-y) + f(y,g)\right) + \frac{\alpha_z}{\tau^2}z,$$

where the partial derivative of the nonlinear forcing term with respect to y is given by

$$\frac{\partial f(y,g)}{\partial y} = (g - y_0)\frac{\partial \tilde{f}_s(y,g)}{\partial y},$$

using (3.12) as well as

$$\frac{\partial \tilde{f}_s(y,g)}{\partial y} = \frac{\partial \tilde{g}(y,g)}{\partial y}\left(1 - \frac{y - y_0}{g - y_0}\right) - \frac{1}{g - y_0}\tilde{g}(y,g),$$

$$\frac{\partial \tilde{g}(y,g)}{\partial y} = \frac{\left(\sum_{i=1}^N \frac{\partial \Psi_{s,i}}{\partial y} w_i\right)\left(\sum_{i=1}^N \Psi_{s,i}\right) - \left(\sum_{i=1}^N \Psi_{s,i} w_i\right)\left(\sum_{i=1}^N \frac{\partial \Psi_{s,i}}{\partial y}\right)}{\left(\sum_{i=1}^N \Psi_{s,i}\right)^2},$$

and

$$\frac{\partial \Psi_{s,i}}{\partial y} = 2h_{s,i}\Psi_{s,i}(y,g)\left(1 - \frac{y - y_0}{g - y_0} - c_{s,i}\right)\frac{1}{g - y_0}.$$

The partial derivative of f with respect to g reads

$$\frac{\partial f(y,g)}{\partial g} = \frac{\partial \tilde{f}_s(y,g)}{\partial g}(g - y_0) + \tilde{f}_s(y,g),$$

with

$$\frac{\partial \tilde{f}(y,g)}{\partial g} = \frac{\partial \tilde{g}(y,g)}{\partial g}\left(1 - \frac{y-y_0}{g-y_0}\right) + \tilde{g}(y,g)\frac{y-y_0}{(g-y_0)^2},$$

$$\frac{\partial \tilde{g}(y,g)}{\partial g} = \frac{\left(\sum_{i=1}^{N}\frac{\partial \Psi_{s,i}}{\partial g}w_i\right)\left(\sum_{i=1}^{N}\Psi_{s,i}\right) - \left(\sum_{i=1}^{N}\Psi_{s,i}w_i\right)\left(\sum_{i=1}^{N}\frac{\partial \Psi_{s,i}}{\partial g}\right)}{\left(\sum_{i=1}^{N}\Psi_{s,i}\right)^2},$$

and

$$\frac{\partial \Psi_{s,i}}{\partial g} = -2h_{s,i}\Psi_{s,i}(y,g)\left(1 - \frac{y-y_0}{(g-y_0)^2} - c_{s,i}\right)\frac{y-y_0}{(g-y_0)^2}.$$

Together with the initial estimate

$$\begin{aligned}\hat{\boldsymbol{x}}_s(0) &= \begin{bmatrix} y(0) & z(0) & \hat{g}(0) & \hat{\tau}(0)\end{bmatrix}^\top \\ &= \begin{bmatrix} 0 & 0 & \hat{g}_0 & \hat{\tau}_0\end{bmatrix}^\top \end{aligned} \tag{5.10}$$

the classical EKF given by (2.29), (2.30) and (2.31) can be formulated for the specialized DMP as,

$$\dot{\hat{\boldsymbol{x}}}_s = \boldsymbol{f}(\hat{\boldsymbol{x}}_s) + \boldsymbol{K}(t)(\boldsymbol{y} - \boldsymbol{C}\hat{\boldsymbol{x}}_s), \tag{5.11}$$

$$\boldsymbol{K}(t) = \boldsymbol{P}(t)\boldsymbol{C}^\top \boldsymbol{R}^{-1}, \tag{5.12}$$

where $\boldsymbol{P}(t)$ is the obtained by solving the Riccati differential equation

$$\dot{\boldsymbol{P}}(t) = \boldsymbol{A}(\hat{\boldsymbol{x}}_s)\boldsymbol{P}(t) + \boldsymbol{P}(t)\boldsymbol{A}(\hat{\boldsymbol{x}}_s)^\top + \boldsymbol{Q} - \boldsymbol{P}(t)\boldsymbol{C}^\top\boldsymbol{R}^{-1}\boldsymbol{C}\boldsymbol{P}(t), \tag{5.13}$$

with initial condition $\boldsymbol{P}(0) = \boldsymbol{P}_0$ and positive definite matrices $\boldsymbol{Q}$, $\boldsymbol{R}$.

Stability

Convergence of the estimates $\hat{\boldsymbol{x}}_s$ to $\boldsymbol{x}_s$ is ensured if the respective assumptions from Section 2.4 hold. Given that Assumption 1 holds for the duration of human motion, i.e., the plant (5.6) is uniformly detectable, it remains to ensure that the nonlinearities satisfy the necessary Lipschitz properties from Assumption 2. The argumentation is almost identical to the original DMP case in Section 4.2.1. Since the centers $c_{s,i}$ and width parameters $h_{s,i}$ can be chosen such that all required boundedness conditions are satisfied locally, Assumption 2 holds.

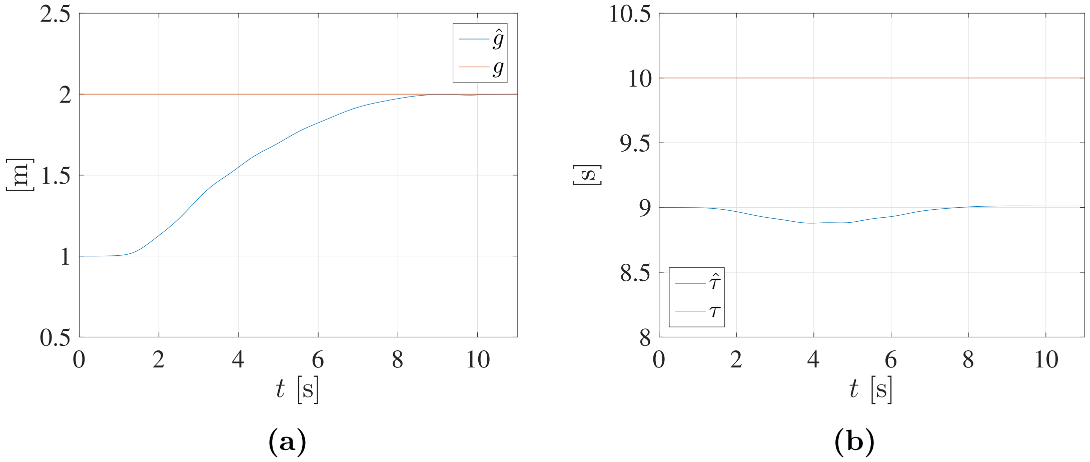

Figure 5.2: On-line estimation of handover position and time with true values $g = 2\,\mathrm{m}$, $\tau = 10\,\mathrm{s}$ and initial parameter estimates $\hat{g}_0 = 1\,\mathrm{m}$, $\hat{\tau}_0 = 9\,\mathrm{s}$ using a classical EKF with $\boldsymbol{P}_0 = 100\boldsymbol{I}$ and a specialized DMP.

Implementation

The EKF given by (5.11)-(5.13) is implemented using the initial estimate from (5.10) with $\hat{g}_0 = 1\,\mathrm{m}$ and $\hat{\tau}_0 = 9\,\mathrm{s}$ for the true values $g = 2\,\mathrm{m}$ and $\tau = 10\,\mathrm{s}$. Choosing $\boldsymbol{P}_0 = 100\boldsymbol{I}$ and matrices $\boldsymbol{R} = \boldsymbol{I}$, $\boldsymbol{Q} = 10\boldsymbol{I}$ yields the convergence results shown in Figure 5.2. The measurements y and $\dot{y}$ are produced using the minimum-jerk trajectory (3.5) shown Figure 3.2. The remaining states $\hat{y}$ and $\hat{z}$ of (5.8) are plotted in Figure A.4. While the estimated position of the human hand $\hat{y}$ coincides with the measured y, the estimated speed of the hand $\hat{z}$ clearly deviates from the measured z. Verification yields, that Assumption 1 can be ensured on the time interval of human motion, as the bounds $\underline{p}_c(t)$ and $\overline{p}_c(t)$ from Figure 5.3 satisfy inequality (2.34).

Our observations are very similar to the case where a classical EKF is designed for the original DMP in Figure 4.7. While the estimated goal $\hat{g}$ slowly converges to the true g, the timescale estimate $\hat{\tau}$ does not converge to the true τ. By choosing a larger $\boldsymbol{P}_0 = 10^5\boldsymbol{I}$, Figure 5.3 shows that faster convergence for $\hat{g}$ to the true goal g and convergence for $\hat{\tau}$ to some constant, which, however, is still subject to a lasting error, can be achieved. The states $\hat{y}$ and $\hat{z}$ of (5.8) are plotted in Figure A.5 and now coincide with the measured y and z everywhere except for $t > \tau$. As before, the bounds on $\boldsymbol{P}(t)$ from Assumption 1 can be confirmed via Figure A.7.

The observed steady state errors in the estimated timescale for different values of $\boldsymbol{P}_0$ motivate the use of a modified EKF with faster convergence, suggested by Reif *et al.* [21].

5.2.2 Modified EKF-Based State Estimation

Again, a nonlinear observer using a modified EKF is designed to perform state estimation for the specialized DMP.

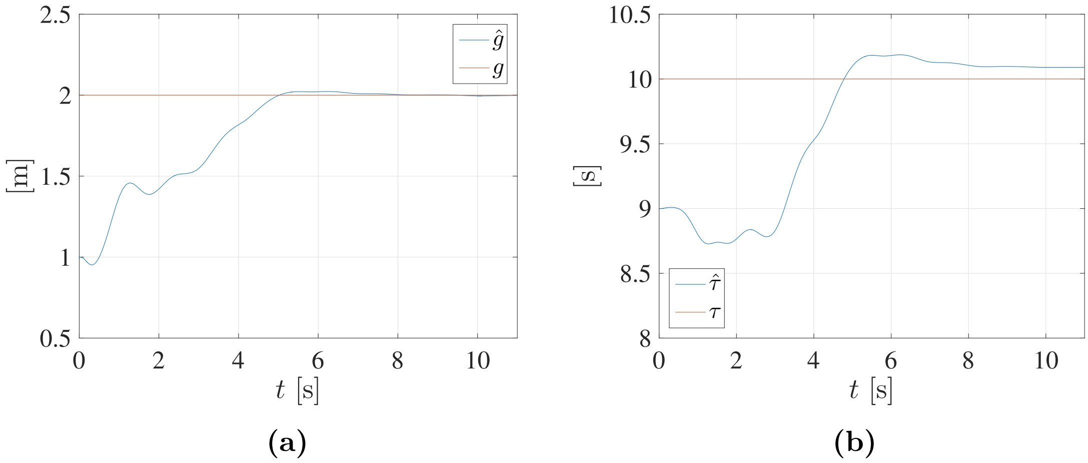

(a) **(b)**

Figure 5.3: On-line estimation of handover position and time with true values $g = 2\,\mathrm{m}$, $\tau = 10\,\mathrm{s}$ and initial parameter estimates $\hat{g}_0 = 1\,\mathrm{m}$, $\hat{\tau}_0 = 9\,\mathrm{s}$ using a classical EKF with $\boldsymbol{P}_0 = 10^5\boldsymbol{I}$ and a specialized DMP.

Observer Formulation

We use the same estimated state vector (5.8) and the plant (5.6) consisting of the specialized DMP dynamics and a random walk model for the unknown timescale and goal, as well as the measurement model (5.7) to design the modified EKF. Following [21], the modified EKF is given by the update law (5.11), the Kalman gain (5.12) and the modified Riccati equation

$$\begin{aligned}\dot{\boldsymbol{P}}(t) = (\boldsymbol{A}(\hat{\boldsymbol{x}}_s) + \alpha_s\boldsymbol{I})\boldsymbol{P}(t) + \boldsymbol{P}(t)(\boldsymbol{A}(\hat{\boldsymbol{x}}_s)^\top + \alpha_s\boldsymbol{I}) + \boldsymbol{Q}\\ -\boldsymbol{P}(t)\boldsymbol{C}^\top\boldsymbol{R}^{-1}\boldsymbol{C}\boldsymbol{P}(t),\end{aligned} \tag{5.14}$$

with $\boldsymbol{P}(0) = \boldsymbol{P}_0$, where $\boldsymbol{A}(\hat{\boldsymbol{x}}_s)$ from (5.9) is the linearization of the process model (5.6) around the current estimate and $\boldsymbol{Q}$ and $\boldsymbol{R}$ are positive definite matrices. The convergence can be tuned via $\alpha_s > 0$.

Stability

The stability analysis for the modified EKF follows similar arguments as in the original DMP case from Section 4.2.2. For simplicity, we again assume that Assumption 1 holds for the plant (5.6) for all times of the time interval of human motion. Thanks to the linearity of the measurement model (5.7), we can conclude that Assumption 4 on the boundedness of $\boldsymbol{C}$ holds. Additionally, since the centers $c_{s,i}$ and widths $w_{s,i}$ can be chosen such that all required boundedness conditions are satisfied, Lipschitz properties of the nonlinearities of (5.6) can be established in a similar manner as in Section 4.2.2. Using the monotony of the integral there exists an $\epsilon_\Phi > 0$ such that Assumption 3 holds as well.

Implementation

The modified EKF consisting of (5.11), (5.12) and (5.14) is implemented using the initial estimate from (5.10) with $\hat{g}_0 = 1\,\mathrm{m}$ and $\hat{\tau}_0 = 9\,\mathrm{s}$ for the true values $g = 2\,\mathrm{m}$

and $\tau = 10\,\mathrm{s}$. Choosing $\alpha_s = 0.5$, $\boldsymbol{P}_0 = 100\boldsymbol{I}$ and matrices $\boldsymbol{R} = \boldsymbol{I}$ and $\boldsymbol{Q} = 10\boldsymbol{I}$ yields the convergence results shown in Figure 5.4. The measurements y and $\dot{y}$ are produced using (3.5).

Convergence of $\hat{g}$ to g can be observed. Assumption 1 can be confirmed with the obtained bounds of $\boldsymbol{P}(t)$ from Figure A.9. The timescale estimate $\hat{\tau}$ does not converge to a constant value within the duration of motion but rather oscillates around the true τ in the final stages of motion, however, due to the small amplitude it still provides a reasonable good estimate of the timescale. The remaining states $\hat{y}$ and $\hat{z}$ of (5.8) are depicted in Figure A.8 and coincide with the measured y and z.

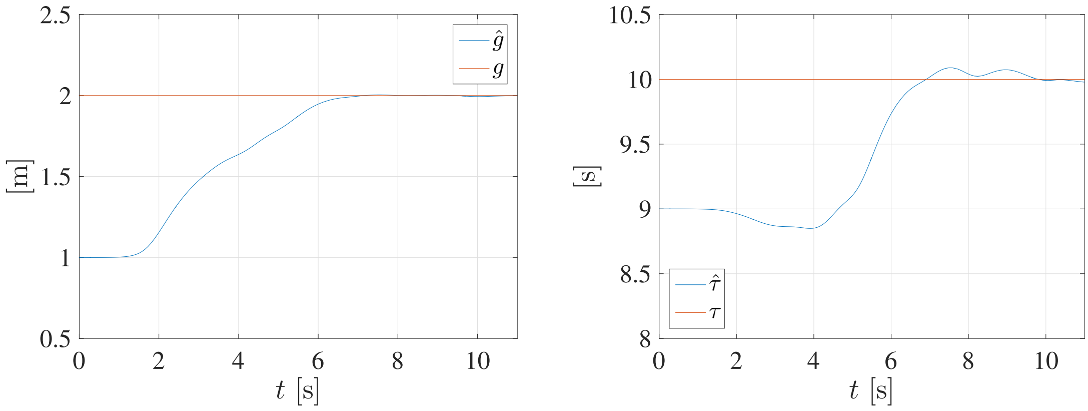

(a) **(b)**

Figure 5.4: On-line estimation of handover position $\hat{g}$ and handover time $\hat{\tau}$ with true values $g = 2\,\mathrm{m}$ and $\tau = 10\,\mathrm{s}$ and initial parameter values $\hat{g}_0 = 1\,\mathrm{m}$ and $\hat{\tau}_0 = 9\,\mathrm{s}$ using a modified EKF with $\boldsymbol{P}_0 = 100\boldsymbol{I}$, convergence parameter $\alpha_s = 0.5$ and a specialized DMP.

We conclude, that EKF-based parameter estimation of specialized DMPs poses a working solution to estimate place and time of a human-robot handover process on-line. While the adaptive law-based on-line estimation scheme only works in a very limited and thus unrealistic environment, the proposed EKF-based estimation schemes were found to be applicable using reasonable gains and are thus expected to also work in a more realistic scenario. The adaptive law-based parameter estimator relies on a high gain to deal with the nonlinear model whereas the EKF-based observers use linearization around current estimates. Both approaches, however, only guarantee convergence to true values for sufficiently good initial guesses of the parameters, which is a typical limitation in nonlinear estimation problems [17, 19, 21].

5.3 Discrete-Time Nonlinear Least-Squares Adaptive Law

It has clearly shown that the estimation performance heavily depends on how nonlinearities are taken into account during the estimator design. As the estimation schemes suggested above all rely on neglecting or linearizing nonlinearities, it is of interest to investigate a nonlinear estimation scheme that directly incorporates the known nonlinearities. In adaptive control, adaptive laws to estimate parameters online are derived using a gradient algorithm to minimize a cost function penalizing output error squares [12]. While for systems that are linear in the unknown parameters this is a convex cost function, systems that are nonlinear in the unknown parameters render such a cost function non-convex. The DMPs used in this thesis pose systems nonlinear in the unknown parameters. In view of this nonlinear optimization problem, a discrete-time approach similar to hybrid adaptive laws allows for designing an on-line nonlinear gradient descent based on well-known nonlinear optimization techniques such as the Levenberg-Marquardt algorithm. For simplicity, we assume that position y, velocity $\dot{y}$ and acceleration $\ddot{y}$ of the human hand are measurable during a handover process.

5.3.1 Optimal Control Formulation

Given a non-convex cost function

$$K(\hat{\boldsymbol{\theta}}) = \sum_{i=0}^{M} \gamma_i \left[\ddot{y}_i - h\left(\hat{\boldsymbol{\theta}}, y(t_i), \dot{y}(t_i)\right)\right]^2, \tag{5.15}$$

penalizing the output error

$$e_o = \ddot{y}_i - h\left(\hat{\boldsymbol{\theta}}, y(t_i), \dot{y}(t_i)\right) \tag{5.16}$$

in a quadratic sense, $t_i = iT_m$ denotes a time-instance and T_m is the sampling rate with which measurements are obtained. Moreover, the optimization horizon M obeys the relation $t = MT_m$, meaning that it increases with time t as more measurement data becomes available. The output error (5.16) at time t_i is weighted by γ_i. In this setup, the optimal value $\hat{\boldsymbol{\theta}}^*$ minimizing (5.15) at time t_M is searched as an estimate of the true parameter vector $\boldsymbol{\theta}$. Using the specialized DMP parameterization (3.13) from Section 3.4,

$$\ddot{y} = h_s(\boldsymbol{\theta}, y(t), \dot{y}(t)) = \frac{1}{\tau^2}(\alpha_z(\beta_z(g-y) - \tau\dot{y}) + f(g, y)),$$

and the parameter vector $\boldsymbol{\theta} = [g, \tau]^\top \in \mathcal{R}^n$ with $n = 2$, we can design an update law minimizing (5.15) in a least-squares sense. With the vector of acceleration measurements

$$\ddot{\boldsymbol{y}} = \begin{bmatrix}\ddot{y}_0 & \dots & \ddot{y}_M\end{bmatrix}^\top, \tag{5.17}$$

the vector of expected accelerations

$$\boldsymbol{h}_s(\hat{\boldsymbol{\theta}}) = \begin{bmatrix} h_s\left(\hat{\boldsymbol{\theta}}, y(t_0), \dot{y}(t_0)\right) \\ h_s\left(\hat{\boldsymbol{\theta}}, y(t_1), \dot{y}(t_1)\right) \\ \vdots \\ h_s\left(\hat{\boldsymbol{\theta}}, y(t_M), \dot{y}(t_M)\right) \end{bmatrix} \in \mathcal{R}^{M+1}, \tag{5.18}$$

and the Jacobian

$$\boldsymbol{J}_h(\hat{\boldsymbol{\theta}}) = \frac{\partial \boldsymbol{h}_s(\hat{\boldsymbol{\theta}})}{\partial \hat{\boldsymbol{\theta}}} \in \mathcal{R}^{(M+1)\times n} = \begin{bmatrix} \partial_{\hat{\boldsymbol{\theta}}} h_s\left(\hat{\boldsymbol{\theta}}, y(t_0), \dot{y}(t_0)\right) \\ \partial_{\hat{\boldsymbol{\theta}}} h_s\left(\hat{\boldsymbol{\theta}}, y(t_1), \dot{y}(t_1)\right) \\ \vdots \\ \partial_{\hat{\boldsymbol{\theta}}} h_s\left(\hat{\boldsymbol{\theta}}, y(t_M), \dot{y}(t_M)\right) \end{bmatrix}, \tag{5.19}$$

with

$$\partial_{\hat{\boldsymbol{\theta}}} h_s\left(\hat{\boldsymbol{\theta}}, y(t_i), \dot{y}(t_i)\right) = \frac{\partial h_s\left(\hat{\boldsymbol{\theta}}, y(t_i), \dot{y}(t_i)\right)}{\partial \hat{\boldsymbol{\theta}}} = \begin{bmatrix} \frac{1}{\hat{\tau}^2}\left(\alpha_z\beta_z + \frac{\partial f(y(t_i),\hat{g})}{\partial \hat{g}}\right) \\ -\frac{2}{\hat{\tau}^3}\left(\alpha_z\beta_z(\hat{g} - y(t_i)) + f(y(t_i), \hat{g})\right) + \frac{\alpha_z}{\hat{\tau}^2}\dot{y}(t_i) \end{bmatrix}^\top, \tag{5.20}$$

for $i = 1, \ldots, M$, we follow [31] and approximate

$$h_s\left(\hat{\boldsymbol{\theta}} + \delta\hat{\boldsymbol{\theta}}, y(t_i), \dot{y}(t_i)\right) \approx h_s\left(\hat{\boldsymbol{\theta}}, y(t_i), \dot{y}(t_i)\right) + \frac{\partial h_s}{\partial \hat{\boldsymbol{\theta}}}\left(\hat{\boldsymbol{\theta}}, y(t_i), \dot{y}(t_i)\right)\delta\hat{\boldsymbol{\theta}}. \tag{5.21}$$

By plugging (5.21) into (5.15), we obtain the approximated cost function

$$\tilde{K}(\hat{\boldsymbol{\theta}} + \delta\hat{\boldsymbol{\theta}}) = \sum_{i=0}^{M} \gamma_i \left[\ddot{y}_i - h_s(\hat{\boldsymbol{\theta}}, y(t_i), \dot{y}(t_i)) - \frac{\partial h_s}{\partial \hat{\boldsymbol{\theta}}}\left(\hat{\boldsymbol{\theta}}, y(t_i), \dot{y}(t_i)\right)\delta\hat{\boldsymbol{\theta}}\right]^2. \tag{5.22}$$

Setting $\gamma_i = \gamma^{M-i}$ with forgetting factor $\gamma > 0$, the matrix of weights

$$\boldsymbol{W} = \begin{bmatrix} \gamma^M & & & & \\ & \gamma^{M-1} & & & \\ & & \ddots & & \\ & & & \gamma^1 & \\ & & & & 1 \end{bmatrix} \in \mathcal{R}^{(M+1)\times(M+1)}, \tag{5.23}$$

is introduced to rewrite (5.22) in vector notation,

$$\begin{aligned} \tilde{K}(\hat{\boldsymbol{\theta}} + \delta\hat{\boldsymbol{\theta}}) &= \left\|\ddot{\boldsymbol{y}} - \boldsymbol{h}_s(\hat{\boldsymbol{\theta}}) - \boldsymbol{J}_h(\hat{\boldsymbol{\theta}})\delta\hat{\boldsymbol{\theta}}\right\|_W^2 \\ &= \left(\ddot{\boldsymbol{y}} - \boldsymbol{h}_s(\hat{\boldsymbol{\theta}}) - \boldsymbol{J}_h(\hat{\boldsymbol{\theta}})\delta\hat{\boldsymbol{\theta}}\right)^\top \boldsymbol{W} \left(\ddot{\boldsymbol{y}} - \boldsymbol{h}_s(\hat{\boldsymbol{\theta}}) - \boldsymbol{J}_h(\hat{\boldsymbol{\theta}})\delta\hat{\boldsymbol{\theta}}\right). \end{aligned} \tag{5.24}$$

As done in the derivation of the Levenberg-Marquardt algorithm from Marquardt [31], the gradient of (5.24) with respect to $\delta\hat{\boldsymbol{\theta}}$ is set to zero and then solved for $\delta\hat{\boldsymbol{\theta}}$. Hence, we have

$$\begin{aligned} \frac{\partial \tilde{K}\left(\hat{\boldsymbol{\theta}} + \delta\hat{\boldsymbol{\theta}}\right)}{\partial \delta\hat{\boldsymbol{\theta}}} &= -2\left(\ddot{\boldsymbol{y}} - \boldsymbol{h}_s(\hat{\boldsymbol{\theta}}) - \boldsymbol{J}_h(\hat{\boldsymbol{\theta}})\delta\hat{\boldsymbol{\theta}}\right)^\top \boldsymbol{W}\boldsymbol{J}_h(\hat{\boldsymbol{\theta}}) \overset{!}{=} \boldsymbol{0} \\ &\Leftrightarrow \left(\boldsymbol{J}_h(\hat{\boldsymbol{\theta}})^\top \boldsymbol{W}\boldsymbol{J}_h(\hat{\boldsymbol{\theta}})\right)\delta\hat{\boldsymbol{\theta}} = \boldsymbol{J}_h(\hat{\boldsymbol{\theta}})^\top \boldsymbol{W}\left[\ddot{\boldsymbol{y}} - \boldsymbol{h}_s(\hat{\boldsymbol{\theta}})\right]. \end{aligned}$$

Introducing a damping term with a damping parameter $\lambda_{LM} \geq 0$, the Levenberg-Marquardt step [31] is thus calculated via

$$\delta\hat{\boldsymbol{\theta}} = (\boldsymbol{J}_h^\top \boldsymbol{W} \boldsymbol{J}_h + \lambda_{LM} \mathrm{diag}(\boldsymbol{J}_h^\top \boldsymbol{W} \boldsymbol{J}_h))^{-1} \boldsymbol{J}_h^\top \boldsymbol{W} (\ddot{\boldsymbol{y}} - \boldsymbol{h}_s(\hat{\boldsymbol{\theta}})). \tag{5.25}$$

Note that a small damping parameter λ_{LM} results into (5.25) behaving similarly to a Gauss-Newton step, meaning that it attempts to directly step to the minimum. This gives fast convergence for objective functions which are close to quadratic. Larger values of λ_{LM} let (5.25) behave more like a gradient descent, taking smaller steps towards the minimum to account for non-quadratic terms in the objective function. As in normal optimization and fitting problems, the optimal value $\hat{\boldsymbol{\theta}}^*$ is obtained by iteratively computing (5.25) and updating

$$\hat{\boldsymbol{\theta}}_{k+1} = \hat{\boldsymbol{\theta}}_k + \delta\boldsymbol{\theta}, \tag{5.26}$$

starting with an initial value $\hat{\boldsymbol{\theta}}_0$ until some terminal condition ensuring $\hat{\boldsymbol{\theta}} \approx \hat{\boldsymbol{\theta}}^*$ is satisfied. In hybrid adaptive control, as presented in Section 2.3.4, parameter updates are conducted at discrete time instances. To obtain a discrete adaptive law for on-line estimation of $\boldsymbol{\theta}$, we propose to use one Levenberg-Marquardt step (5.25) at each update time t_k to design a discrete version of the gradient algorithm from [12] and update the estimated parameter vector $\hat{\boldsymbol{\theta}}$ with a sampling time of $T_c > T_m$. This proposed algorithm is closely related to moving horizon estimation, as we basically increase the optimization horizon M over time and solve an optimization problem at each update time-instant t_k on-line [22].

5.3.2 Implementation

The discrete adaptive law is given by the update law (5.26) based on the Levenberg-Marquardt step (5.25). It uses the vector of measurements (5.17), the vector of expected accelerations (5.18), the Jacobian (5.19), (5.20) and the matrix of weights (5.23), which are all obtained for the specialized DMP representation of human motion from Section 3.4 with $N = 100$ basis functions. We choose a rather small damping parameter $\lambda = 1 \cdot 10^{-8}$ as we would ideally like to directly step into the optimum at each parameter update based on the quadratically approximated cost function (5.22). For simulation we choose a realistic measurement sampling time of $T_m = 0.01\,\mathrm{s}$ and, to obtain a considerable amount of information and to not make the update law sensitive to measurement noise, we choose a considerably slower controller sampling time of $T_s = 0.5\,\mathrm{s}$ to update the parameter estimates. The measurements y, $\dot{y}$ and $\ddot{y}$ are simulated using the functional minimum-jerk representation (3.5) and its derivatives. The estimated parameter vector is set to

$$\hat{\boldsymbol{\theta}} = \begin{bmatrix} \hat{g} & \hat{\tau} \end{bmatrix},$$

and the initial value of $\hat{\boldsymbol{\theta}}_0 = [\hat{g}_0, \hat{\tau}_0]^\top$ with $\hat{g}_0 = 1\,\mathrm{m}$ and $\hat{\tau}_0 = 9\,\mathrm{s}$ for the true values $g = 2\,\mathrm{m}$ and $\tau = 10\,\mathrm{s}$ is chosen.

Nonlinear Least-Squares without Forgetting

Initially, the pure version of the presented nonlinear least-squares algorithm is implemented by setting the forgetting factor to $\gamma = 1$, which results in equal weighting of all collected measurements and thus no forgetting. Simulation results are plotted in Figure 5.5. Convergence of the estimates to their true values for both the goal estimate $\hat{g}$ and the timescale estimate $\hat{\tau}$ can be observed. The true values are reached after about 5 s which is half the transition time of the simulated motion of the human hand. The prominent estimation error in the initial phase of the motion can be attributed to the already discussed relatively large fitting errors of the specialized DMP during that phase of the motion. This requires a sufficiently close initial guess of the parameters to obtain convergence to true values. It was found that smoothness and fitting of the nonlinear forcing term (3.11) of the specialized DMP play a key role in the performance obtained using the discrete nonlinear least-squares-based parameter estimation scheme. These properties heavily depend on the number of basis functions N, the spacing of centers (3.18) and widths (3.19) of the basis functions.

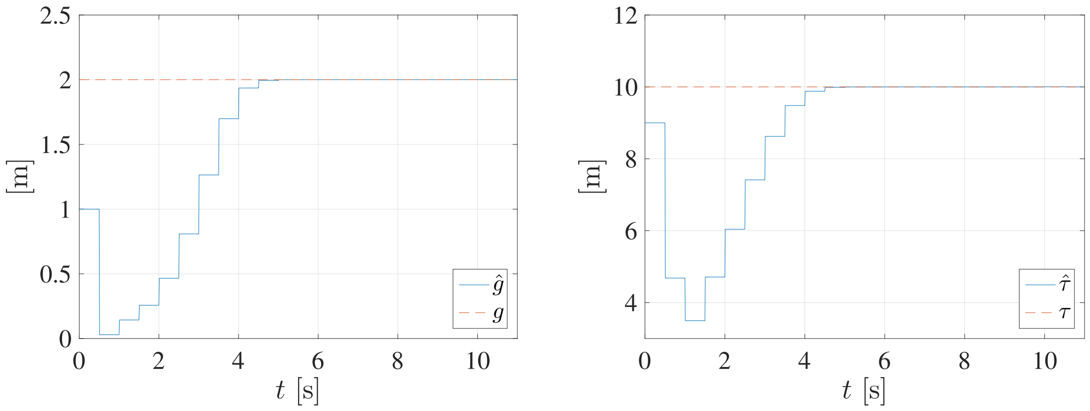

(a) **(b)**

Figure 5.5: On-line estimation of handover position and time with true values $g = 2\,\text{m}$, $\tau = 10\,\text{s}$ and initial parameter values $\hat{g}_0 = 1\,\text{m}$, $\hat{\tau}_0 = 9\,\text{s}$ using a discrete-time nonlinear least-squares adaptive law without forgetting with $T_c = 0.5\,\text{s}$ and $T_m = 0.01\,\text{s}$ for a specialized DMP.

Nonlinear Least-Squares with Forgetting

Now using a forgetting factor of $\gamma = 0.8$, the discrete-time nonlinear least-squares adaptive law with the update step (5.26) based on (5.25) is implemented. Simulation results are depicted in Figure 5.6. While faster convergence in combination with some oscillation around the true values was expected, convergence of the estimated goal $\hat{g}$ became slower with slight oscillation around the true g. The estimated timescale $\hat{\tau}$ exhibits large deviations from the true τ. Interestingly, in Figure 5.6b $\hat{\tau}$ seems to converge towards τ during the middle stage of the human motion. This is also the stage in which the specialized DMP fits the minimum-jerk profile best.

An explanation for the observed bad behavior of the nonlinear least-squares with forgetting can therefore be found based on the fitting error from Figure 3.8 of the specialized DMP. Forgetting causes past measurements to be 'forgotten' after some time. Hence, the current measurement has a greater impact on the estimate than past measurements. In Figure 5.6b, past measurements are forgotten towards the end and good estimates $\hat{\tau}$ from around $t = 6\,\mathrm{s}$ are changed to wrong estimates based on a badly fitted model in the final stage of the observed human motion.

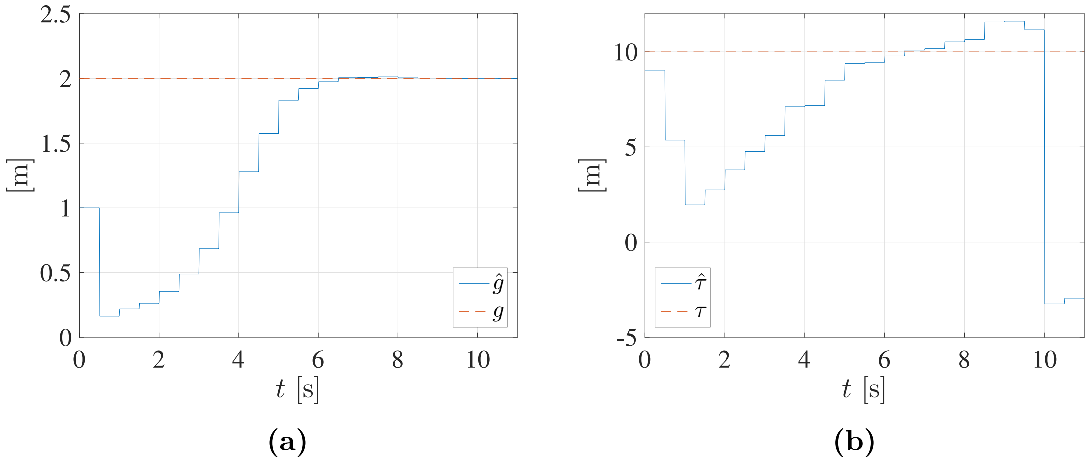

Figure 5.6: On-line estimation of handover position and time with true values $g = 2\,\mathrm{m}$, $\tau = 10\,\mathrm{s}$ and initial parameter values $\hat{g}_0 = 1\,\mathrm{m}$, $\hat{\tau}_0 = 9\,\mathrm{s}$ using discrete-time nonlinear least-squares adaptive law with forgetting factor $\gamma = 0.8$, $T_c = 0.5\,\mathrm{s}$ and $T_m = 0.01\,\mathrm{s}$ for a specialized DMP.

To conclude, the suggested discrete-time nonlinear least-squares based adaptive law poses a promising alternative to the high-gain or linearization based parameter estimation laws investigated in this section. Using the algorithm without forgetting seems to allow for fast convergence for the specialized DMP. Several approaches to improve the proposed discrete-time parameter estimation law exist. Instead of updating the parameter estimate with one Levenberg-Marquardt step, several iterations can be done to obtain solutions that are closer to the optimal values. Additionally, constraints on the parameters can be added to only produce feasible estimates and also possibly speed up convergence. Many of these approaches are common features and problems of moving horizon estimation, which highlights that the presented nonlinear least-squares based parameter estimator can be considered a moving horizon estimator.

6

Results

Evaluation of the predictors consisting of the different presented DMPs as parameterizations and estimators is conducted to ensure applicability for the prediction of handover place and time in a realistic scenario.

6.1 Evaluation of the Parameterizations

To compare the two different DMP representations, we conduct off-line learning of both the original DMP and the specialized DMP based on the minimum-jerk trajectory from (3.5) with starting point $y_0 = 0\,\mathrm{m}$, endpoint $g = 2\,\mathrm{m}$ and duration $\tau = 1\,\mathrm{s}$. The DMP parameters are set to $\alpha_z = 25$, $\beta_z = \alpha_z/4$ and $\alpha_x = \alpha_z/3$ as suggested in [9] to ensure a critically damped transformation system. The fitting error $\epsilon_{fit}(t_k) = f_{target,k} - f(y(t_k), g)$ which is obtained using (2.8) at time instances t_k with $k = 1, \ldots, P$ as defined in Section 2.2.4, is illustrated both for the original DMP as well as the specialized DMP in Figure 6.1a. Figure 6.1b depicts the squared fitting error $\epsilon_{fit}^2(t_k)$. Clearly, the fitting errors and their squares are much lower for the original DMP than for the specialized DMP. Albeit absolute values of the fitting error are significantly lower for the original DMP, both DMP versions have larger fitting errors in the beginning and in the end of the learned minimum-jerk motion compared to the errors during the middle stage of motion. Since off-line learning of

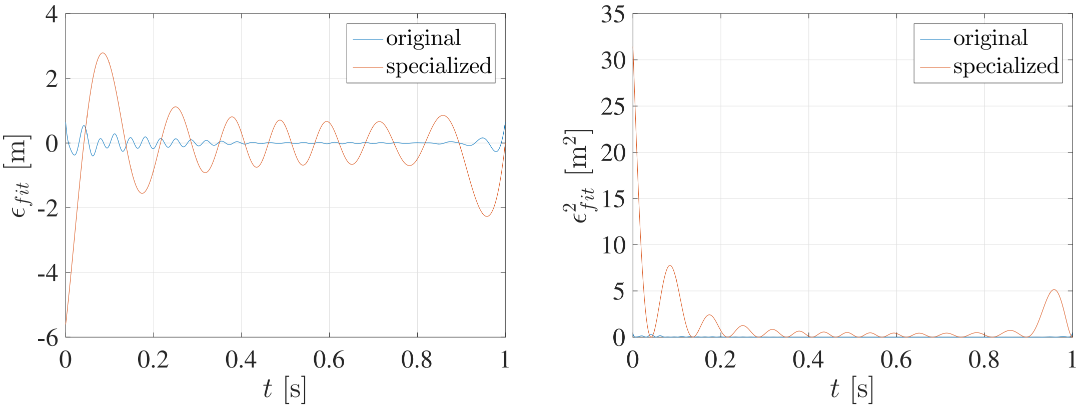

(a) **(b)**

Figure 6.1: Fitting errors ϵ_{fit} and squared fitting errors ϵ_{fit}^2 for original and specialized DMP for a minimum-jerk trajectory with starting point $y_0 = 0\,\mathrm{m}$, endpoint $g = 2\,\mathrm{m}$ and duration $\tau = 1\,\mathrm{s}$.

a DMP is done through fitting the nonlinear forcing term f with (2.8), large and oscillating fitting errors, as observed for the specialized DMP in Figure 6.1, affect the smoothness of the nonlinear forcing term, which in turn can make the design of an appropriate observer or parameter estimator more difficult. The poor fitting of the specialized DMP originates in the chosen widths of the basis functions. They are set via (3.8) and do not achieve equally sized Gaussians in time, as could already be seen in Figure 3.6. A different choice of $h_{s,i}$, allowing for equally sized Gaussians, would allow for low fitting errors similar to those of the original DMP since the basis functions of the original DMP resemble slightly distorted, equally spaced and sized Gaussians in time, as shown in Figure 4.6a.

The advantage of the specialized DMP is that by exploiting the consideration of monotone point-to-point motion, it does not require the use of a canonical system. As a consequence it has less states than the original DMP, which can simplify DMP-based state and parameter estimation. Additionally, in our context, DMPs are used to represent human motion. Without a canonical system, all appearing DMP states originating in the second-order transformation system have a physical meaning and can therefore be measured if required. In the present case of human motion, the specialized DMP states represent position and velocity of the human hand, which are signals that can be measured with appropriate sensors. However, bearing in mind that the specialized DMP can only be applied to monotone point-to-point motion and considering the original DMP's superior fitting performance, using the original DMP as a parameterization of human motion is beneficial.

6.2 Parameter Estimation Performance

In a realistic human-robot handover process, both place and time of the handover are initially unknown. As discussed before, it is therefore necessary to treat both the goal g, describing the handover place, and the timescale τ, describing the handover time, as unknown. We introduce the estimation errors

$$\begin{aligned}\tilde{g} &= g - \hat{g},\\ \tilde{\tau} &= \tau - \hat{\tau},\end{aligned}$$

to evaluate the performance of the parameter estimation schemes presented in this thesis.

6.2.1 Original DMP

Since the classical least-squares and integral adaptive laws from [12] do not give promising performance for the nonlinear DMP, we only evaluate the performance of the EKF-based estimation laws from Section 4.2. Using a minimum-jerk trajectory with parameters from Table 6.1 to fit the DMP with $N = 100$ basis functions and to generate measurements, we compare EKF-based state and parameter estimation for the original DMP. Using position y and velocity $\dot{y}$ measurements with the formulations from Section 4.2 with $\boldsymbol{P}_0 = 100\boldsymbol{I}$, $\boldsymbol{R} = \boldsymbol{I}$, $\boldsymbol{Q} = 10\boldsymbol{I}$ and $\alpha = 2$ for both state and parameter estimation cases, we obtain the trajectories from Figure 6.2.

The filter parameter of the EKF-based parameter estimator is set to $\lambda_f = 5$. Both estimation laws yield estimates very close to the true parameters after about 3 seconds. This would allow a robot to reach the handover place in time for the handover taking place after $\tau = 5\,\mathrm{s}$. We note, that the EKF-based parameter estimation law, having a state vector with a lower dimension than that of the state estimation case, shows slightly faster convergence. Apart from that, the EKF-based state estimation shows some oscillation of the timescale estimation error $\tilde{\tau}_{se}$ just before the end of motion at $t = 5\,\mathrm{s}$ and a small lasting error $\tilde{\tau}_{se}$ after the end of motion.

Parameter	**Value**	**Description**
τ	5 s	Timescale
y_0	0 m	Starting point
g	2 m	Endpoint/Goal

Table 6.1: Parameters of the minimum-jerk trajectory used to generate measurements.

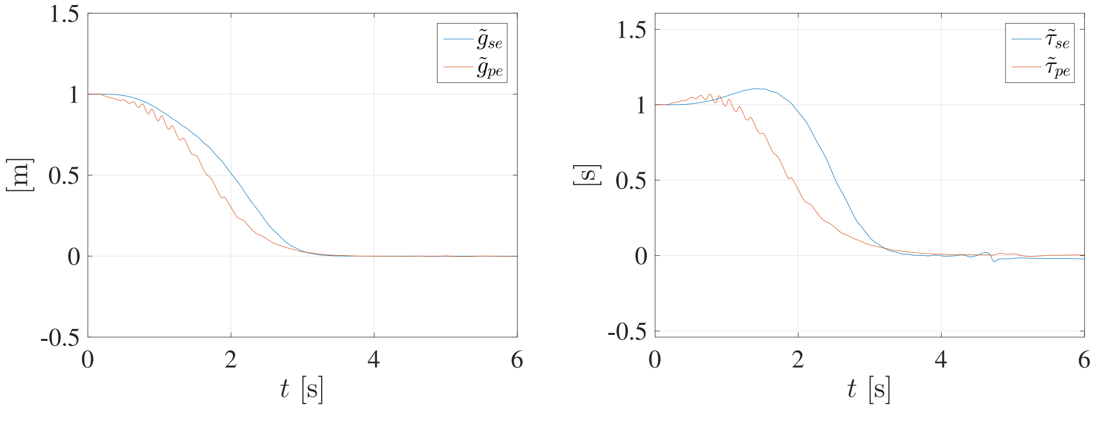

(a) **(b)**

Figure 6.2: Estimation errors $\tilde{g}_{se}$, $\tilde{\tau}_{se}$ using EKF-based state estimation and $\tilde{g}_{pe}$, $\tilde{\tau}_{pe}$ using EKF-based parameter estimation with initial guesses $\hat{g}_0 = 1\,\mathrm{m}$, $\hat{\tau}_0 = 4\,\mathrm{s}$ for true values $g = 2\,\mathrm{m}$, $\tau = 5\,\mathrm{s}$.

6.2.2 Specialized DMP

Using a minimum-jerk trajectory with the parameters from Table 6.1 to generate measurements, we compare the parameter estimation laws that are designed based on a specialized DMP. As done in Section 3.4 we choose $N = 100$ basis functions to get a sufficiently good fitting to the minimum-jerk trajectory from Table 6.1 for the algorithms designed for specialized DMPs to work. Setting the parameters of the EKF from Section 5.2.2 to $\boldsymbol{R} = \boldsymbol{I}$, $\boldsymbol{P}_0 = 100\boldsymbol{I}$, $\boldsymbol{Q} = 10\boldsymbol{I}$ and $\alpha = 2$ and implementing the discrete-time nonlinear least-squares based update law from Section 5.3 with forgetting factor $\gamma = 1$, damping parameter $\lambda = 1 \cdot 10^{-8}$ and sampling times $T_m = 0.01\,\mathrm{s}$ and $T_c = 0.5\,\mathrm{s}$, we obtain the trajectories from Figure 6.3.

Clearly both parameter sets of EKF and discrete-time adaptive law pose reasonable and realizable choices since none of the used tuning parameter values are excessively large. As can be seen, both estimation laws provide a working means to predict place and time of a human-robot handover through providing good estimates of goal and timescale after slightly more than half of the chosen duration $\tau = 5\,\mathrm{s}$ of human motion. The EKF-based estimations exhibit an overshoot and an oscillation just before the end of motion at $t = 5\,\mathrm{s}$. A small lasting error of the timescale estimate after the motion is finished at $t = 5\,\mathrm{s}$, as shown in Figure 6.3b, is expected to be due to the fact, that modeling errors, causing estimation errors, are also present as a result of the erroneous fitting of the specialized DMP.

In total, the discrete-time nonlinear least-squares adaptive law seems slightly superior from a precision point of view. However, its low damping parameter λ and therefore relatively large optimization based update step, make it sensitive to fitting errors, which is why a good fitting has to be ensured via a high number of basis functions for it to work. Choosing a larger λ would reduce this sensitivity at the cost of slower convergence.

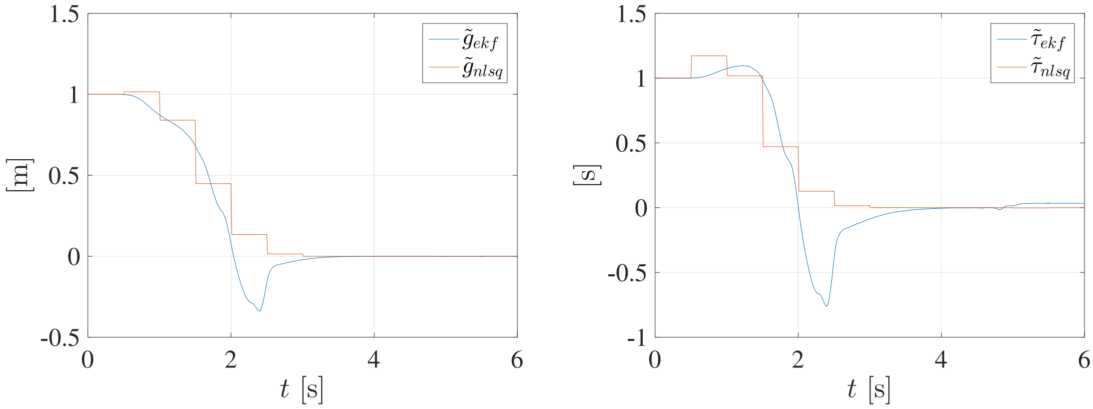

(a) **(b)**

Figure 6.3: Estimation errors $\tilde{g}_{ekf}$, $\tilde{\tau}_{ekf}$ using EKF-based state estimation and $\tilde{g}_{nlsq}$, $\tilde{\tau}_{nlsq}$ using discrete-time nonlinear least-squares-based parameter estimation with initial guesses $\hat{g}_0 = 1\,\mathrm{m}$, $\hat{\tau}_0 = 4\,\mathrm{s}$ for true values $g = 2\,\mathrm{m}$, $\tau = 5\,\mathrm{s}$ of a specialized DMP.

6.3 Parameter Estimation Performance Using Experimental Data

Using a motion capture system, a series of human-human handovers was conducted and the corresponding position trajectories were measured. [1] They are shown in Figure 6.4a. Clearly, a small variation of timescale and goal can be observed, while their shapes appear relatively similar in Figure 6.4b.

---

[1] The handover trajectories were captured by Axel Demborg and Elon Såndberg in a motion capture lab at KTH as part of their Bachelor's thesis [32].

6.3.1 Qualitative Evaluation of the Parameter Estimators

Considering the modified EKFs based on original DMPs with parameters from Table 6.2 for the state estimation EKF and parameters from Table 6.3 for the parameter estimation EKF, we first fit an original DMP to a captured handover trajectory via demonstration learning. This training trajectory is shown in Figure 6.4 and has goal $g = -0.8920\,\mathrm{m}$ and timescale $\tau = 1.5667\,\mathrm{s}$. Since the estimation schemes presented in this thesis also rely on measurements of the velocities, we produce them via numerical differentiation. Choosing initial guesses $\hat{g}_0 = -1.5\,\mathrm{m}$ and $\hat{\tau}_0 = 2\,\mathrm{s}$, estimation with the two EKFs based on the original DMP is performed. We use the measurements captured for the training trajectory and the corresponding velocity measurements produced via numeric differentiation. Results are shown in

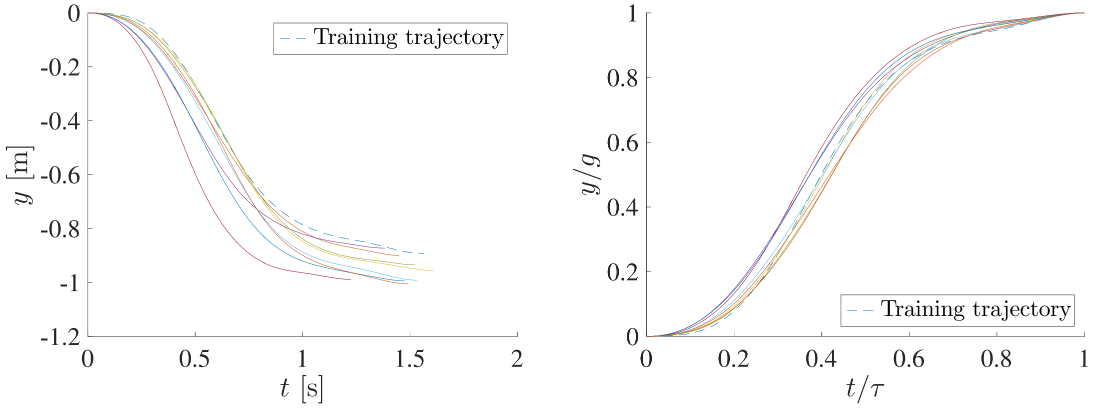

(a) **(b)**

Figure 6.4: Captured trajectories of the human hand during a human-human handover.

Parameter	Value
$\boldsymbol{P}_0$	$100\boldsymbol{I}$
$\boldsymbol{R}$	$0.001\boldsymbol{I}$
$\boldsymbol{Q}$	$10\boldsymbol{I}$
α	5

Table 6.2: Parameters of the modified EKF used for state estimation.

Parameter	Value
$\boldsymbol{P}_0$	$100\boldsymbol{I}$
$\boldsymbol{R}$	1
$\boldsymbol{Q}$	$10\boldsymbol{I}$
α	5
λ_f	10

Table 6.3: Parameters of the modified EKF used for parameter estimation.

Figure 6.5. Despite the relatively fast true timescale, the estimation errors converge to zero within the first 0.7 seconds for the state estimation EKF and with 0.4 seconds even faster for the parameter estimation EKF. Towards the end of motion, the state estimation EKF shows a small error in the timescale as has already been observed for minimum-jerk trajectories in Chapter 4. A possible explanation could be fitting errors that cause the nonlinear forcing term to be highly nonlinear, thus resulting in bad performance due to the linearization used by the EKF. From a practical point of view the estimates from Figure 6.5 are all useful, as the goal estimates are very precise and the errors in the timescale relatively small. Also, bad estimates in the end could be neglected by using a special control policy to guide the robot hand towards the handover place during the final stage of motion.

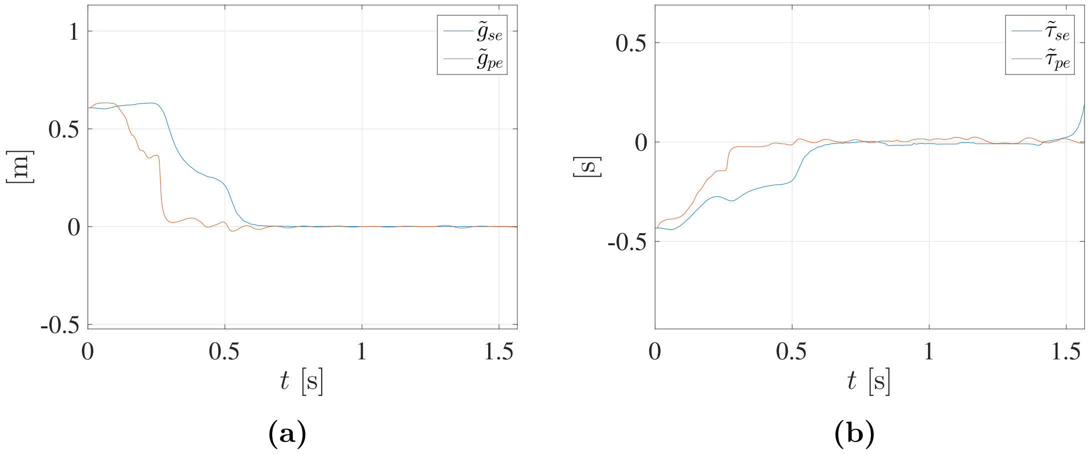

Figure 6.5: Estimation errors $\tilde{g}_{se}$, $\tilde{\tau}_{se}$ using EKF-based state estimation and estimation errors $\tilde{g}_{pe}$, $\tilde{\tau}_{pe}$ using EKF-based parameter estimation with initial guesses $\hat{g}_0 = -1.5\,\text{m}$, $\hat{\tau}_0 = 2\,\text{s}$ for a captured human handover with true values $g = -0.8920\,\text{m}$, $\tau = 1.5667\,\text{s}$ which was also used as training data.

When applying the same EKFs to another captured human handover trajectory with goal $g = -0.9451\,\text{m}$ and timescale $\tau = 1.5250\,\text{s}$, the estimates shown in Figure 6.6 are obtained. While the goal estimate converges after slightly over 0.5 seconds, the timescale estimate is erroneous. The estimation error $\tilde{\tau}_{se}$ obtained by the state estimation EKF is quite large, whereas $\tilde{\tau}_{pe}$ is vanishing towards the end of motion. Similar to previous simulations, we observe that the timescale estimate is more prone to errors in the presence of model errors than the goal estimate. In the scenario considered here, a slight difference in shape between the training trajectory and the tested one could cause these estimation errors.

Testing the estimation laws designed for the specialized DMP with $N = 100$ basis functions, we again use the captured training trajectory from Figure 6.4a with goal $g = -0.8920\,\text{m}$ and timescale $\tau = 1.5667\,\text{s}$. As it is strictly monotonically decreasing, a specialized DMP representing it can be learned. The parameters of the modified EKF from Section 5.2.2 are shown in Table 6.4 and those of the discrete-time nonlinear least-squares adaptive law are shown in Table 6.5. Using the training trajectory and its derivatives as measurements and initial guesses $\hat{g}_0 = -1.5\,\text{m}$, $\hat{\tau}_0 = 2\,\text{s}$, we obtain the estimates from Figure 6.7. While the goal estimates from

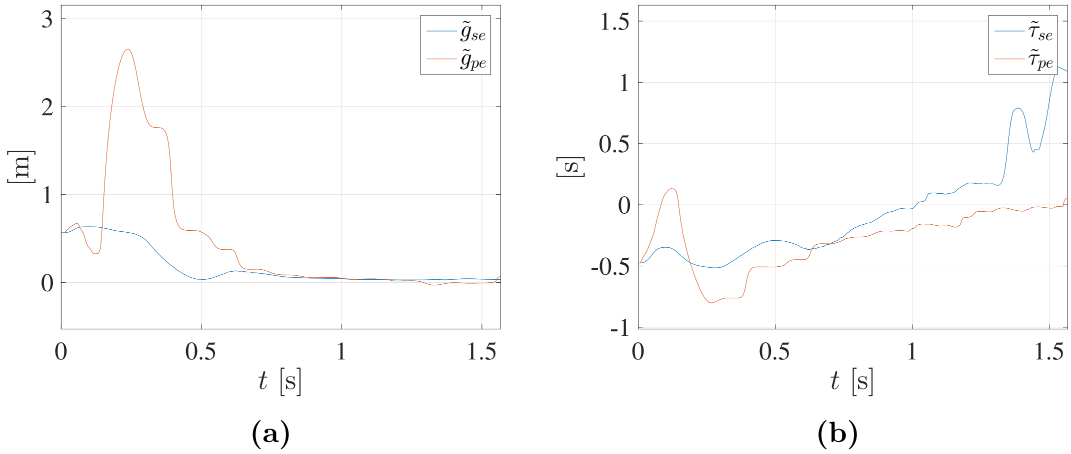

Figure 6.6: Estimation errors $\tilde{g}_{se}$, $\tilde{\tau}_{se}$ using EKF-based state estimation and $\tilde{g}_{pe}$, $\tilde{\tau}_{pe}$ using EKF-based parameter estimation with initial guesses $\hat{g}_0 = -1.5\,\mathrm{m}$, $\hat{\tau}_0 = 2\,\mathrm{s}$ for a captured human handover with true values $g = -0.9451\,\mathrm{m}$, $\tau = 1.5250\,\mathrm{s}$.

Parameter	**Value**
$\boldsymbol{P}_0$	$100\boldsymbol{I}$
$\boldsymbol{R}$	$1\boldsymbol{I}$
$\boldsymbol{Q}$	$10\boldsymbol{I}$
α	5

Table 6.4: Parameters of the modified EKF designed for a specialized DMP used for state estimation.

Figure 6.7a converge to the true value, there are significant errors in the timescale estimate.

The same estimation laws designed for a specialized DMP are now used for a different handover trajectory with goal $g = -0.9451\,\mathrm{m}$ and timescale $\tau = 1.5250\,\mathrm{s}$. The resulting estimates are plotted in Figure 6.8. Again, the goal estimates converge, especially for the EKF, while the timescale estimates exhibit considerable errors. Performance of the specialized DMP based laws could be improved using more aggressively tuned estimation laws, however, the relatively bad fitting of the specialized DMP has been found to be a challenge when it comes to numerically stable simulations.

Generally, performance on the testing trajectory is worse than on the training data due to the difference in shape between the trajectories and the thus present

Parameter	**Value**
λ	$5 \cdot 10^{-2}$
γ	1
T_m	$0.01\,\mathrm{s}$
T_c	$0.5\,\mathrm{s}$

Table 6.5: Parameters of the discrete adaptive law designed for a specialized DMP.

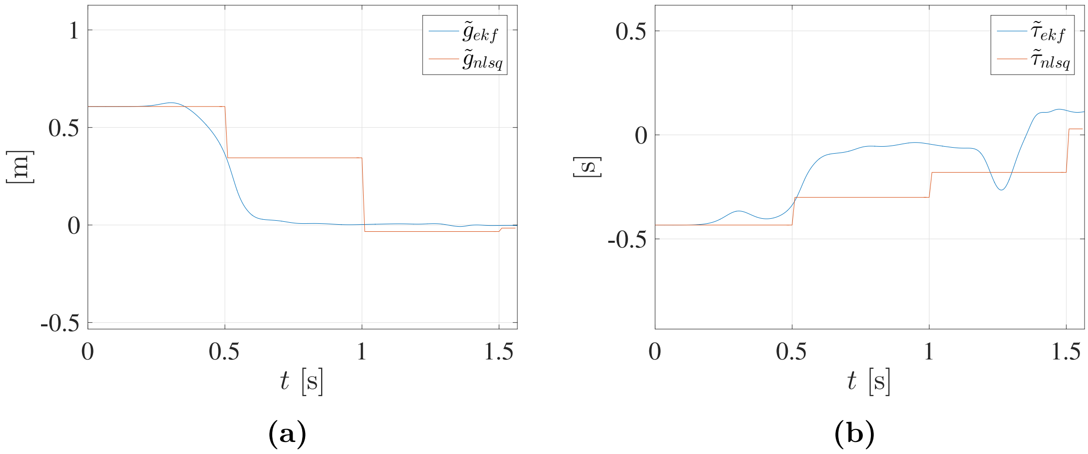

Figure 6.7: Estimation errors $\tilde{g}_{ekf}$, $\tilde{\tau}_{ekf}$ using EKF-based state estimation for a specialized DMP and estimation errors $\tilde{g}_{nlsq}$, $\tilde{\tau}_{nlsq}$ using EKF-based parameter estimation for a specialized DMP. Initial guesses are $\hat{g}_0 = -1.5\,\mathrm{m}$, $\hat{\tau}_0 = 2\,\mathrm{s}$ for the training trajectory with true values $g = -0.8920\,\mathrm{m}$, $\tau = 1.5667\,\mathrm{s}$.

modeling errors of the DMP. However, in all the presented cases good performance of the goal estimation could be observed. Even in case the timescale estimation does not perform well, sufficiently fast goal estimation allows a robot to move towards the thereby predicted handover place fast to ensure the robot hand is there to receive an object even before the human hand reaches the handover place.

6.3.2 Quantitative Evaluation of the EKF-Based Parameter Estimator Using a DMP

After these illustrative evaluations, we now pick the predictor consisting of the modified EKF-based filtered parameter estimator for the original DMP from Section 4.2.3 to conduct a more thorough testing of the parameter estimation performance on all human-human handover trajectories available from experiments.

The parameters of the filtered EKF-based parameter estimator using measurements of position y and velocity $\dot{y}$ are set to those from Table 6.6.

Parameter	Value
$\boldsymbol{P}_0$	$10^4\boldsymbol{I}$
$\boldsymbol{R}$	1
$\boldsymbol{Q}$	$\boldsymbol{I}$
α	2
λ_f	20

Table 6.6: Parameters of the filtered EKF-based parameter estimator using a DMP for the prediction of real human-human handovers.

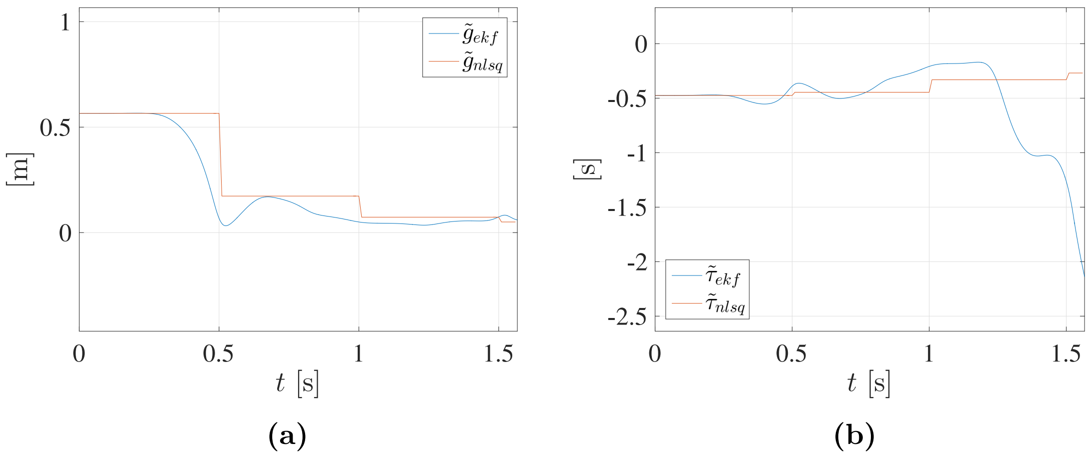

(a) **(b)**

Figure 6.8: Estimation errors $\tilde{g}_{ekf}$, $\tilde{\tau}_{ekf}$ using a state estimation EKF for a specialized DMP and estimation errors $\tilde{g}_{nlsq}$, $\tilde{\tau}_{nlsq}$ using a parameter estimation EKF for a specialized DMP with initial guesses $\hat{g}_0 = -1.5\,\mathrm{m}$, $\hat{\tau}_0 = 2\,\mathrm{s}$ for the training trajectory with true values $g = -0.9451\,\mathrm{m}$, $\tau = 1.5250\,\mathrm{s}$.

Basic Handover Trajectory

We fit an original DMP to the simple captured training trajectory with goal $g = -0.8920\,\mathrm{m}$ and timescale $\tau = 1.5667\,\mathrm{s}$ from Figure 6.4 via demonstration learning.

Choosing initial guesses $\hat{g}_0 = -1.5\,\mathrm{m}$ and $\hat{\tau}_0 = 2\,\mathrm{s}$, estimation using the filtered EKF-based parameter estimation on the original DMP is performed for all captured human-human handover trajectories. The velocity measurements $\dot{y}$ required in addition to the shown position measurements y are produced via numeric differentiation.

Obtained estimation errors $\tilde{g}$ of the goals are shown in Figure 6.9. While the estimation error $\tilde{g}_{training}$ obtained for the training trajectory clearly converges to zero fastest, goal estimates get close to zero for all captured trajectories after slightly more than half the duration τ of the human motion. Figure 6.10 shows a close-up of the goal estimation errors $\tilde{g}$ from Figure 6.9. We observe that the goal estimation errors are less than $0.2\,\mathrm{m}$, resulting in a relative error of less than 22% after 0.6τ for all test trajectories. At $t = \tau$ most of the goal estimates exhibit an error of approximately 10% or less.

The timescale estimation errors $\tilde{\tau}$ from Figure 6.11 are generally larger than those for the goals. They do converge, albeit to non-zero values. We observe that the timescale estimation errors are within $1\,\mathrm{s}$ after 0.6τ, which means large relative errors of up to 66%. Even at the end of the human motion at $t = \tau$, the timescale estimation errors are of similar scope for many of the test trajectories of Figure 6.4.

Estimation errors appear due to modeling errors as a result of differences in shapes between training and test trajectories. The estimation of place and time of the handover hence works well for test trajectories exhibiting shapes close to that of the training trajectory in Figure 6.4b. Note, that it seems sensible to simply use goal and timescale of the training trajectory as initial values for the parameter estimation with test trajectories in reality. However, due to the small differences in goals and timescales of the present captured handover trajectories, initial conditions

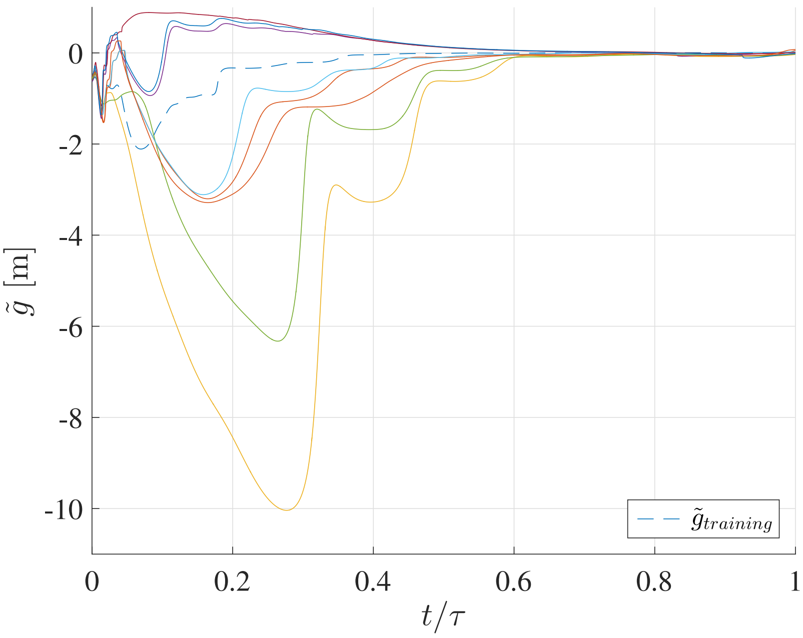

Figure 6.9: Obtained goal estimation errors $\tilde{g}$ for the captured basic handover trajectories.

were deliberately chosen to be rather far from the true parameter values to obtain more illustrative results.

Generally, we observe that timescale estimates are more prone to modeling errors than goal estimates. This was observed in several simulations throughout this thesis. As discussed before, poor timescale estimates can be dealt with by simply moving to the more reliably estimated handover place fast enough to reach it before the human hand does. Reliable goal estimates and thus precise handover place predictions, however, are crucial to achieve seamless handovers since the transfer of an object can only be performed when human and robot hand meet at the same place.

We conclude that the prediction of place and time of a human-robot handover by using an EKF-based parameter estimator and a DMP to parameterize human motion works better, the closer training and test trajectory are in terms of shape, since in that case, the DMP is a good representation of the motion of the human hand.

Extended Handover Trajectory

Thanks to the versatility of using a DMP as a parameterization of human motion, it is also possible to consider an extended version of a human handover trajectory which not only includes the reaching of the human hand towards the robot, but also the part where the human picks up an object before reaching towards the robot. Figure 6.12 shows these extended handover trajectories captured in human-human handovers. They vary in timescale and goal while also exhibiting shapes that are not entirely similar to each other.

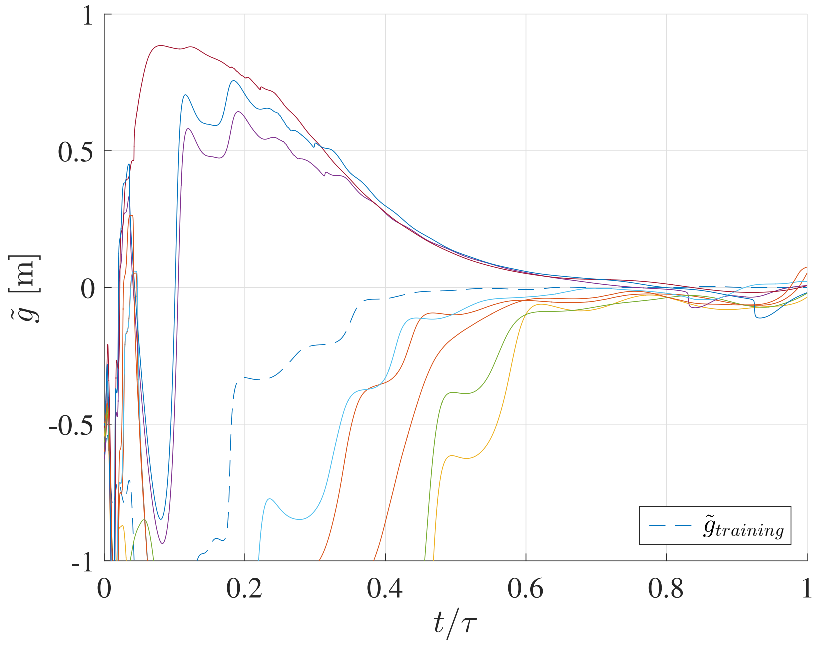

Figure 6.10: Close-up of the obtained estimation errors $\tilde{g}$ for the captured basic handover trajectories.

Using the training trajectory from Figure 6.12 with goal $g = -0.3542\,\mathrm{m}$ and timescale $\tau = 2.1833\,\mathrm{s}$, an original DMP is learned via demonstration. As before, the modified EKF-based filtered parameter estimator from Section 4.2.3 with parameters from Table 6.6 is used to predict handover place and time by estimating the parameters of the learned DMP on-line. With initial guesses $\hat{g}_0 = -1\,\mathrm{m}$ and $\hat{\tau}_0 = 2\,\mathrm{s}$, the estimation errors from Figure 6.13 are obtained.

Again, convergence of the estimates is fastest for the training trajectory. After 0.6τ, the goal estimates are within $0.2\,\mathrm{m}$ of the true goals for all trajectories. In this case, we have a relative goal estimation error of less than 55% for all trajectories. This large relative error originates in the large differences in shapes for some of the extended handover trajectories. Many of the closer test trajectories yield relative errors of less than about 29%. The final goal estimates are within $0.02\,\mathrm{m}$ of the true value, resulting in a final relative estimation error of around 6% . The timescale estimates for the extended handover trajectory are within $0.2\,\mathrm{s}$ after 0.6τ, implying a relative error of less than 10% for the different trajectories. The final relative timescale estimation error is less than 2%.

Generally, the final estimation errors are lower than those obtained with the basic handover trajectories from above. The more sophisticated shapes of the captured extended handover trajectories are expected to facilitate parameter estimation as they contain more information, or as is often used in adaptive control, they have a higher level of excitation. Considering the low relative errors of the timescale estimates, this seems to especially improve the estimation of the timescale. Relatively clear differences in the shapes of the extended handover trajectories from Figure 6.12 explain the erroneous goal estimates in the earlier stages of the motion.

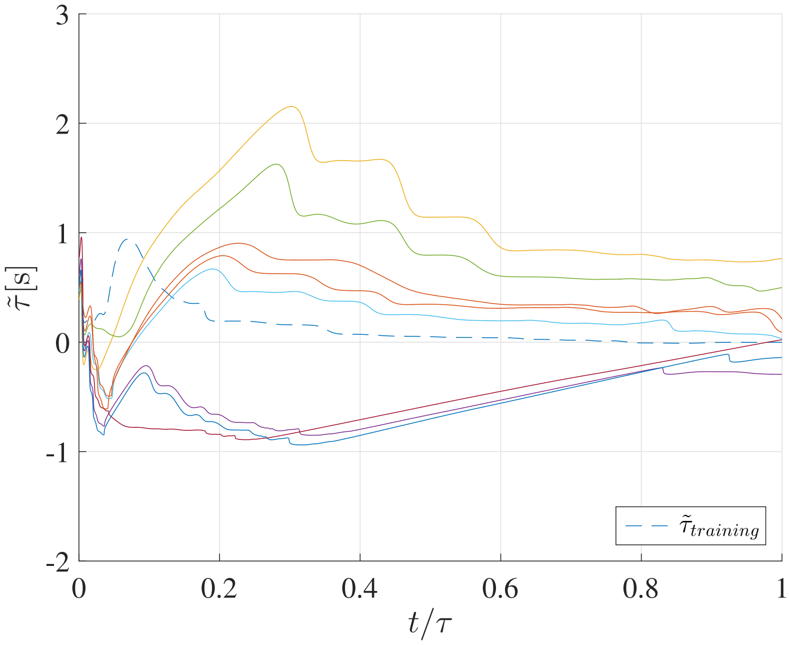

Figure 6.11: Obtained estimation errors $\tilde{\tau}$ for the captured basic handover trajectories.

On the whole, good performance for the extended handovers can be observed. The higher level of excitation allows for good estimates for both goal and timescale even in the face of significant differences in shape. For trajectories with shapes similar to the training trajectory, very good convergence is observed. Clearly, place and time of a handover can be predicted in the case of extended handovers. Thanks to the higher level of excitation, it is therefore beneficial to consider the extended handover instead of the basic handover.

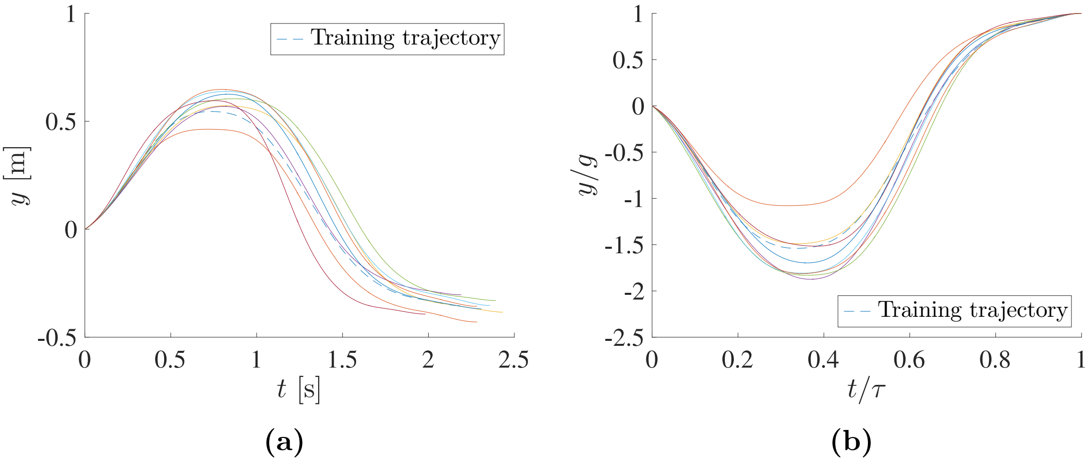

Figure 6.12: Captured extended trajectories of the human hand during a human-human handover.

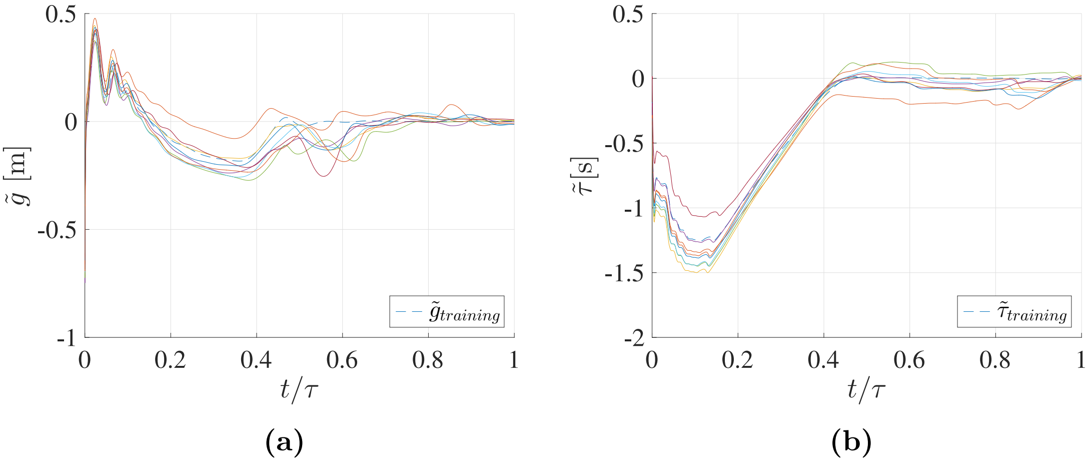

Figure 6.13: Estimation errors $\tilde{g}$ and $\tilde{\tau}$ for the captured extended handover trajectories.

7

Conclusions and Future Work

Seamless human-robot handover as a scenario of human-robot collaboration is aimed for in this thesis. To allow for natural interaction, we proposed a predictor enabling the robot agent to predict place and time of a handover while the human hand is reaching towards the robot. After having formulated the prediction problem as a model-based parameter estimation problem, we used dynamic movement primitives (DMPs) to parameterize human motion and employed parameter estimation strategies originating from adaptive control to estimate point attractor and timescale of the DMP. Using the fact that the point attractor and the timescale of a DMP can represent place and time of a handover, we were able to predict these characteristic parameters of a handover.

Human motion was parameterized with two versions of the off-line learnable DMP. The original DMP from Schaal *et al.*, consisting of a transformation system and a canonical system, showed low fitting errors. Exploiting the fact that human trajectories in handovers can be considered as point-to-point motions, a specialized DMP without a canonical system was presented. While fitting errors became larger, all states of the specialized DMP have a physical interpretation and can theoretically be measured.

Both adaptive laws and estimators designed based on the extended Kalman filter were used to estimate the parameters of the original DMP. While the adaptive laws failed to cope with the nonlinearity in the parameters of the DMP, convergence of the EKF-based estimators, using a linearization of the DMP with respect to the parameters, could be shown. A low number of unknown parameters was found to be beneficial for convergence speed as less information was required to obtain good parameter estimates.

Similarly, adaptive laws and EKF-based estimators were designed to estimate parameters of a specialized DMP. Again, convergence for the EKF-based estimators could be shown. An adaptive law with a high gain also achieved convergence in one unrealistic scenario. This motivated the proposition of a discrete-time nonlinear least-squares based adaptive law originating in the gradient algorithm commonly used to derive adaptive laws for linear parametric models. Convergence of the parameter estimates could be observed for some cases. A disadvantage of the presented parameter estimators based on the specialized DMP is their reliance on measurements of position, velocity and acceleration of the human hand. Contrastingly, estimation schemes based on the original DMP require position and speed measurements of the human hand only.

Evaluation of the promising predictors consisting of the different parameterizations and estimators was performed based on human handover trajectories artificially generated as minimum-jerk trajectories and on data captured from real human-human handover experiments. Equal performance for the EKF-based estimators designed for the original DMP as well as the EKF-based estimator and the discrete-time nonlinear least-squares adaptive law designed for the specialized DMP was observed for the generated minimum-jerk trajectories. For the data captured from a real human-human handover, the estimators using an original DMP performed better than those using a specialized DMP. Differences in the shapes of the captured handover trajectories gave rise to estimation errors with magnitude proportional to modeling errors. Modeling errors arise due to the difference in shape between the test trajectories and the training trajectory used to learn the DMP.

In conclusion, the proposed predictor structure consisting of a DMP, parameterizing human motion, and a parameter estimator, which estimates the parameters of the DMP describing place and time of a handover, has shown promising results. The combination of an original DMP with an EKF-based parameter estimator allowed prediction of the handover place for all captured handover trajectories with around 22% accuracy after slightly more than half the duration of human motion and around 10% accuracy at the end of motion. The handover time predictions were found to be more sensitive to modeling errors. The more similar the shape of handover trajectories were to the training trajectory, the better the prediction of handover place and time worked. Extended handover trajectories including the fetching of the object allowed for good prediction of both place and time of the handover due to their higher level of excitation. Significant differences in the shapes of the extended trajectories led to a higher relative error for the predicted handover place in the early stages of human motion. In the final stages of the human motion, the predictions of both handover place and time were quite precise and allowed for smooth handovers.

Seamless handovers may even be achieved by controlling the robot agent to reach the estimated handover place sufficiently fast to be able to receive an object once the human hand reaches the handover place without using the estimated handover time. It can thus be said that the proposed EKF-based parameter estimator allows for more efficient collaboration between human and robot in handover tasks both when considering basic and when considering extended handover trajectories. Furthermore, the proposed combination of DMP and EKF-based parameter estimator was found to be very versatile as different point-to-point trajectories can be represented by a DMP and their timescale and point attractor can be estimated on-line with the presented EKF-based parameter estimator.

The proposed method to predict handover place and time has only been applied to one-dimensional motion in this thesis. Future work can extend the predictor structure to cope with multidimensional trajectories. It is even possible to exploit the temporal couplings of the separate dimensions of human motion in the DMP framework: One joint canonical system can be used to modulate the temporal evolution of human motion in all dimensions, while measurements of position and velocity in the different dimensions increase the number of measurable outputs of the corresponding system. Thus, the additional information available in a multi-dimensional case might be used to improve the precision of the predictions of handover place and time.

For the presented predictor to work in a realistic scenario, it is essential to detect when the DMP presentation becomes valid and measurements can be used to predict handover place and time. Since we learn our DMP from a demonstrated handover trajectory, the robot would have to be able to decide when the human starts a handover by reaching towards the robot. What is more, a human might change their behavior when interacting with a robot and thereby render the learned DMP an erroneous model. Given this, a learning strategy repeatedly updating the learned DMP might produce better results than the supervised learning used in this thesis.

Since a handover is an example of two agents synchronizing with each other, it also seems possible to generalize the method proposed in this thesis to achieve synchronization of multiple systems without resorting to explicit communication. In this context, a rigorous proof, possibly using the notion of persistence of excitation, showing convergence of the goal and timescale estimates of a DMP obtained using an EKF is yet to be done as well.

Bibliography

[1] K. W. Strabala, M. K. Lee, A. D. Dragan, J. L. Forlizzi, S. Srinivasa, M. Cakmak, and V. Micelli, "Towards seamless human-robot handovers," *Journal of Human-Robot Interaction*, vol. 2, no. 1, pp. 112–132, 2013.

[2] M. Huber, M. Rickert, A. Knoll, T. Brandt, and S. Glasauer, "Human-robot interaction in handing-over tasks," in *RO-MAN 2008 - The 17th IEEE International Symposium on Robot and Human Interactive Communication*, Aug 2008, pp. 107–112.

[3] T. Flash and N. Hogan, "The coordination of arm movements: an experimentally confirmed mathematical model," *The journal of Neuroscience*, vol. 5, no. 7, pp. 1688–1703, 1985.

[4] J. Kim, J. Park, Y. K. Hwang, and M. Lee, "Advanced grasp planning for handover operation between human and robot," in *2nd International Conference on Autonomous Robots and Agents*, 2004, pp. 13–15.

[5] A. Edsinger and C. C. Kemp, "Human-robot interaction for cooperative manipulation: Handing objects to one another," in *RO-MAN 2007 - The 16th IEEE International Symposium on Robot and Human Interactive Communication*, Aug 2007, pp. 1167–1172.

[6] S. M. Khansari-Zadeh and A. Billard, "Learning stable nonlinear dynamical systems with gaussian mixture models," *IEEE Transactions on Robotics*, vol. 27, no. 5, pp. 943–957, Oct 2011.

[7] S. Schaal, J. Peters, J. Nakanishi, and A. Ijspeert, "Learning movement primitives," in *Robotics Research. The Eleventh International Symposium.* Springer, 2005, pp. 561–572.

[8] A. J. Ijspeert, J. Nakanishi, and S. Schaal, "Learning attractor landscapes for learning motor primitives," Tech. Rep., 2002.

[9] A. J. Ijspeert, J. Nakanishi, H. Hoffmann, P. Pastor, and S. Schaal, "Dynamical movement primitives: learning attractor models for motor behaviors," *Neural computation*, vol. 25, no. 2, pp. 328–373, 2013.

[10] M. Prada and A. Remazeilles, "Dynamic movement primitives for human robot interaction," in *IEEE/RSJ Int. Conf. on Intelligent Robots and Systems, workshop on Robot Motion Planning: online, reactive and in Real-time, Algarve, Portugal*, 2012.

[11] M. Prada, A. Remazeilles, A. Koene, and S. Endo, "Implementation and experimental validation of dynamic movement primitives for object handover," in *2014 IEEE/RSJ International Conference on Intelligent Robots and Systems*, Sept 2014, pp. 2146–2153.

[12] P. A. Ioannou and J. Sun, *Robust adaptive control.* Courier Corporation, 2012.

[13] J.-J. E. Slotine, W. Li *et al.*, *Applied nonlinear control.* Prentice-hall Englewood Cliffs, NJ, 1991, vol. 199, no. 1.

[14] S. Sastry and M. Bodson, *Adaptive control: stability, convergence and robustness.* Courier Corporation, 2011.

[15] V. Stepanyan and N. Hovakimyan, “Robust adaptive observer design for uncertain systems with bounded disturbances,” *IEEE Transactions on Neural Networks*, vol. 18, no. 5, pp. 1392–1403, Sept 2007.

[16] I. Y. Tyukin, E. Steur, H. Nijmeijer, and C. Van Leeuwen, “Adaptive observers and parameter estimation for a class of systems nonlinear in the parameters,” *Automatica*, vol. 49, no. 8, pp. 2409–2423, 2013.

[17] G. Besançon, *Nonlinear observers and applications.* Springer, 2007, vol. 363.

[18] R. M. Murray, “Optimization-based control,” *California Institute of Technology, CA*, 2009.

[19] S. Bonnabel and J. J. Slotine, “A contraction theory-based analysis of the stability of the deterministic extended kalman filter,” *IEEE Transactions on Automatic Control*, vol. 60, no. 2, pp. 565–569, Feb 2015.

[20] B. Ni and Q. Zhang, “Stability of the kalman filter for output error systems,” *IFAC-PapersOnLine*, vol. 48, no. 28, pp. 1106–1111, 2015.

[21] K. Reif, F. Sonnemann, and R. Unbehauen, “An ekf-based nonlinear observer with a prescribed degree of stability,” *Automatica*, vol. 34, no. 9, pp. 1119–1123, 1998.

[22] J. B. Rawlings and D. Q. Mayne, *Model predictive control: Theory and design.* Nob Hill Pub., 2009.

[23] E. L. Haseltine and J. B. Rawlings, “Critical evaluation of extended kalman filtering and moving-horizon estimation,” *Industrial & engineering chemistry research*, vol. 44, no. 8, pp. 2451–2460, 2005.

[24] Y. Maeda, T. Hara, and T. Arai, “Human-robot cooperative manipulation with motion estimation,” in *Proceedings of the IEEE/RSJ International Conference on Intelligent Robots and Systems*, vol. 4, 2001, pp. 2240–2245 vol.4.

[25] H. K. Khalil and J. Grizzle, *Nonlinear systems.* Prentice hall New Jersey, 1996, vol. 3.

[26] W. Lohmiller and J.-J. E. Slotine, “On contraction analysis for non-linear systems,” *Automatica*, vol. 34, no. 6, pp. 683–696, 1998.

[27] A. Ude, A. Gams, T. Asfour, and J. Morimoto, “Task-specific generalization of discrete and periodic dynamic movement primitives,” *IEEE Transactions on Robotics*, vol. 26, no. 5, pp. 800–815, Oct 2010.

[28] H. Hoffmann, P. Pastor, D. H. Park, and S. Schaal, “Biologically-inspired dynamical systems for movement generation: Automatic real-time goal adaptation and obstacle avoidance,” in *IEEE International Conference on Robotics and Automation*, May 2009, pp. 2587–2592.

[29] E. A. Jackson, *Perspectives of nonlinear dynamics.* CUP Archive, 1992, vol. 1.

[30] K. Eriksson, D. Estep, and C. Johnson, *Applied Mathematics: Body and Soul: Volume 1: Derivatives and Geometry in IR3.* Springer Science & Business Media, 2013.

[31] D. W. Marquardt, “An algorithm for least-squares estimation of nonlinear parameters,” *Journal of the society for Industrial and Applied Mathematics*, vol. 11, no. 2, pp. 431–441, 1963.

[32] A. Demborg and E. Såndberg, “Common representations for human-robot handovers,” 2016.

A

Appendix

A.1 Derivations of Lipschitz Continuity for the EKF

The components of (4.31) are

$$\tilde{h}(x) = 2\frac{\left(\sum_{i=1}^{N} \Psi_i'(\hat{x}) w_i\right)\left(\sum_{i=1}^{N} \Psi_i(\hat{x})\right) - \left(\sum_{i=1}^{N} \Psi_i(\hat{x}) w_i\right)\left(\sum_{i=1}^{N} \Psi_i'(\hat{x})\right)}{\left(\sum_{i=1}^{N} \Psi_i(\hat{x})\right)^2}$$

and

$$\begin{aligned}
\tilde{g}(x) =& \frac{\left(\sum_{i=1}^{N} \Psi_i''(\hat{x}) w_i\right)\left(\sum_{i=1}^{N} \Psi_i(\hat{x})\right) - \left(\sum_{i=1}^{N} \Psi_i'(\hat{x}) w_i\right)\left(\sum_{i=1}^{N} \Psi_i'(\hat{x})\right)}{\left(\sum_{i=1}^{N} \Psi_i(\hat{x})\right)^2} \\
&- \frac{\left(\left(\sum_{i=1}^{N} \Psi_i'(x) w_i\right)\left(\sum_{i=1}^{N} \Psi_i'(x)\right) + \left(\sum_{i=1}^{N} \Psi_i(x) w_i\right)\left(\sum_{i=1}^{N} \Psi_i''(x)\right)\right)\left(\sum_{i=1}^{N} \Psi_i(x)\right)^2}{\left(\sum_{i=1}^{N} \Psi_i\right)^4} \\
&+ 2\frac{\left(\sum_{i=1}^{N} \Psi_i(x) w_i\right)\left(\sum_{i=1}^{N} \Psi_i'(x)\right)\left(\sum_{i=1}^{N} \Psi_i(x)\right)\left(\sum_{i=1}^{N} \Psi_i'(x)\right)}{\left(\sum_{i=1}^{N} \Psi_i\right)^4}.
\end{aligned}$$

A.2 Additional Plots

A.2.1 EKFs for the original DMP

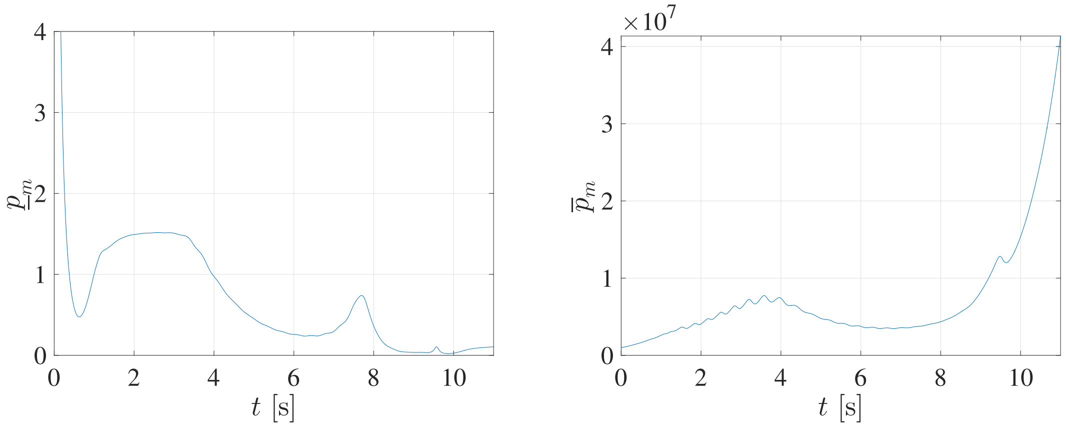

(a) **(b)**

Figure A.1: Lower bound $\underline{p}_m(t)$ and upper bound $\overline{p}_m(t)$ of $\boldsymbol{P}(t)$ using a modified EKF to estimate the states of an original DMP.

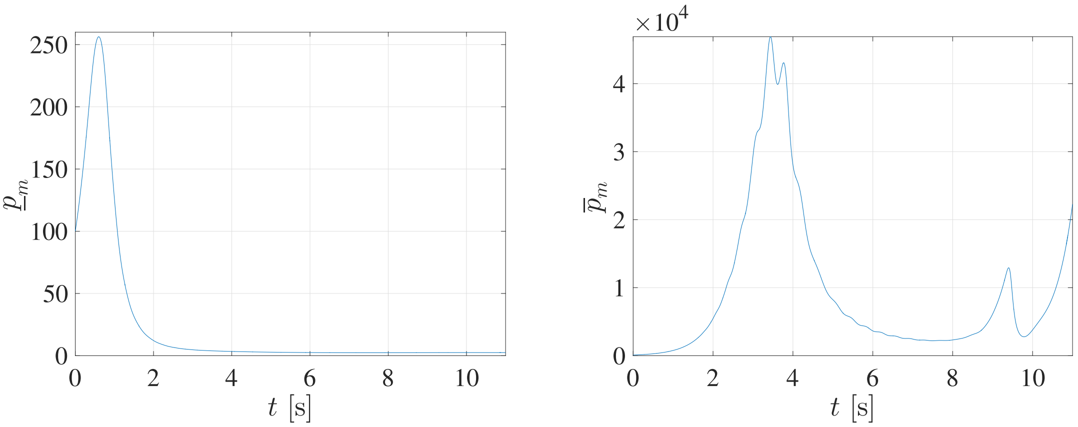

(a) **(b)**

Figure A.2: Lower bound $\underline{p}_m(t)$ and upper bound $\overline{p}_m(t)$ of $\boldsymbol{P}(t)$ using a modified EKF to estimate the parameters of an original DMP.

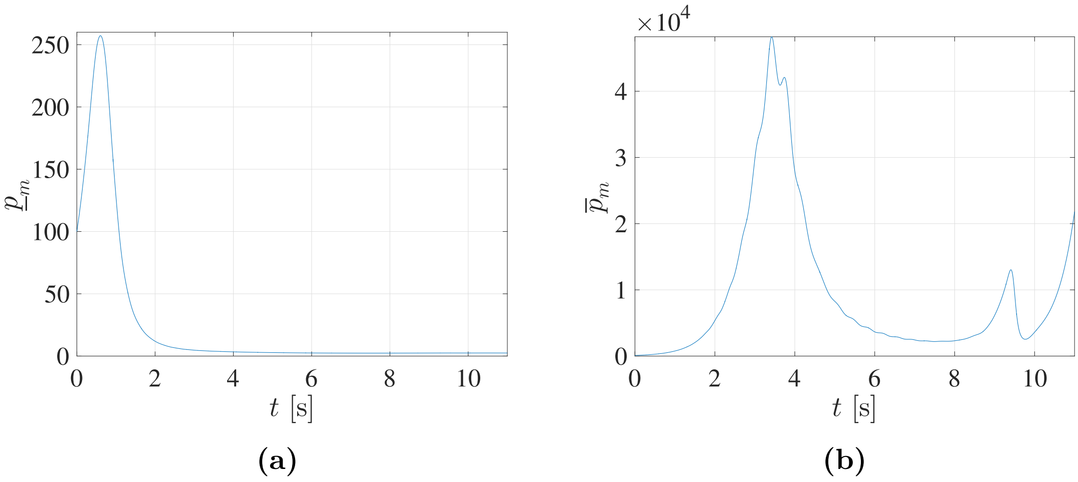

(a) **(b)**

Figure A.3: Lower bound $\underline{p}_m(t)$ and upper bound $\overline{p}_m(t)$ of $\boldsymbol{P}(t)$ using a filtered version of the modified EKF to estimate the parameters of an original DMP.

A.2.2 EKFs for the Specialized DMP

Classical EKFs

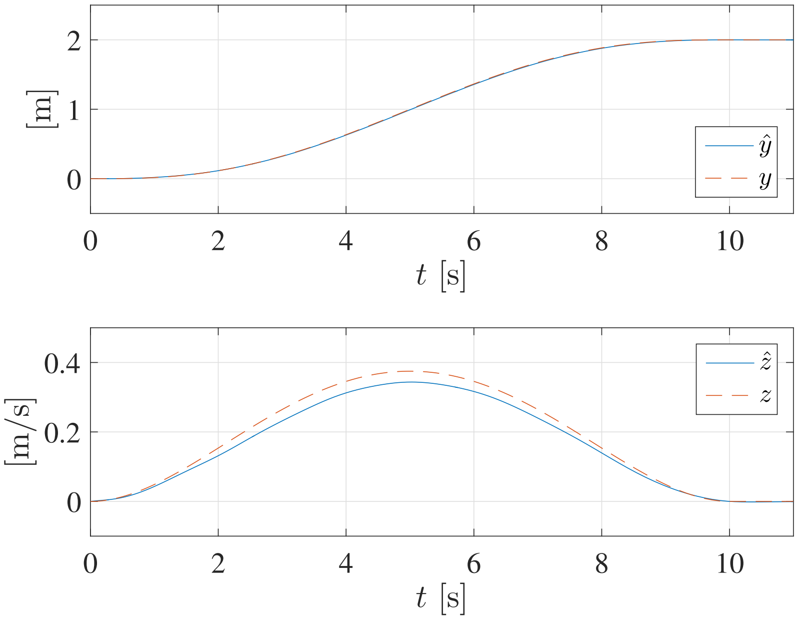

Figure A.4: Estimates $\hat{y}$ and $\hat{z}$ using a classical EKF with $\boldsymbol{P}_{0,s} = 100\boldsymbol{I}$ and a specialized DMP.

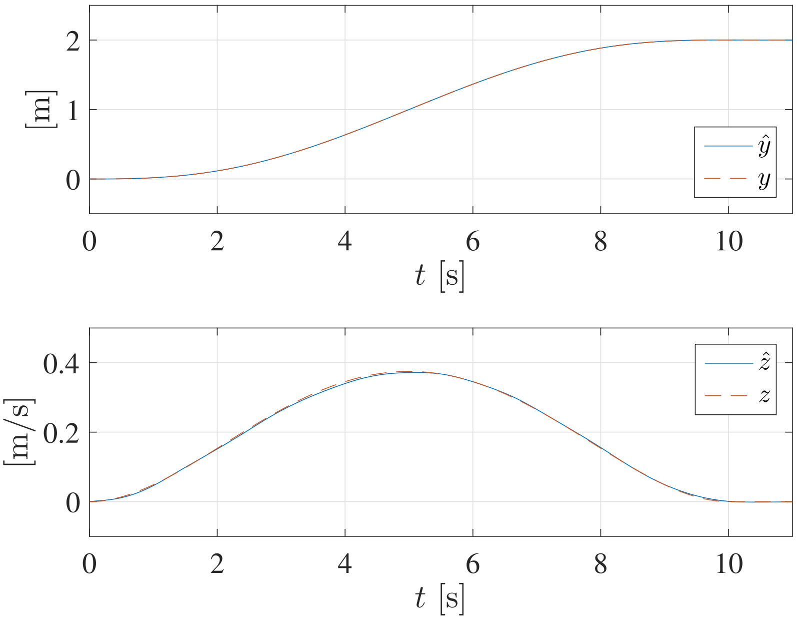

Figure A.5: Estimates $\hat{y}$ and $\hat{z}$ using a classical EKF with $\boldsymbol{P}_{0,s} = 10^5\boldsymbol{I}$ and a specialized DMP.

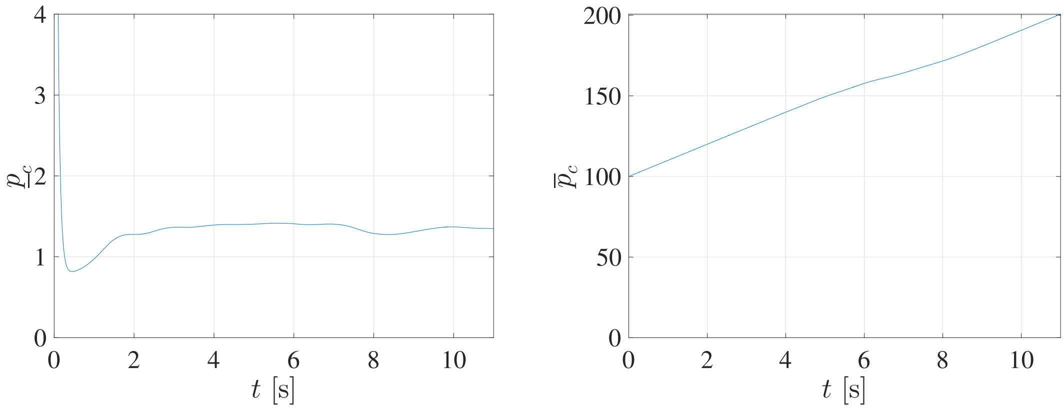

(a)

(b)

Figure A.6: Lower bound $\underline{p}_c(t)$ and upper bound $\overline{p}_c(t)$ of $\boldsymbol{P}(t)$ using a classical EKF with $\boldsymbol{P}_0 = 100\boldsymbol{I}$ to estimate the states of a specialized DMP.

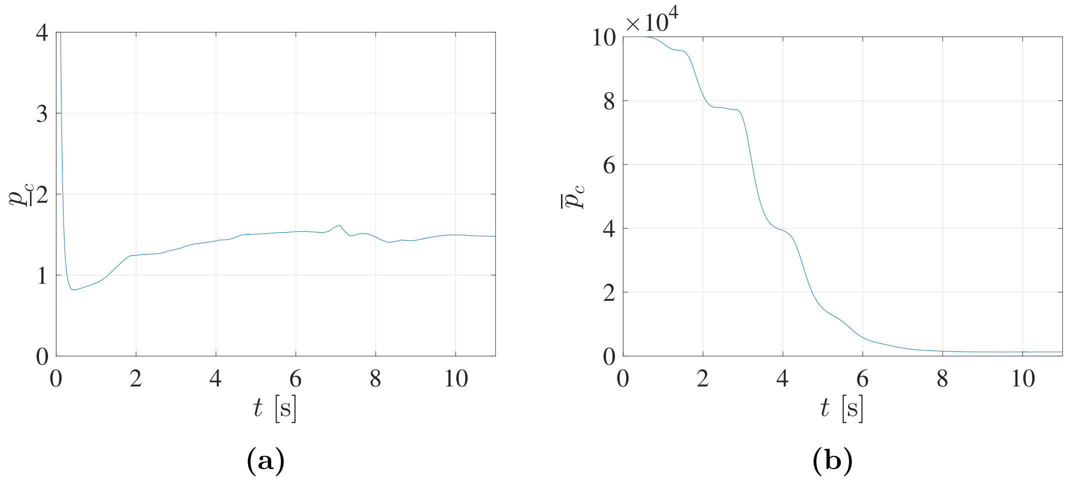

Figure A.7: Lower bound $\underline{p}_c(t)$ and upper bound $\overline{p}_c(t)$ of $\boldsymbol{P}(t)$ using a classical EKF with $\boldsymbol{P}_0 = 10^5\boldsymbol{I}$ to estimate the states of a specialized DMP.

Modified EKF

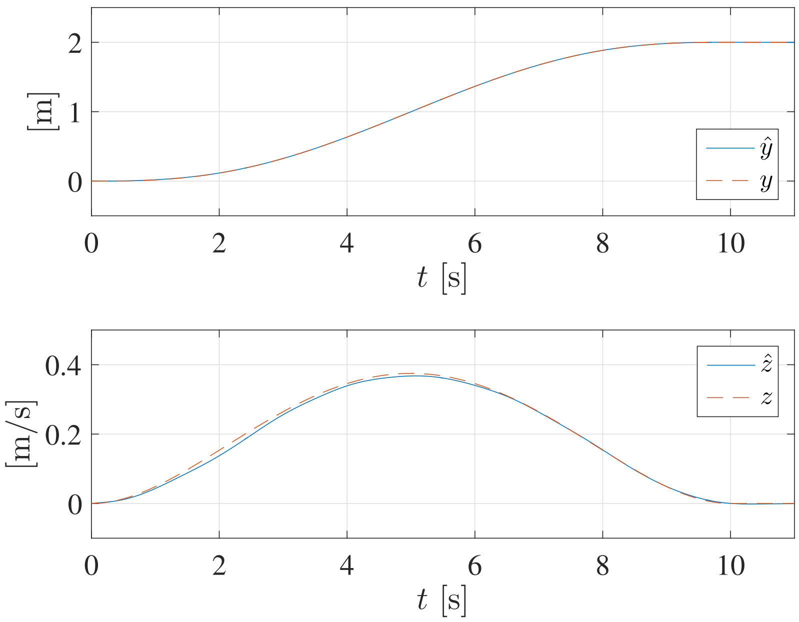

Figure A.8: Estimates $\hat{y}$ and $\hat{z}$ using a modified EKF with $\boldsymbol{P}_{0,s} = 100\boldsymbol{I}$, convergence parameter $\alpha_s = 0.5$ and a specialized DMP.

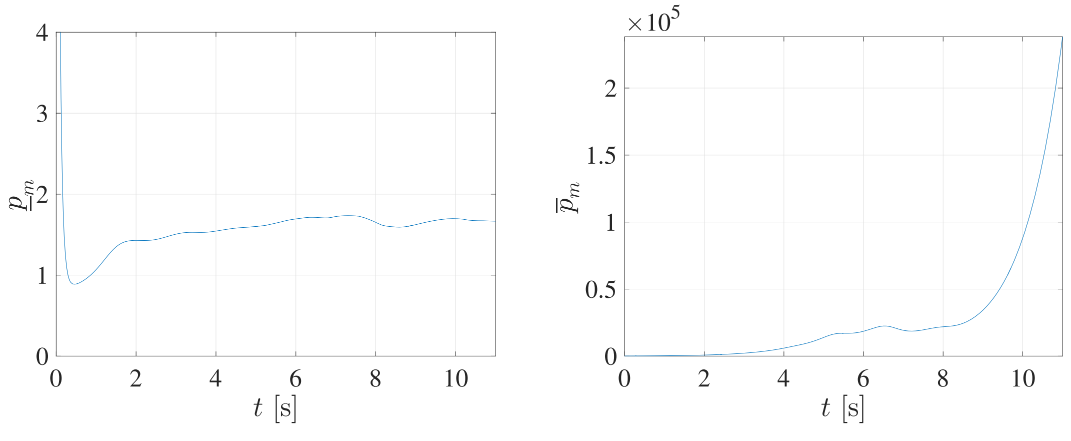

(a) **(b)**

Figure A.9: Lower bound $\underline{p}_m(t)$ and upper bound $\overline{p}_m(t)$ of $\boldsymbol{P}(t)$ using a modified EKF to estimate the states of a specialized DMP.